

Identification of factors involved in the biogenesis of thylakoid membranes in cyanobacteria

Dissertation

zur Erlangung des Grades eines Doktors der Naturwissenschaften an der
Fakultät für Biologie der
Ludwig-Maximilians-Universität München

vorgelegt von

Julia Constanze Hamm

München, 2021



Erstgutachter: Herr Prof. Dr. Jörg Nickelsen

Zweitgutachter: Frau PD Dr. Serena Schwenkert

Tag der Abgabe: München, den 26. Mai 2021

Tag der mündlichen Prüfung: München, den 27. August 2021

TABLE OF CONTENTS

TABLE OF CONTENTS	I
SUMMARY	1
ZUSAMMENFASSUNG	2
1. INTRODUCTION	3
1.1 Photosynthesis.....	3
1.1.1 Electron transport chain	4
1.2 Model organism <i>Synechocystis</i> sp. PCC 6803.....	5
1.3 Cyanobacterial Photosynthetic complexes.....	7
1.3.1 PSII	7
1.3.2 PSI	9
1.4 <i>De novo</i> Biogenesis of Photosystem II.....	11
1.5 PSII repair	13
1.6 Thylakoid membranes in <i>Synechocystis</i>	15
1.7 Aims of this work	18
2. MATERIAL AND METHODS	19
2.1 Materials.....	19
2.2 Methods	27
2.2.1 Bioinformatic tools	27
2.2.2 Growth conditions	28
2.2.3 Molecular biology methods.....	28
2.2.3.1 Transformation of <i>E.coli</i> cells	29
2.2.3.2 Plasmid isolation	29
2.2.4 Genetic screen	29
2.2.5 Transformation of <i>Synechocystis</i>	30
2.2.5.1 Strain generation of <i>Synechocystis</i>	30

2.2.6 Microscopy	31
2.2.6.1 Immunofluorescence and fluorescence microscopy.....	31
2.2.6.2 Transmission electron microscopy (TEM) and correlative light-electron microscopy (CLEM)	31
.....	31
2.2.7 Measurement of chlorophyll and oxygen consumption/evolution.....	32
2.2.8 Fluorescence measurements.....	32
2.2.8.1 P ₇₀₀ ⁺ reduction kinetics and relative electron transport rate.....	32
2.2.8.2 77 K Measurements	32
2.2.9 Protein analysis.....	33
2.2.9.1 SDS-PAGE.....	33
2.2.9.2 Blue Native (BN)-PAGE / 2D-PAGE	33
2.2.9.3 Western Blotting	34
2.2.10 Protein purification.....	35
2.2.10.1 Maltose binding protein (MBP) Tagged Proteins	35
2.2.10.2 His Tagged Proteins.....	36
2.2.11 Antibody purification.....	36
2.2.12 Whole cell protein isolation.....	36
2.2.13 Analysis of cyanobacterial membrane complexes.....	37
2.2.13.1 Solubility Test	37
2.2.13.2 Analysis membrane complexes using 2D-PAGE	37
2.2.13.3 Pulse-labeled Proteins.....	37
2.2.13.4 Membrane fractionation.....	38
2.2.13.5 Co-Immunoprecipitation (Co-IP) of α CurT in PDM and TM	38
2.2.14 Mass spectrometry (MS)	39
2.2.15 Protein interaction studies using microscale thermophoresis (MST).....	40
2.2.16 Accession numbers.....	40
3. RESULTS	41
3.1 PrtA complex.....	41
3.2 Proteomic screen	45
3.3 Genetic screen	48
3.3.1 Primary analysis of the ORF <i>hik43</i> and <i>cyt_{CM}</i>	51
3.4 Analysis of <i>ancM</i>	53
3.4.1 Recombinant overexpression of AncM for antibody production	54
3.4.1 Generation of <i>ancM</i> related strains.....	55
3.4.2 <i>ancM</i> has a photosynthetic phenotype	58

Table of contents

3.4.3 The effect of highlight treatment in <i>ancM</i> ⁻ and related strains	60
3.4.4 Molecular phenotype of <i>ancM</i> ⁻	62
3.4.5 Distribution of photosynthetic complexes	65
3.4.6 Localisation of AncM	68
3.4.7 The loss of AncM affects the thylakoid membrane structure	77
4. DISCUSSION	80
4.1 PrtA Complex	80
4.2 Proteomic screen	81
4.3 Genetic Screen	82
4.3.1 Characterisation of AncM	83
4.3.1.1 Properties of recombinant AncM	83
4.3.1.2 <i>ancM</i> ⁻ and the phenotypes of the related strains	83
4.3.1.3 <i>ancM</i> ⁻ has a molecular photosynthetic phenotype	84
4.3.1.4 AncM is localised at the PDM	85
4.3.1.5 The relationship of CurT and AncM	86
4.3.1.6 Comparison of PDM and TM	86
4.3.1.7 AncM - The membrane anchor.	87
BIBLIOGRAPHY	90
ABBREVIATIONS	108
ANNEX	111
CURRICULUM VITAE	126
LIST OF PUBLICATION	127
DANKSAGUNG	128
EIDESSTAATLICHE VERSICHERUNG UND ERKLÄRUNG	129

SUMMARY

Photosynthesis is the key reaction that has enabled the evolution of complex life on earth. The gram-negative cyanobacterium *Synechocystis* sp. PCC 6803 (hereinafter *Synechocystis*) is a well-established model organism for research on photosynthesis.

The *Synechocystis* cell is surrounded by an outer membrane and a plasma membrane. Photosynthesis takes place in the thylakoid membranes (TMs) localised in the cytoplasm, which are shaped towards the plasma membrane and form the converging zone. The resulting converging zone is the region of early Photosystem II (PSII) assembly steps. The precursor form of D1 (pD1) is preloaded with manganese by the processing associated tetrapeptide (TPR) protein (PratA) in a subcompartment of the TM. The PratA defined membrane (PDM) represents the converging zones. Moreover, PratA forms a 200 kDa complex with the high temperature requirement homologue A (HhoA) and pilin protein Q (PilQ) in the periplasm. Beside PratA, the protein Curvature Thylakoid1 (CurT) plays an important role in the formation of the converging zones. A reduced photosynthetic performance and the absence of convergence zones is caused by knocking out CurT.

This photosynthetic phenotype can be suppressed by the formation of suppressor lines of *curT*⁻: *sucurT*. To get a better understanding of the convergence zones two different screening methods were performed: a proteomic screen with the focus on PratA and a genetic screen focused on *curT* and its suppressor *sucurT*.

In the primary analysis some selected candidates of the screen showed defects in photosynthetic performance and growth. The open reading frame (ORF) *slr2070* encodes for a protein named anchoring of convergence membranes (AncM). AncM was found independent in both screens. Concerning this, AncM is reduced in *pratA*⁻ and co-expressed with CurT. In *sucurT* *ancM* contains a STOP codon in the N-terminus at the amino acid position 164 in front of a transmembrane domain (TMD). Based on that, AncM was not detected in *sucurT* by immunoblotting. Immunofluorescence and sucrose density gradients localised the membrane protein AncM at the PDM. Moreover a photosynthetic phenotype was observed in *ancM*. In some regions AncM is colocalised with CurT. Electron microscopy studies of *ancM* shows thylakoids that are not connected to the plasma membrane. This reveals a structuring function of AncM relating to CurT. It is suggested that AncM anchors the thylakoids and offers a fixing point for the thylakoids at the converging zones.

Based on the important function of AncM at the converging zones the independent screens offer a powerful method to investigate convergence zones as a specialised compartment of the thylakoids.

ZUSAMMENFASSUNG

Die Photosynthese ist die Schlüsselreaktion, die das höhere Leben auf der Erde ermöglicht. Dabei etablierte sich das gram negative Cyanobakterium *Synechocystis* sp. PCC 6803 (*Synechocystis*) als Modelorganismus für die Photosyntheseforschung. Das Bakterium ist von einer äußeren Membran und der Plasmamembran umrundet. Im Cytoplasma befinden sich die photosynthetisch aktiven Membranen, die Thylakoide. Die Thylakoide bilden Konvergenz Zonen, welche in Richtung der Plasmamembran geformt sind und auf molekularer Ebene den Startpunkt der Photosystem II (PSII) Assemblierung sind. Dabei wird die Vorläufer Form von D1 (pD1) von dem Tetrakopeptid Protein PrtA mit Mangan beliefert. Die Beladung von pD1 findet in einer spezialisierten Region der Thylakoidmembran statt, die PrtA enthaltende Membran (PDM), welche repräsentativ für die Konvergenz Zonen ist. Das Mangan bindende Protein PrtA bildet im Periplasma mit den mit der Protease HhoA und dem Pilin Protein Q (PilQ) einen Komplex mit einer Größe von 200 kDa. Ein weiterer wichtiger Faktor der Konvergenz Zonen ist das Protein mit dem Namen Curvature Thylakoid (CurT). Der Verlust des Proteins führt zu einer Abwesenheit von Konvergenz Zonen sowie zu einer drastischen Reduktion der photosynthetischen Leistung. Durch eine genetische Veränderung kann der Photosynthese Phänotyp von *curT*⁻ in dem Suppressor von *sucurT*⁻ supprimiert werden.

Um ein besseres Verständnis der Konvergenz Zonen zu erlangen, wurden zwei unterschiedliche Screens durchgeführt: zum einen ein proteomischer Screen mit dem Fokus auf PrtA und zum anderen ein genetischer Screen, in dem die Genome *sucurT*⁻ und *curT*⁻ miteinander verglichen wurden. Die daraus resultierenden Leserahmen (ORF), liefern Kenntnisse über die Konvergenz Zonen. Erste Analysen der generierten knock-out Mutanten haben defekte im Wachstum bzw. einen photosynthetischen Phänotyp. Besonders interessant ist der ORF *slr2070*, der aufgrund der Ergebnisse dieser Arbeit Anker der Konvergenz Membranen (AncM) heißt. AncM wurde in beiden Screens unabhängig voneinander als Kandidat identifiziert. So ist AncM in *prtA*⁻ reduziert und wird mit CurT coexprimiert. Der Verlust von AncM führt zu einer reduzierten Photosynthese Leistung. Dabei übernimmt der N-Terminus von AncM eine gesonderte Rolle ein. So besitzt der ORF *ancM* in *sucurT*⁻ an der Aminosäure stelle 164, kurz vor der Transmembrandomäne (TMD) ein STOP Codon. Dies hat zur Folge, dass AncM in *sucurT*⁻ nicht immunologisch detektiert werden kann. Die TMD führt zu einer Lokalisierung von AncM in den PDMs und zu einer Colokalisierung mit CurT. Elektronenmikroskopische Aufnahmen von *ancM* zeigen von der Plasmamembran losgelöste Thylakoide. Dabei offeriert AncM sich als ein Anker für Thylakoide, der wie ein Kleber die Membranen an den Konvergenz Zonen fixiert. Die beiden Screens haben sich dabei als eine sehr nützliche Methode erwiesen, um einen detaillierten Blick in den Aufbau der Konvergenz Zonen zu erhalten.

1. INTRODUCTION

1.1 Photosynthesis

For ~2.4 billion years, light energy in the form of photons has been converted by photosynthetic active bacteria to produce chemical energy (Raymond and Segrè, 2006; Hohmann-Marriott and Blankenship, 2011). Moreover, this physiological process has been responsible for the rise of biomass on earth. In addition to producing biomass, oxygen is released to the atmosphere and builds up an ozone layer in the stratosphere. The ozone layer is crucial, since it protects the earth from mutagenic UV light and therefore has increased the stability of DNA macromolecules (Blankenship, 1992). Upon the presence of oxygen on earth, the carbon dioxide resulting from the heterotrophic lifestyle emerged. Beside the release of oxygen during oxygenic photosynthesis, other sources such as sulphur can also be formed by anoxygenic photosynthesis. Anoxygenic photosynthesis takes place for example in purple bacteria and uses electron sources like hydrogen sulfide (Brocks *et al.*, 2005). During oxygenic photosynthesis, an organism uses water as an electron donor and molecular oxygen is produced. The oxygenic photosynthesis can be divided into light and dark reactions. The net equation is summarised below, dioxide (CO₂) and water (H₂O) are used to form carbohydrate (CH₂O), water H₂O and oxygen (O₂) (Van Niel, 1932).



The light dependent reactions occur in the thylakoid membranes (TM) and can be parted in a cyclic and a linear electron flow. The linear electron chain involves four membrane bound protein complexes: Photosystem II (PSII), Cytochrome *b₆f* complex (Cyt *b₆f*), Photosystem I (PSI) and adenosine triphosphate synthase (ATPase) (Figure 1). During the dark reactions, also called the Calvin Cycle, CO₂ is fixed to form of glucose by using the energy from light reaction transiently stored as nicotinamide adenine dinucleotide hydrophosphate (NADPH) and adenosine triphosphate (ATP) (Benson and Calvin, 1947).

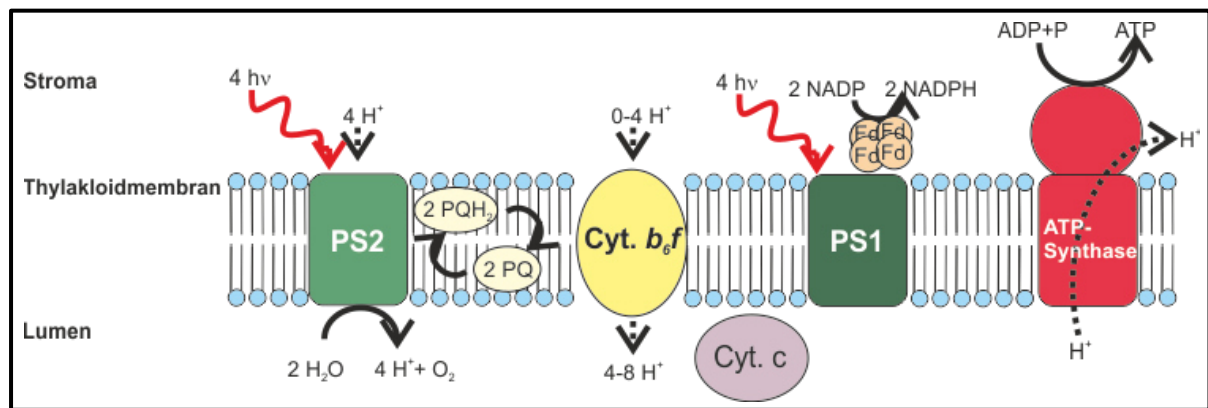


Figure 1: Light reaction of photosynthesis. Photons from sunlight are absorbed by the Photosystem II and I (PSII, PSI) thereby electrons from the water splitting complex get released and transferred via Cytochrome b_6f (Cyt b_6f) complexes across PSI to the terminal electron acceptor Ferredoxin (Fd). During the last step NADP⁺ is reduced to NADPH by FNR. The pumped protons are used to produce ATP by the ATP Synthase (ATPase).

1.1.1 Electron transport chain

Excitation of the PSII reaction centre P_{680} by photons from sunlight causes a charge separation. While one electron is transferred via pheophytin to plastoquinone A (Q_A) in a second step the electron moves on to plastoquinone B (Q_B). The Q_B has a redox potential of -0.06 V and can be reduced twice following Q_B accepts a second electron and is released as plastoquinone (PQH_2) from the Q_B binding pocket. Subsequently the P_{680} chlorophyll radical pair is reduced by uptake of one electron from the tyrosine residue Y_z (Holzwarth *et al.*, 2006). The regeneration of the formed tyrosine radical is done via the Kok Cycle (Kok *et al.*, 1970; Chrysin *et al.*, 2019). During the Kok-Cycle the oxygen evolving complex (OEC) provides four electrons derived from the splitting of water to oxygen. The OEC passes through four oxidation states from the ground state S_0 to S_4 . Altogether, four electrons get released and the resulting electron gap gets balanced by the splitting of water (Kok *et al.*, 1970; Cox *et al.*, 2014; Suga *et al.*, 2015; Chrysin *et al.*, 2019).

Back at the stromal side of PSII, the quinone PQH_2 transfers the electrons to the luminal side of the Cyt b_6f complex (Kurusu *et al.*, 2003). Within the Cyt b_6f complex the PQH_2 is oxidised to plastoquinone by the Rieske iron-sulphur cluster (Rieske *et al.*, 1964; Veit *et al.*, 2016). Afterwards, the electrons get transferred via haem groups to the single electron carrier plastocyanin. During the electron transfer inside Cyt b_6f complex, two protons get pumped by the Q-cycle into the lumen that are later on used for ATP synthesis (Kurusu *et al.*, 2003; Stroebel *et al.*, 2003). Plastocyanin (in some cases cytochrome c_6) transfer the electron to PSI.

Upon the absorption of photons at the reaction centre of PSI (P_{700}) a second charge separation takes place, and one electron is released to phylloquinone resulting a chlorophyll radical $P_{700}\bullet$ ($Chl a$)₂^{*}. Plastocyanin reduces the ($Chl a$)₂^{*} and is oxidised itself. Finally, the electron gets transferred via three iron-sulphur clusters to the electron acceptor Ferredoxin

(Fd) located at the stromal side of the TM (Fromme *et al.*, 2001). During the last step, NADP⁺ is reduced to NADPH by Ferredoxin NADP Reductase (FNR) (Karplus and Bruns, 1994).

In addition, a proton gradient is formed in the lumen, which is used by the ATP-Synthase. The proton motive force causes a conformational change in the binding site of ADP and the free phosphate. Based on the conformational change ATP can be synthesised (Mitchell, 1966; Noji *et al.*, 1997).

Beside the described linear electron transport the cyclic electron flow increases the ATP amount but not the NADP⁺ reduction. During cyclic electron flow several mechanisms are discussed, thereby one possible mechanism in cyanobacteria is the transfer of excited electron from the PSI via Fd into the plastoquinone pool and Cyt *b₆f* back to PSI (Munekage *et al.*, 2004; Yeremenko *et al.*, 2005; Lea-Smith *et al.*, 2016). The role of the photosynthetic complex I, the NDH-complex, is under debate. Latest cryo-electron microscope studies suggest that Fd directly mediates the transfer between PSI and NDH-complex (Schuller *et al.*, 2019).

In order to absorb photons in a highly efficient way from sunlight, light harvesting complexes (LHC) in higher plants conduct the energy to the inner of the reaction centre (Liu *et al.*, 2004; Standfuss *et al.*, 2005). In contrast in cyanobacteria, phycobilisomes are associated with the TMs at the cytoplasmic side and transfer the absorbed light energy to PSI and PSII (Mullineaux, 1992; Arteni *et al.*, 2009). In order to adapt to the environmental conditions, phycobilisomes can move between PSII and PSI. These state transitions balance the ratio of absorbed photons at PSII and PSI (Mullineaux and Allen, 1990; Watanabe *et al.*, 2014; Ranjbar *et al.*, 2018).

1.2 Model organism *Synechocystis* sp. PCC 6803

Synechocystis sp. PCC 6803 (hereafter *Synechocystis*) from the Pasteur Culture Collection (PCC) in Paris is a unicellular gram-negative fresh water cyanobacteria, which was isolated in 1968 in Oakland California (Stanier *et al.*, 1971; Rippka and Herdman, 1992). In contrast to *Cyanothece* sp. or *Nostoc* sp., which are able to form heterocytes to fix nitrogen, *Synechocystis* is not able to fix nitrogen (Rippka *et al.*, 1979; Campbell *et al.*, 2007; Bandyopadhyay *et al.*, 2011).

The *Synechocystis* cell has a diameter of two µm and is surrounded by an outer membrane and the plasma membrane (Liberton *et al.*, 2006; Van De Meene *et al.*, 2006). Like in gram-negative bacteria a peptidoglycane layer is located between the outer membrane and plasma membrane. On top of the outer membrane a surface layer (S-Layer) encloses the cell (Trautner and Vermaas, 2013) (Figure 2).

Introduction

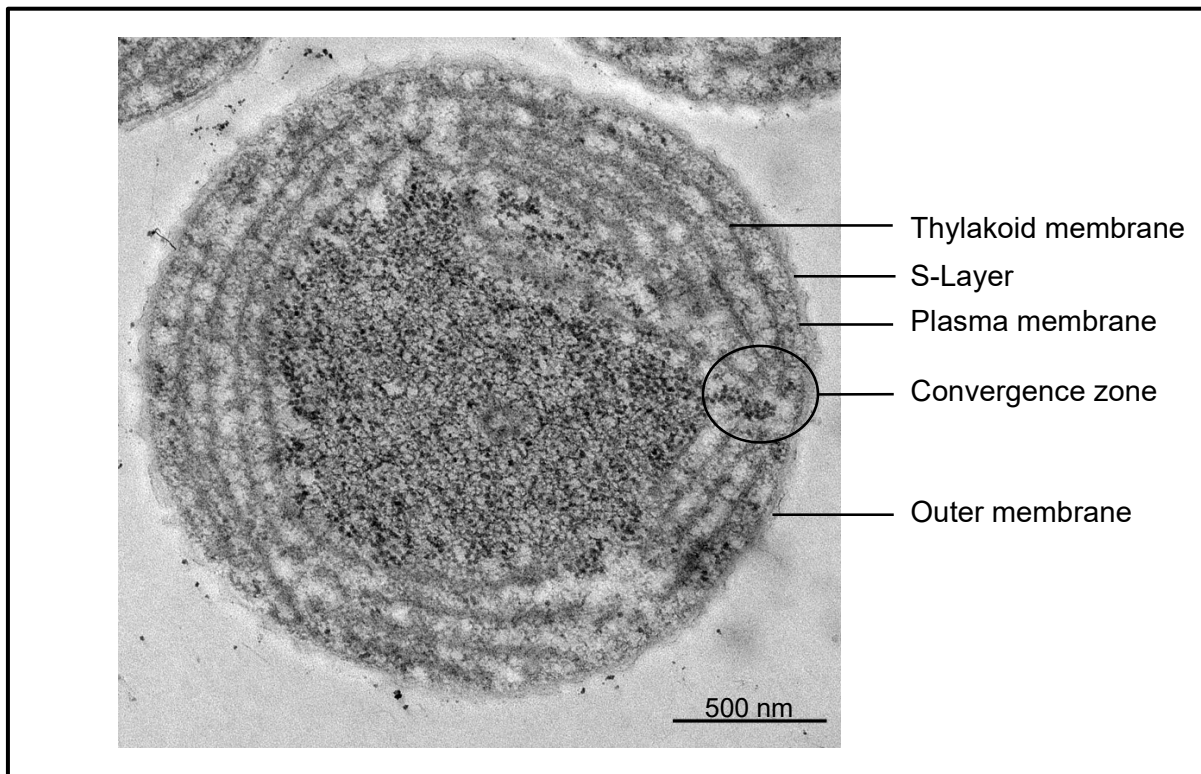


Figure 2: Electron microscope picture of *Synechocystis*. The cell is surrounded by surface layer (S-Layer), outer membrane and plasma membrane. The thylakoids are shaped towards the plasma membrane and form the convergence zone (Rast, unpublished data). Balk: 500 nm.

The genome of *Synechocystis* is completely sequenced and contains 3.57 mega base pairs (Mbp). It is organised in one chromosome and three small plasmids (pCA2.4, pCB2.4, PCC5.2) and four large plasmids (pSYSM, pSYSA, pSYSG and pSYSX) (Kaneko *et al.*, 2003). Recent studies reported that the genome of *Synechocystis* contains 218 copies during the motile phase (Griese *et al.*, 2011). As is the case with many other bacteria the transcriptome of *Synechocystis* is parted in transcriptomic units (Kopf *et al.*, 2014). Moreover, the genome can be manipulated easily with foreign DNA by homologous recombination (Kufryk *et al.*, 2002).

In order to fix CO₂ *Synechocystis* has special microcompartments containing Ribulose-1.5-bisphosphate carboxylase (RubisCO) termed carboxysomes (Kerfeld and Melnicki, 2016). Polyphosphate bodies are located close to the TM. These vesicles contain a high amount of phosphate, which is used for DNA synthesis (Seki *et al.*, 2014). Beside polyphosphate bodies and carboxysomes, the cytoplasm contains the TM, which is arranged in layers and located along the cell membrane (Liberton *et al.*, 2006; Van De Meene *et al.*, 2006; Van De Meene *et al.*, 2012; Rast *et al.*, 2019). The TM in *Synechocystis* is connected to a network structure in contrast to the grana stacks present in chloroplasts of higher plants. (Shimoni *et al.*, 2005; Van De Meene *et al.*, 2006; Rast *et al.*, 2019). The membranes are shaped towards the plasma membrane and form the biogenesis centres (Liberton *et al.*, 2006; Van De Meene *et al.*, 2006; Stengel *et al.*, 2012; Heinz *et al.*, 2016b; Rast *et al.*, 2019). In accordance with the

endosymbiont theory, cyanobacteria are the ancestors of chloroplasts, which are found in plants and algae (Falcon *et al.*, 2010).

Due to the short doubling time of ~8 h, the ability to grow both photo-autotrophically and heterotrophically in the presence of glucose, and the easy genomic manipulation, *Synechocystis* has become a model organism for photosynthesis research.

1.3 Cyanobacterial Photosynthetic complexes

Photosystems are supercomplexes containing several subunits that are localised in the TM (Fromme *et al.*, 2001; Umena *et al.*, 2011). The complexes absorb and funnel light energy to their reaction centre. Additionally, PSII splits water and provides the electrons and protons required for reduction of the energy carrier NADP and ADP (Lea-Smith *et al.*, 2016).

1.3.1 PSII

Monomeric PSII contains 20 subunits and has a size of 350 kilodalton (kDa) (Umena *et al.*, 2011). PSII can oligomerise to a dimer. Several crystal structures of cyanobacterial PSII are available with a resolution of 3.8-2.9 Ångström (Å) (Zouni *et al.*, 2001; Ferreira *et al.*, 2004; Loll *et al.*, 2005; Guskov *et al.*, 2009). Recent structure of the supercomplex from the thermophilic cyanobacteria *Thermosynechococcus vulcanus* provides the highest resolution of the supercomplex at 1.9 Å (Umena *et al.*, 2011). Besides 20 protein subunits, the complex is composed of more than 80 cofactors. These include 35 chlorophyll *a* molecules, two pheophytins and plastoquinones, 11 β-carotenoids, more than 20 lipids, two hemes, one non-heme iron, one bicarbonate, three carbonates and the OEC (Umena *et al.*, 2011) (Figure 3).

The central intrinsic subunits of PSII, D1 and D2 (PsbA, PsbD) bind the special chlorophyll pair in the reaction centre of PSII (P₆₈₀) and the electron carrier pheophytin. In particular the Q_B binding site and the Tyr_z residue are located in the D1 subunit whereas Q_A is located in the D2 subunit (Umena *et al.*, 2011). D1 undergoes a high turnover due to photo damaging (Vermaas *et al.*, 1995). Furthermore, D1 and D2 form together with cytochrome *b*₅₅₉ (Cyt *b*₅₅₉) and PsbI the reaction centre complex (RC) complex including the manganese cluster (Zheleva *et al.*, 1993; Vasil'ev *et al.*, 2001; Komenda *et al.*, 2004; Umena *et al.*, 2011). The Cyt *b*₅₅₉ is not directly involved in the electron transport chain in PSII, but it is supposed that it protects against photoinhibition as a heme binding protein PSII (Thompson and Brudvig, 1988; Barber and De Las Rivas, 1993; Chu and Chiu, 2015).

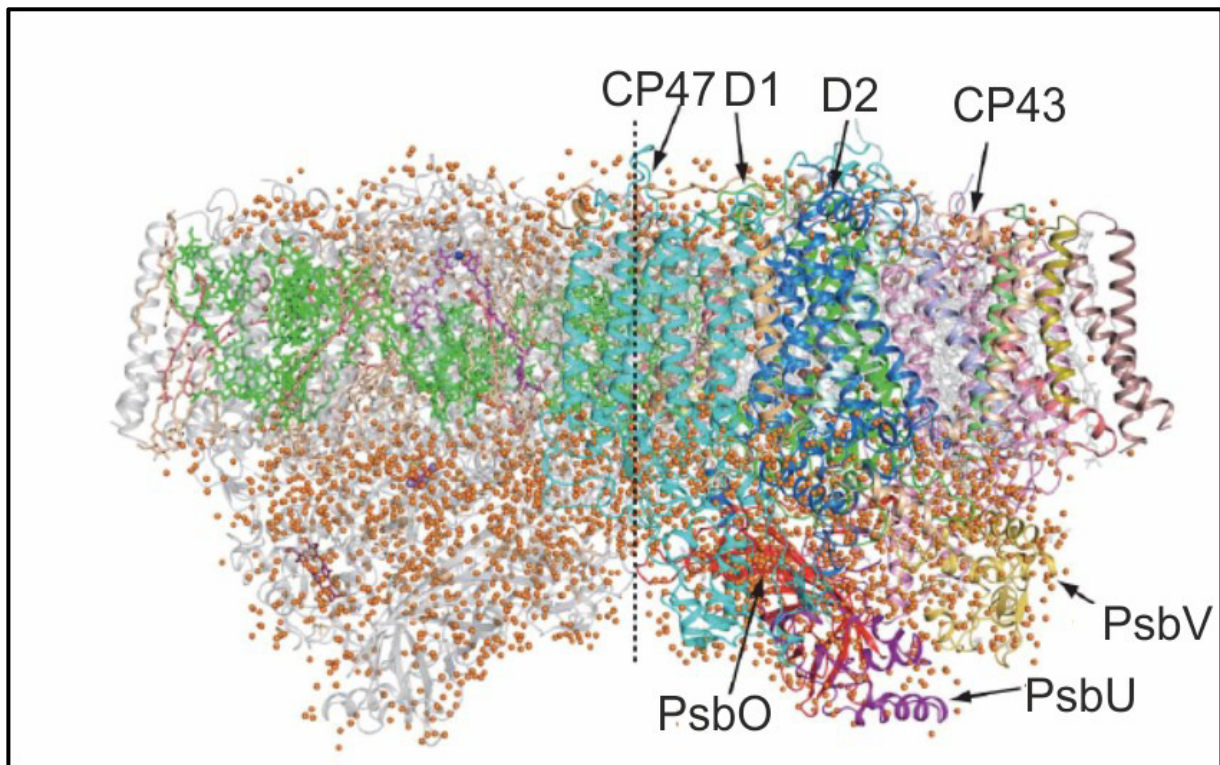


Figure 3: Crystal structure of dimeric PSII from the organism *Thermosynechococcus vulcanus* with a resolution of 1.9 Å. PSII subunits CP47, D1, D2, CP43, PsbO, PsbU and PsbV are marked by black arrows. Modified after Umena *et al.* (2011).

The RC-complex is flanked by the core antenna chlorophyll binding proteins CP43 and CP47 (PsbB, PsbC). The subunit CP43 binds 13 chlorophyll molecules whereas CP47 contains 16 molecules (Vasil'ev *et al.*, 2001).

The manganese ions are clustered with calcium and oxygen to Mn_4CaO_5 and form the OEC. Moreover, the OEC is surrounded in cyanobacteria by the extrinsic subunits PsbU, PsbV and PsbO and binds to the intrinsic subunits of PSII (Umena *et al.*, 2011). Higher plants like *Arabidopsis thaliana* have the extrinsic subunits PsbP and PsbQ instead of PsbU and PsbV in cyanobacteria (Shen and Inoue, 1993). Homologues of PsbP and PsbQ in cyanobacteria are called CyanoP and CyanoQ (Kashino *et al.*, 2002; Thornton *et al.*, 2004; Cormann *et al.*, 2014). CyanoP binds to the luminal site of inactive PSII, that lacks PsbO, PsbV and PsbU (Cormann *et al.*, 2014). The main role of the extrinsic subunits is to optimise the oxygen evolution at physiological calcium and chloride ion concentration as well as to protect the OEC from exogenous reductants (Murata and Miyao, 1985; Murray and Barber, 2006; Ifuku and Noguchi, 2016).

Some herbicides bind as a plastoquinone analogue to PSII and inhibit the linear electron transport chain. One well-studied inhibitor is the phenyl urea derivate 3-(3,4-Dichlorophenyl)-1,1-dimethylurea (DCMU) (Trebst, 1979). DCMU binds to the Q_B binding pocket and inhibits irreversibly the electron transport chain (Trebst, 1979).

1.3.2 PSI

The second charge separation happens at PSI, a multimeric protein complex. *In vivo* PSI is a trimer in cyanobacteria and the monomer has a size of 300 ± 20 kDa (Rögner *et al.*, 1990). To date, the crystal structure of PSI complex from the thermophilic cyanobacterium *Thermosynechococcus elongatus* is solved at a resolution of 2.5 Å (Jordan *et al.*, 2001). In addition, single particle cryo-electron microscopy image analysis has provided a PSI structure at a resolution of 3.3 Å from the cyanobacterium *Anabaena* sp. PCC 7120 (Kato *et al.*, 2019). Therein one monomer contains 12 subunits, 127 cofactors including 96 chlorophyll molecules, two phylloquinones, three iron-sulphur cluster (Fe_4S_4), 22 carotenoids, four lipids and one putative Ca^{2+} ion (Jordan *et al.*, 2001). Like PSII, the RC of PSI contains two chlorophyll *a* molecules, which absorbs at a wavelength maximum of 700 nm (Mullet *et al.*, 1980; Jordan *et al.*, 2001).

PSI contains nine protein subunits with transmembrane α -helices: PsaA, PsaB, PsaF, PsaI, PsaJ, PsaK, PsaK, PsaM and PsaX (Jordan *et al.*, 2001) (Figure 4). Moreover, the integral subunit PsaA and PsaB show a high homology to each other and form the central part of the PSI complex (Fish *et al.*, 1985; Mühlhoff *et al.*, 1993). Both subunits contain eleven transmembrane α -helices. The C-terminal regions of PsaA and PsaB coordinate the cofactor transport and have some structural and functional similarities to the subunits D1/D2 of PSII (Schubert *et al.*, 1998; Jordan *et al.*, 2001). Furthermore, both subunits bind the central chlorophyll pair P_{700} (Jordan *et al.*, 2001). In addition to binding the central chlorophyll pair, PsaA binds 40 chlorophyll molecules, whereas PsaB binds 39 (Jordan *et al.*, 2001). By comparison of PSI with PSII, more chlorophyll molecules are bound to PSI (Jordan *et al.*, 2001; Umena *et al.*, 2011). It is supposed that the hydrophobic side chains of PsaA and PsaB are involved in the interaction with plastocyanin (Sun *et al.*, 1999; Fromme *et al.*, 2001). However, the eukaryotic organism *Chlamydomonas reinhardtii* demonstrates that the aromatic side chains of PsaA and PsaB are essential for the recognition of plastocyanin (Sommer *et al.*, 2002; Sommer *et al.*, 2004).

The small intrinsic subunits PsaF, PsaI, PsaJ, PsaK, PsaK, PsaL PsaM and PsaX are located peripheral to the subunits PsaA and PsaB and stabilise the protein complex. The subunit PsaL and PsaI are required for trimerisation of PSI (Chitnis and Chitnis, 1993; Xu *et al.*, 1995). Beside the intrinsic subunits, PSI has three stromal subunits: PsaC, PsaD and PsaE.

iron-sulphur F_B (Fischer *et al.*, 1999; Jordan *et al.*, 2001). Moreover, a direct interaction between PsaD a ~18 kDa protein and Fd was demonstrated by cross-linking studies (Zanetti and Merati, 1987; Pandini *et al.*, 1999). In addition, PsaE promotes the anchoring of Fd and this small subunit plays a role in the cyclic electron flow (Rousseau *et al.*, 1993; Sonoike *et al.*, 1993; Yu *et al.*, 1993).

1.4 *De novo* Biogenesis of Photosystem II

The assembly of PSII is highly coordinated and separated in time and space. This regulated process starts with the insertion of the precursor form of D1 (pD1) into the plasma membrane. The insertion of pD1 is mediated by YidC insertase in interaction with the SecYEG translocase (Ossenbühl *et al.*, 2006; Gathmann *et al.*, 2008; Sachelaru *et al.*, 2013; Chidgey *et al.*, 2014). Chloroplast of higher plants contain the homolog of YidC named Albino3 (Spence *et al.*, 2004). The PSII assembly factor Ycf39, the chlorophyll synthase (ChlG) and the chlorophyll-binding one-helix proteins C and D (HliD), which belong to the high-light-inducible protein (Hlip) family, interact with pD1 and deliver chlorophyll to pD1 (Chidgey *et al.*, 2014; Knoppová *et al.*, 2014).

Afterwards, pD1 binds to the small PSII subunit PsbI and these form a subcomplex (Dobáková *et al.*, 2007). The PrtA protein binds manganese ions and delivers the manganese to pD1, which is required for the formation of the OEC (Klinkert *et al.*, 2004; Schottkowski *et al.*, 2009b). Thereby PrtA interacts with the C-terminal region of pD1 in a sub-compartment of TM so called the PrtA-defined membrane (PDM) (Klinkert *et al.*, 2004; Stengel *et al.*, 2012). Beside the interaction with pD1 PrtA forms with ORFs *slr1277* and *sll1679* a complex in the periplasm (Heinz *et al.* in preparation; (Schottkowski *et al.*, 2009b)). The secretin-like protein Slr1277 is part of the PilQ family and involved in the biosynthesis of type IV pili in *Synechocystis* (Yoshihara *et al.*, 2001; Nudleman and Kaiser, 2004; Gold *et al.*, 2015). Furthermore PilQ forms the pore in the type IV pili machinery in the outer membrane (Hospenthal *et al.*, 2017). PilQ builds a huge membrane-bound multimer. Two pools of PilQ can be experimentally distinguished, one being an insoluble membrane-bound complex and the other one in its non-assembled form in the periplasm, which is identified as PrtA interaction partner. The second identified interaction partner is Sll1679, which encodes for one of the three periplasmic Deg proteases: HhoA (Cheregi *et al.*, 2016). HhoA is part of an ATP-independent serine protease that is present in bacteria and eukaryotes (Clausen *et al.*, 2002; Huesgen *et al.*, 2007; Huesgen *et al.*, 2011).

During the next step, pD1 is processed by the C-terminal processing protease (CtpA) (Anbudurai *et al.*, 1994; Komenda *et al.*, 2007a). The intermediate form of D1 (iD1) binds to the subcomplex D2-Cyt *b*₅₅₉ and build up the RC (Nanba and Satoh, 1987; Komenda *et al.*, 2004). Thereby the PSII assembly factor Ycf48 stabilises pD1 and mediates the binding to D2-

Introduction

Cyt b_{559} (Komenda *et al.*, 2008; Rengstl *et al.*, 2013; Yu *et al.*, 2018). The early PSII assembly factor CyanoP interacts with C-terminus of D2 at the luminal side and forms with Ycf48 a complex to build the RC complex (Cormann *et al.*, 2014; Knoppová *et al.*, 2016; Yu *et al.*, 2018).

The later steps of PSII assembly occur in the TM (Rengstl *et al.*, 2011). In consequence the RC47 complex is formed by binding of the antenna protein CP47 and the low molecular-weight subunits PsbH, PsbL, PsbM, PsbT; PsbX and PsbY (Boehm *et al.*, 2012a). The assembly intermediate is stabilised by Psb28 and the PSII assembly factor SII0933 (Dobáková *et al.*, 2009; Armbruster *et al.*, 2010; Boehm *et al.*, 2012a). During the formation of RC47, iD1 is processed a second time to the mature form of D1 (mD1) by CtpA (Komenda *et al.*, 2004; Komenda *et al.*, 2007a; Komenda *et al.*, 2007b; Boehm *et al.*, 2012a). The PSII assembly factors SII0933 and Ycf48 are directly interacting with RC47 subcomplex (Rengstl *et al.*, 2013). In addition, a strong interaction has been shown between SII0933 and Ycf48 and the PSII assembly factor Slr0151 (Rast *et al.*, 2016). Following this, the low molecular subunits PsbK, PsbZ, Psb30 and the assembly factors SII0933 and Psb27 bind to CP43 (Komenda *et al.*, 2007b; Boehm *et al.*, 2011; Rengstl *et al.*, 2013). Afterwards, the CP43 module binds to RC47 to form the PSII-Psb27 intermediate (Komenda *et al.*, 2012). In addition, the subunit PsbJ at the luminal face has not been detected at the RC47 complex (Boehm *et al.*, 2012b).

Photoactivation of PSII takes place by reorganisation of manganese ions and the binding of calcium ions (Ananyev and Dismukes, 1997). This process is mediated by the PSII assembly factor Psb27 as well as CyanoP (Roose and Pakrasi, 2008; Cormann *et al.*, 2014). Psb27 indicates a direct interaction with PSII at the site that will bind PsbO later on (Cormann *et al.*, 2009; Cormann *et al.*, 2014). Finally, the active PSII monomer is formed by detachment of Psb27 (Roose and Pakrasi, 2008). In addition, the extrinsic subunits PsbO, PsbU and PsbV bind to the complex and stabilise the manganese cluster (Nowaczyk *et al.*, 2006; Umena *et al.*, 2011). This suggests that these late assembly step is under the assistance of the assembly factor CyanoQ, the cyanobacterial homologue to PsbQ of plants (Roose *et al.*, 2007; Liu *et al.*, 2015). The PSII dimerisation is facilitated by the low molecular weight subunits PsbI and PsbM (Kawakami *et al.*, 2011). In order to optimise the energy transfer the attachment of the phycobilisomes takes place (Acuña *et al.*, 2018) (Figure 5). This suggests that the extrinsic subunit PsbU stabilises electron transport during the assembly of phycobilisomes and PSII (Veerman *et al.*, 2005).

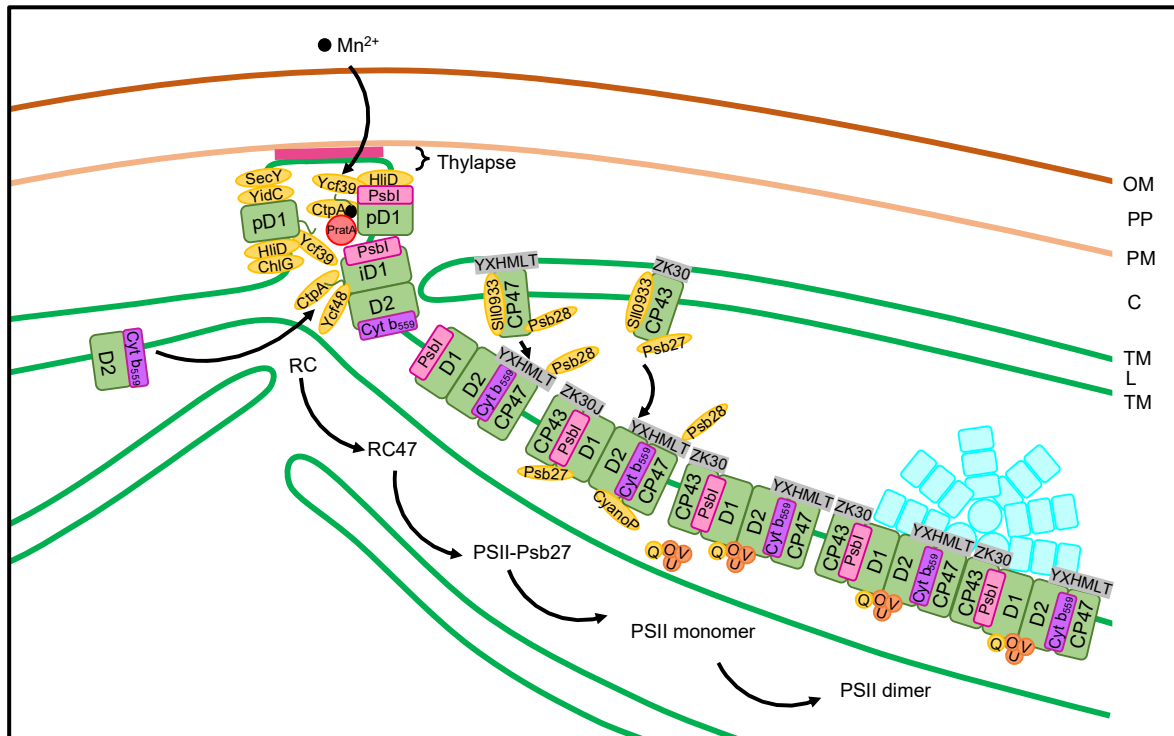


Figure 5: PSII biogenesis in *Synechocystis*. The precursor form of D1 (pD1) gets preloaded with Mn by PratA. Afterwards pD1 is processed by the C-terminal processing protease (CtpA). The resulting intermediate form of D1 (iD1) binds to the subcomplex D2-Cyt b_{559} and build up the reaction centre (RC) complex. The RC47 complex is formed by binding of the antenna protein CP47 and the low mass subunits PsbH, PsbL, PsbM, PsbT; PsbX and PsbY. Following this the CP43 module is attached to the RC47 complex and form the PSII-Psb27 subcomplex. Completion of PSII assembly by dimerisation of the PSII monomer including the extrinsic subunits PsbO, PsbU, PsbV (orange circle) and phycobilisomes. The intrinsic subunits D1, D2 and the chlorophyll binding proteins CP43, CP47 are green, PsbI pink, Cyt b_{559} purple, low mass subunits in grey, extrinsic subunits orange, phycobilisomes turquoise, transiently binding PSII assembly factors in yellow and manganese binding factor PratA in a red circle, outer membrane (OM), periplasm (PP), plasma membrane (PM), cytoplasm (C), thylakoid membrane (TM), lumen (L).

1.5 PSII repair

The PSII subunit D1 is *in vivo* under a constant turnover because of photo damage (Edelman and Mattoo, 2008). During the repair cycle damaged D1 is replaced by a newly synthesised D1 copy (Ohad *et al.*, 1984). Under high light treatment D1 has a half time of approximately 20 min (Tyystjärvi *et al.*, 1994). Besides high light intensities, also reactive oxygen species (ROS) such as hydrogen peroxide and other oxygen radicals, which are byproducts of photosynthesis, harm D1 (Apel and Hirt, 2004; Kale *et al.*, 2017). High light conditions are accompanied by the rise of ROS, especially when phycobilisomes, or in case of plants light harvesting complexes, absorb more photons than PSII can channel into the electron transport chain. Damage of the PSII complex caused by high light leads to irreversible photoinhibition. At the acceptor site of PSII, photoinhibition causes an over-reduction of the PQ-Pool, while photoinhibition at the donor site occurs when the oxidation of water does not correspondent to the rate of P_{680} oxidation (Pospíšil, 2009; Nixon *et al.*, 2010). The resulting

Introduction

P_{680} radicals can damage amino acid residues fairly close to it based on its oxidative potential (Nixon *et al.*, 2010). Also, under low light conditions, damage of D1 occurs by electron back flow from Q_B to the OEC (Keren *et al.*, 1997). In addition, it is discussed if the manganese cluster itself is the first step of photoinhibition (Hakala *et al.*, 2005; Hakala *et al.*, 2006).

It has been demonstrated that FtsH and Deg proteases participate in the degradation of D1 as a response to light stress. The cyanobacteria *Synechocystis* contains three Deg proteases and four FtsH proteases (Nixon *et al.*, 2005). *In vitro* studies show that the degradation of photo-damaged D1 is a two-step mechanism initiated by the cleavage by Deg protease of the stromal loop that connects transmembrane helices of D1 and, afterwards, degradation of the N-terminal D1 fragment by FtsH (Spetea *et al.*, 1999; Haußühl *et al.*, 2001; Nixon *et al.*, 2005). The FtsH2 and FtsH3 form a heterocomplex, which is involved in D1 degradation (Boehm *et al.*, 2012b). The proteases FtsH2 and FtsH3 are localised in TM at specialised repair zones (Komenda *et al.*, 2006; Sacharz *et al.*, 2015).

Similar to the *de novo* biogenesis of PSII, newly synthesised pD1 is integrated into the membrane via the same machinery. During PSII assembly, pD1 is stabilised by the biogenesis factor Ycf48 (Komenda *et al.*, 2008). In contrast during PSII repair, pD1 is enclosed by CP43 and the CP43 subunit and this complex is stabilised by Psb27 and Sll0933 (Nowaczyk *et al.*, 2006; Grasse *et al.*, 2011; Komenda *et al.*, 2012; Rengstl *et al.*, 2013). In addition, yeast two hybrid assays could show a direct interaction between Slr0151 with CP43 and D1 (Yang *et al.*, 2014). The interaction studies and a reduced growth of the knockout strain during high light conditions allows the conclusion to be drawn that Slr0151 plays a role in PSII repair cycle (Yang *et al.*, 2014; Rast *et al.*, 2016). Similar to PSII assembly, during PSII repair the processing of the integrated pD1 is performed by CtpA (Komenda *et al.*, 2007a).

It is assumed that the chlorophyll molecules that are released during the repair cycle of PSII are recycled by the Hlip protein family. This protein family is sometimes designated as small chlorophyll *a/b* binding protein (CAB)-like proteins (SCPs) and they transport the chlorophyll molecules to pD1 by YCF39 (Dolganov *et al.*, 1995; Vavilin *et al.*, 2007; Knoppová *et al.*, 2014) (Figure 6).

Introduction

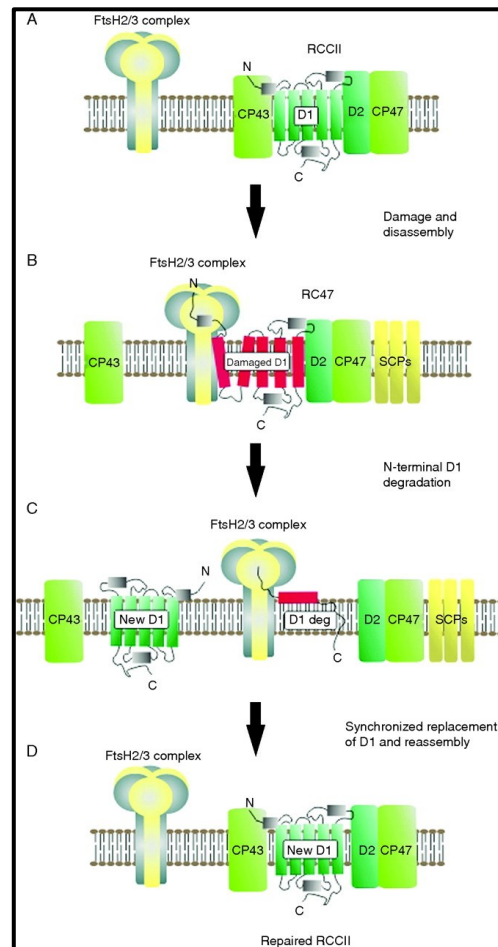


Figure 6: Replacement of damaged D1 during PSII repair. Damaged D1 is N-terminal degraded by the FtsH2/3 complex. The insertion of newly synthesised D1 into the TM is synchronised with the attachment of CP43 and the CP47 module. It is supposed that the chlorophyll molecules are recycled by SCP/Hlip protein family (Nixon *et al.*, 2010).

1.6 Thylakoid membranes in *Synechocystis*

Photosynthetic electron transport, *de novo* biogenesis and repair of PSII repair take place at TM. The TM forms in chloroplasts grana stacks and contains more than 70% proteins (Kirchhoff *et al.*, 2002). Based on this high protein amount a matrix of lipids is necessary in bioenergetic membranes to stabilise the photosynthetic protein complexes (Boudière *et al.*, 2014).

The glycerol lipids in the photosynthetic membrane are conserved during the evolution from cyanobacteria to chloroplast (Boudière *et al.*, 2014). However, the thylakoids contain four main lipid types, the polar lipids monogalactosyldiacylglycerol (MGDG) and digalactosyldiacylglycerol (DGDG), and the lipids with a negatively charged head group sulfoquinovosyldiacylglycerol (SQDG) and phosphatidylglycerol (PG) (Allen and Good, 1971). Based on the distribution of thylakoids in cyanobacteria, plants and algae, MGDG (48% in spinach) are the most abundant lipids on earth (Gounaris *et al.*, 1983). The galactolipids MGDG and DGDG with a polar head group (> 70% in spinach) form the most abundant group of lipids in thylakoids (Gounaris *et al.*, 1983). The small head group of MGDG is able to form

Introduction

hexagonal structures (Lee, 2000; Bottier *et al.*, 2007). The structure of the bilayer is determined by the head group (Gounaris *et al.*, 1983). It is supposed that DGDG forms a stable bilayer in contrast to MGDG, which reinforces the curvature of thylakoids (Gounaris *et al.*, 1983; Jarvis *et al.*, 2000; Rast *et al.*, 2015). This theory is supported by a higher ratio of MGDG/DGDG in grana stacks compared to stroma lamellae in spinach chloroplasts (Gounaris *et al.*, 1983). In addition, DGDG is required for the stabilisation of the OEC (Sakurai *et al.*, 2007). Moreover, it could be shown that the negatively charged PG is an essential for the photoautotrophic growth in *Synechocystis* (Hagio *et al.*, 2000; Sato *et al.*, 2000).

The sulphur containing lipid SQDG can be replaced by PG during phosphate limitation (Benning *et al.*, 1993; Boudière *et al.*, 2014).

In addition to the influence of lipids on the shape of membranes, membrane binding proteins can be involved in the shape of TM. For example, the vesicle inducing protein in plastids 1 (Vipp1) is suggested to be essential for membrane formation in cyanobacteria, algae and plants (Kroll *et al.*, 2001; Westphal *et al.*, 2001; Göhre *et al.*, 2006; Rütgers and Schroda, 2013; Siebenaller *et al.*, 2019). Cryo-electron microscopy studies demonstrate an oligomeric structure of Vipp1 that is organised in rings and rods that engulf liposomal membranes (Siebenaller *et al.*, 2019; Theis *et al.*, 2019) However, localisation studies with GFP-tagged Vipp1 show some of the signals at the cell periphery (Bryan *et al.*, 2014).

Beside all the predictions and possible functions of Vipp1, an important shaping protein factor of cyanobacterial membranes is CurT, which homologous to the grana-shaping family CURVATURE THYLAKOID1 (CURT1) from *Arabidopsis thaliana* (Armbruster *et al.*, 2013; Heinz *et al.*, 2016b; Pribil *et al.*, 2018). In *A. thaliana* the CURT1 family contains four members named CURT1A-D (Armbruster *et al.*, 2013; Pribil *et al.*, 2018). Moreover, CurT is a membrane protein containing two TMD and one N-terminal amphipathic α -helix (Armbruster *et al.*, 2013; Heinz *et al.*, 2016b). Immunogold labelling of CURT1 in *A. thaliana* localises the protein at the grana stack margins (Armbruster *et al.*, 2013). Overexpression studies in *A. thaliana* of the CURT1A protein results in an increase and intensification of TM curvature in chloroplasts (Pribil *et al.*, 2018).

In contrast, in *Synechocystis* fluorescence localisation studies with GFP tagged CurT demonstrate a tubular network pattern at the cellular periphery with a local concentration at convergence zones (Heinz *et al.*, 2016b). Sucrose density gradients allow a more detailed localisation of CurT in the in PDM, TM and in the plasma membrane fraction (Heinz *et al.*, 2016b). *In vitro* assays demonstrate, that CurT can build up oligomers and tubulate liposomes (Armbruster *et al.*, 2013; Heinz *et al.*, 2016b). Interestingly, in absence of CurT, ultrastructural analysis reveals a loss of biogenesis centres and unordered thylakoids (Heinz *et al.*, 2016b). The loss of CurT in *Synechocystis* has a dramatic effect on the photosynthetic performance (Heinz *et al.*, 2016b).

Introduction

Moreover, cryo-electron micrographs of *Synechocystis* allow a detailed view of the convergence zone (Rast *et al.*, 2019) (Figure 7). The tomograms of these biogenic regions show a high curvature of thylakoids at the convergence zone. The convergence tubule is shaped towards the contact site with the plasma membrane. The specialised zone in the thylakoid that forms the contact site called the thylapse (Rast *et al.*, 2019). The proposed biogenic function of the convergence zones is supported by the absence of phycobilisomes as marker (Rast *et al.*, 2019). So far, the exact function of the thylapse is unclear. It is surmised that these structures play a role in the manganese ion uptake (Heinz *et al.*, 2016b; Rast *et al.*, 2019).

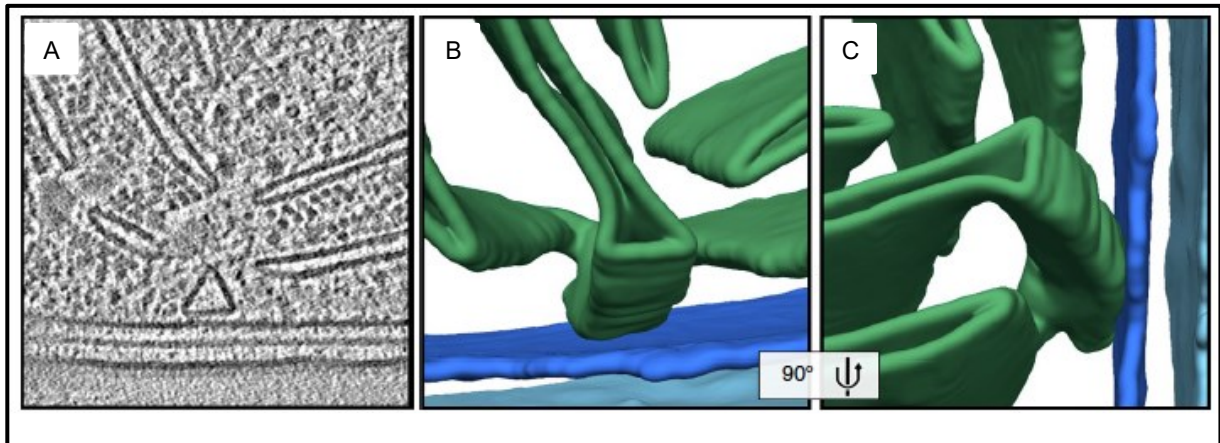


Figure 7: Convergence zones in *Synechocystis* (Rast *et al.*, 2019). (A) Cryo-electron tomogram of convergence zones in the cyanobacterium *Synechocystis*. (B and C) Related 3-D segmentation. Convergence tubule (green) come close to the plasma membrane (dark blue), outer membrane (light blue).

1.7 Aims of this work

Since the first PSII assembly factors were found the PSII assembly machinery is under ongoing discussion. Over the years many PSII assembly factors were found by various research groups. The first steps of the highly coordinated process that is separated in time and space takes place at the convergence zones. Recent studies performed by Rast *et al.* 2019 have demonstrated a new structuring element of the convergence zones - the thylapse. So far, the function of this structure is unclear.

The data in this work represents a new method for identifying putative candidates involved in structuring of the convergence zones and the assembly of PSII. The genetic and proteomic screens that were performed are based on the two main players of the convergence zones:

- i) Curt a, a well characterised structural protein and
- ii) PratA, the manganese binding protein.

Besides looking for new candidates, one part of this work was focused on PratA that forms a 200 kDa complex in the periplasm. Thereby, possible interactions of the complex have been quantitative analysed that offer a new aspect of the primary PSII assembly steps.

2. MATERIAL AND METHODS

2.1 Materials

Table 1: Chemicals used.

Chemical	Company
2,3-Dihydroxybutan-1,4-dithiol, 1,4-Dithioerythritol (DTT)	AppliChem GmbH (Darmstadt, Germany)
3-(3,4-Dichlorophenyl)-1,1-dimethylurea (DCMU)	Sigma-Aldrich (St. Louis, USA)
³⁵ S-Methionin	Hartmann Analytik GmbH (Braunschweig, Germany)
4-(2-Hydroxyethyl)piperazine-1-ethanesulfonic acid (HEPES)	Carl Roth GmbH (Karlsruhe, Germany)
6-aminohexanoic acid	Merck KGaA (Darmstadt, Germany)
Acetic acid (99-100%)	VWR (Radnor, USA)
Acetone	J.T. Baker (Deventer, Netherlands)
Acetonitrile	Merck KGaA (Darmstadt, Germany)
Acrylamid/Bis-solution, 37.5:1 30% (w/v) (Acrylamide)	Serva Electrophoresis GmbH, (Heidelberg, Germany)
Agar-Agar Kobe I	Carl Roth GmbH (Karlsruhe, Germany)
Agarose	Genaxxon bioscience (Ulm, Germany)
Ammonium ferric citrate	Sigma-Aldrich (St. Louis, USA)
Ammonium hydrogen bicarbonate (NH ₄ CO ₃)	Carl Roth GmbH (Karlsruhe, Germany)
Ammonium persulfate (APS)	Carl Roth GmbH (Karlsruhe, Germany)
Ampicillin sodiumsolt	AppliChem GmbH (Darmstadt, Germany)
Amylose Resin	New England Biolabs (Ipswich, USA)
Bis(2-hydroxyethyl)-amino-tris(hydroxymethyl)-methane (Bis-tris)	Carl Roth GmbH (Karlsruhe, Germany)
Boric acid	Carl Roth GmbH (Karlsruhe, Germany)
Bovine serum albumin (BSA)	Sigma-Aldrich (St. Louis, USA)
Bromophenol blue	AppliChem GmbH (Darmstadt, Germany)
Calbiochem FluorSave™ Reagent	Merck KGaA (Darmstadt, Germany)
Calcium dichloride dihydrate (CaCl ₂)	Carl Roth GmbH (Karlsruhe, Germany)
Cetyltrimethylammoniumbromide (CTAB)	Carl Roth GmbH (Karlsruhe, Germany)

Material and Methods

Chemical	Company
Chloramphenicol	Carl Roth GmbH (Karlsruhe, Germany)
Citric acid	Sigma-Aldrich (St. Louis, USA)
Cobalt(II) nitrate $\text{Co}(\text{NO}_3)_2$	Carl Roth GmbH (Karlsruhe, Germany)
Complete (Mini) EDTA-free	Roche AG (Basel, Switzerland)
Coomassie Brilliant Blue R-250	AppliChem GmbH (Darmstadt, Germany)
Copper(II) sulfate CuSO_4	Sigma-Aldrich (St. Louis, USA)
D(+)-Glucose monohydrate (Glucose)	Carl Roth GmbH (Karlsruhe, Germany)
D(+)-Maltose monohydrate (Maltose)	Carl Roth GmbH (Karlsruhe, Germany)
D(+)-Sucrose (Sucrose)	Carl Roth GmbH (Karlsruhe, Germany)
Deoxyribonucleoside triphosphate (dNTPs)	Genaxxon bioscience (Ulm, Germany)
Dimethyl pimelidate dihydrochloride	Sigma-Aldrich (St. Louis, USA)
Dimethyl sulfoxide (DMSO)	Carl Roth GmbH (Karlsruhe, Germany)
Dipotassium hydrogen phosphate (K_2HPO_4)	Carl Roth GmbH (Karlsruhe, Germany)
Disodium hydrogen phosphate dihydrate (Na_2HPO_4)	Carl Roth GmbH (Karlsruhe, Germany)
Ethanol (99.97%)	VWR (Radnor, USA)
Ethanolamine	Sigma-Aldrich (St. Louis, USA)
Ethylenediaminetetraacetate disodium salt dihydrate (Na-EDTA)	Carl Roth GmbH (Karlsruhe, Germany)
Formaldehyde	Carl Roth GmbH (Karlsruhe, Germany)
Glacial acetic acid	Carl Roth GmbH (Karlsruhe, Germany)
Glycerol	Carl Roth GmbH (Karlsruhe, Germany)
Glycin	Carl Roth GmbH (Karlsruhe, Germany)
Hydrochloric acid 37% (HCl)	VWR (Radnor, USA)
Hydrogen peroxide (H_2O_2)	AppliChem GmbH (Darmstadt, Germany)
Imidazol	Carl Roth GmbH (Karlsruhe, Germany)
Iron(II) sulfate heptahydrate	Merck KGaA (Darmstadt, Germany)
Isopropyl- β -D-thiogalactopyranosid (ITPG)	Carl Roth GmbH (Karlsruhe, Germany)
Kanamycin sulfate	Carl Roth GmbH (Karlsruhe, Germany)
Luminol	Sigma-Aldrich (St. Louis, USA)
Magnesium dichloride hexahydrate (MgCl_2)	Carl Roth GmbH (Karlsruhe, Germany)
Magnesium sulfate heptahydrate (MgSO_4)	Sigma-Aldrich (St. Louis, USA)
Mangan(II) dichloride dihydrate (MnCl_2)	Merck KGaA (Darmstadt, Germany)

Material and Methods

Chemical	Company
Methanol 99.9%	VWR (Radnor, USA)
Midorri green	NIPPON Genetics (Düren, Germany)
Milk powder	Carl Roth GmbH (Karlsruhe, Germany)
<i>N,N,N',N'</i> -tetramethylethane-1,2-diamine (TEMED)	Carl Roth GmbH (Karlsruhe, Germany)
<i>n</i> -Dodecyl- β -D-Maltoside (β -DM)	Carl Roth GmbH (Karlsruhe, Germany)
Nonidet P-40 (NP40)	Sigma-Aldrich (St. Louis, USA)
Osmium(IV) oxide (OsO ₄)	Science Services GmbH (München, Germany)
<i>p</i> -Cumaric acid	Sigma-Aldrich (St. Louis, USA)
Peptone from casein tryptical digest	Carl Roth GmbH (Karlsruhe, Germany)
Phenylmethylsulfonyl fluoride (PMSF)	Carl Roth GmbH (Karlsruhe, Germany)
Ponceau S	AppliChem GmbH (Darmstadt, Germany)
Potassium acetate (K-acetate)	Carl Roth GmbH (Karlsruhe, Germany)
Potassium chloride (KCl)	J.T. Baker (Deventer, Netherlands)
Potassium dihydrogen phosphate (KH ₂ PO ₄)	Carl Roth GmbH (Karlsruhe, Germany)
Protein A Agarose Beads	Roche AG (Basel, Switzerland)
Protino [®] Ni-NTA Agarose	Machery-Nagel GmbH (Düren, Germany)
ROTI [®] Load 2x non reducing	Carl Roth GmbH (Karlsruhe, Germany)
ROTI [®] Load, 4x reducing	Carl Roth GmbH (Karlsruhe, Germany)
ROTI [®] Phenol/ Chloroform/ Isoamylalkohol	Carl Roth GmbH (Karlsruhe, Germany)
RotiQuant	Carl Roth GmbH (Karlsruhe, Germany)
Rubidium chloride (RbCl)	Carl Roth GmbH (Karlsruhe, Germany)
Silver nitrate (AgNO ₃)	Carl Roth GmbH (Karlsruhe, Germany)
Sodium carbonate (Na ₂ CO ₃)	Carl Roth GmbH (Karlsruhe, Germany)
Sodium dodecyl sulfate (SDS)	Carl Roth GmbH (Karlsruhe, Germany)
Sodium hydroxide (NaOH)	Carl Roth GmbH (Karlsruhe, Germany)
Sodium molybdate dehydrate (Na ₂ MoO ₄)	AppliChem GmbH (Darmstadt, Germany)
Sodium nitrate (NaNO ₃)	Carl Roth GmbH (Karlsruhe, Germany)
Sodium thiosulfate pentahydrate (Na ₂ S ₂ O ₃)	Carl Roth GmbH (Karlsruhe, Germany)
Sodiumazid	Merck KGaA (Darmstadt, Germany)
Sodiumchloride (NaCl)	Carl Roth GmbH (Karlsruhe, Germany)
β -Mercaptoethanol	Carl Roth GmbH (Karlsruhe, Germany)
Tricine	Carl Roth GmbH (Karlsruhe, Germany)

Material and Methods

Chemical	Company
Triethanolamine	Sigma-Aldrich (St. Louis, USA)
Tris(hydroxymethyl)aminomethane (Tris)	Carl Roth GmbH (Karlsruhe, Germany)
Triton® X-100	Carl Roth GmbH (Karlsruhe, Germany)
Tween-20	Carl Roth GmbH (Karlsruhe, Germany)
Uranyl acetate	Science Services GmbH (München, Germany)
Urea	Carl Roth GmbH (Karlsruhe, Germany)
Yeast extract	Carl Roth GmbH (Karlsruhe, Germany)
Zinc sulfate heptahydrate (ZnSO ₄)	Carl Roth GmbH (Karlsruhe, Germany)

Kits and consumables are used in this study listed in Table 2.

Table 2: Kits and consumables used in this study.

Kits	Company
CloneJET PCR Cloning Kit	ThermoFisher Scientific (Waltham, USA)
Monoilith Protein Labeling Kit RED NHS (Amine Reaction)	NanoTemper Technologies GmbH (Munich, Germany)
Monolith NT.115 Premium Capillaries	NanoTemper Technologies GmbH (Munich, Germany)
NucleoBond Xtra Midi kit for transfection-grade plasmid DNA	Machery-Nagel GmbH (Düren, Germany)
NucleoSpin Gel and PCR Clean-up	Machery-Nagel GmbH (Düren, Germany)

Enzymes that are used in this work listed in Table 3.

Table 3: Enzymes used in this work.

Enzyme	Company
RQ1 RNase-Free DNase	Promega (Fitchburg, USA)
RNase A	Genaxxon bioscience (Ulm, Germany)
FastDigest <i>EcoRI</i>	ThermoFisher Scientific (Waltham, USA)
FastDigest <i>BamHI</i>	ThermoFisher Scientific (Waltham, USA)
Lysozym	Carl Roth GmbH (Karlsruhe, Germany)
FastDigest <i>XbaI</i>	ThermoFisher Scientific (Waltham, USA)
FastDigest <i>SaI</i>	ThermoFisher Scientific (Waltham, USA)
FastDigest <i>XhoI</i>	ThermoFisher Scientific (Waltham, USA)
FastDigest <i>PstI</i>	ThermoFisher Scientific (Waltham, USA)
FastDigest <i>BamHI</i>	ThermoFisher Scientific (Waltham, USA)

Material and Methods

Enzyme	Company
FastDigest <i>EcoRI</i>	ThermoFisher Scientific (Waltham, USA)
FastDigest <i>SmaI</i>	ThermoFisher Scientific (Waltham, USA)
FastDigest <i>MunI</i>	ThermoFisher Scientific (Waltham, USA)
T4 DNA Ligase (1 U/ μ l)	ThermoFisher Scientific (Waltham, USA)
Q5 High fidelity DNA Polymerase	New England Biolabs (Ipswich, USA)

Oligos used in this study are listed in Table 4. All oligos were purchased from Sigma-Aldrich (St. Louis, USA).

Material and Methods

Table 4: Oligos used for cloning.

Oligo name	Sequence (5'-3')
fwd-fraH-seg	TTGCCCAGAAAAATCCTTCC
rev-fraH-seg	GTTGATTGTAATAGCGGAGC
fwd-cyt _M -seg	ATCCAATACCGATGCCA
rev-cyt _M -seg	AAGCGGCTACCAACCAAA
fwd-hik43-seg	TTTTGTTGCTCACCCGCC
rev-hik43-seg	GTCCATCCCTAGCCTGTT
fwd-ancMa	GGTAAATGTGGATGCCAT
rev-ancMa	AAGTCGACCTAGCTAGCCCTCAAAC
fwd-ancMb	AAGGATCCGCCCATTGCCGCCAGG
rev-ancMb	AATCTAGAATTTCTGAGCCGCCGCC
fwd-ancM-seg	AAATTCCAAGCTAGCACC
rev-ancM-seg	CCCATCTAAACCCAAAAATTCC
fwd-ancM ^{164HisSTOP}	AAGAGCTCCAGGTCCTGGGATTGTTGG
rev-ancM ^{164HisSTOP}	AAGAGCTCCTAATGATGGTGGTGGTGGTGGTGGCAGCCGGAGTATGG
fwd-curT-seg	TAGTACCTGGTCTTCCATGGCGT
rev-curT-seg	CTTTCGGCCTTAGCTAAATAGGCTTC
fwd-slr2071a	GGAGTTAGTGAACAGTTG
rev-slr2071a	AAAGTCGACAAAGAATTCAAAGGATCCCTTGGTAAATACTTCCGC
fwd-slr2071b	AAAGGATCCGATCACCCCAAACCTGAAGACT
rev-slr2071b	AAAGTCGACCACCAAGGAGTGAGGGAA
fwd-slr2071-seg	CCCCAGTAGTTCCCATTT
rev-slr2071-seg	GCCATGACCCAGAGATTT
fwd-MBP-AncM	AAAGGATCCGTGCTAAATGTCCGGAG
rev-MBP-AncM	AAACTGCAGCTAGCTAGCCCTCAAAC
fwd-HisCP47	AAGGATCCAATGCCACCACCCCATC
rev-HisCP47	AACTGCAGTTAGGGACTGGTGCGBAATACAC
fwd-MBP-PilQ	TTGGATCCGAAACGGTTTCCCAGTCAAAT
rev-MBP-PilQ	TTCTGCAGCTATGGCTGAGCCTGAACG
fwd-His-PratA	GATCGGATCCAGGCAGTTCAATGAGCTACTG
rev-His-PratA	GATCGTGCAGCTGGTAAAGTTTT TTCGCTTC

Gene-block fragments used for gene disruption in *Synechocystis* were ordered from Integrated DNA Technology (IDT) (Coraville, USA).

Material and Methods

Table 5: Synthetic gene-block fragments.

G-block	DNA Sequence (5'→ 3')
<i>G-fraH</i>	GGTCTGGTCTTGCCATCGCCCCGCCATAATACGCAGATAATTACCCAAGC TTTGTTCCAGTTGTTGATGGGAAAACACCAGGCTAGGGGAGTCGGGAGC CGTCGTTACCGTCGGGAGAGTTAGGGATAATCGGACAAAGTTTCCCTGG GGGACTAATTGCCACTCAGGATGGGGTGTGTCGTCACTCATCAAAAAAAT TTAGAATTTTGCCGTAGGATCGCCCTTACCTTAGCACTTCACTTTCCCGG ACCGTCCTCCTCCCAGGGGGTCAATTCGAGCTGGGGTGGAGATTTTTTGC CCTGGGGCCGGGAGGGTTAGGAAAGACAAATTTTTTCGCTACGATTGAAGA GAATCCTGCCATACTCCGCTGTGGTATTTAACATTAATCCCTACATTATTT GAATCAAAAAAGGATCCTCCCAGGCAACCGTCATTTACTGCGTCCCGGC GATCGCCTTGCTTTGGGCAAAGGGGATTTGGTCACATTTATATTTTCAGTTG CATTAGGTTGCCCCCACTTTGCTCAGGAATTAATCCACCATTGAATATT GAGATCCCCTAGGCGCATGGAAATTCCCGTCCGCTATCAACCCCGCCTTT TAACTCCGGAGGAAAGGGCAGGTTATCTAGATTGGTCTTTGGATTTTTTTA CCGACGATCGCCTATTGCAAATTCCTACATTGATTTGACGTTGCAATTGG ATGTGACCAATGCCTATGGAGTTTACCAACAACAAAAGGACAGCCCAGGC AGTTTTTTTTGCTTTTTTGGCTCTGGCATTGGATGCAATGTTTGCAAACCATT GGGAATTCGGCTCCGCTATTACAATCAACAATGGTATGTGTTGGATAATC CGCCGGCCATG
<i>G-cyt_M</i>	CCCTAGGTTTAGACGGTCTTTTCCTATTAGCCAATGATCCCAATACCGATG CCATTGCCGCCGGGGTAACGGTGTGGAGACCCAATCCTTCAGCGATGG GCCTAGTTTAGTGGCAGCCCTAAAACTACCCTCCAACCAGGCGATCGCC TCCTGTTTAAAGCATCCAATTCGGTCTAGGGGCTGTGGTCAGTCAG TTGTTGGCAGAAAATCCCCTTCGGTTTAAAACGGCAAGGCTTGAGTCAG TAAAAATGGGGTTAATCTCACTCCAGCGGGATCAATCGAGATCAATAGG TGTGGGGTTGGTTGGCAGTGGCATCCAACAAATGGCCTAAAACCAGATG GTTAAGAACATGGCTAAAACGTCTATCCAAACCAATCTGGCCTTATCCCT GGATCCAAAAAAGAATTCGGGTTAAGAACGATTGGTCAAGGTGGCCAGAA CCACCACTCAGAACTTAATCTAACTTAATCTATTGTATTGATGCCGGGCA TTCTGTCTTTGCTCAGTCCCAGATTGAAGTCCGGATTAACCCTGTTGACA AACTAAAACCTCCCCGATATCGATACCCAGAATTTTCCTAGGTCCGGGGG GGAGCATTGACAAAAATCTATCCAGCTCGGCCCAATGGATCAGCAAGGG CCCGCCGGCTTATAGGGGAGCAACTTGCACTTCCACCGTAGCGATGACTT CGGGGTGCAGTTTGATTTGGGTTGGTAAAACCAGTTTTGTGGATATCCG

Material and Methods

G-block	DNA Sequence (5' -> 3')
	GCAGACTGATGCCCCGGCGATCGAGACTTTGGTTGGTAGCCGCTTCCAC TGCATCGGCCACTTCC
<i>G-hik43</i>	ATCCTGGCCCCTACTACTATCCGCCGGATTTGGTCACCGACCAGCCGGA ACGGTTCATTATGGCCGAGTTAATTCGGGAGCAGATTTTGTGCTCACC CGCCAGGAGGTGCCTCACTCCGTGGCGATCGCCATTGAGAAGGTGGAA GAAACGCCCGAACGCACCAATGTTTTTGCCGCCATCACAGTGGAAGAG GTTCCCAAAGGGCATTATCATTGGCCAAAAGGTAGTATGCTTCAGGC GATCGGCACTGCGGCCCGGCAACAAATTCAAAATTAATTTCCGGGGAT GTTTATTTAAAAC TATTTGTGAAAGTTGAACCAAATGGCGGCAGTCTCG CCAGCAGTTGTTAGAATTTGGATACCGTGTGGAAGAGTAGCAAGAAGCA GAATTCAAAAAAGGATCCAGGGGAAGAAGAAATTGTTATCAAGCAAATTG AAGGGCCCATTCCAAACCTCCAGGCATTGCCGGGGCTACCGTGCGGG GGGATGGTAGCATCATGCCATTGCCGATGTTTTGGAAGTATCGAAAT TGCCAGGGTTCGTCTCCGCACTGACAGCAGTGGTGGACTATGGCGCAA AACCTGACCCCCACGGTCAATGAAGTCCACATGGACCCCACTGTGCTA ATTGTGGACGACTCCATCACGGTGC GGGAATTGCTCTCCCTCAGTTTCA AAAAAGCTGGTTTCCGGGTAGAACAGGCTAGGGATGGACAGGAAGCCT GGGATCAACTCAAGTCTGGTCTGCCCTGTGACTTGGTCTTCTGTGACAT TGAAATGCCCCGCAAAAATGGCTTGGA
<i>G-ancM</i>	GGGGGCACTGGCACTCGGTAAATGTGGATGCCATCGACCATTTCTGG GACGGACTTTCTCTGTGGCCACGGTAATTAATGGATCTCATAGCCCT GTTGAACTAATTCTGGGTAGAGTTCTGCCACATGGCGAGCAATGCCGCC GACAATGCGGGGGGAAATTCCCAAGCTAGCACCAAGATTTTCATGGCT GTGACCAATTTTTGTGAGTGCATGGAGGGAAAGTCGGGGCTATTGGTGT CGTGGGCACTCTAAAACATTATGCGCAATCGTGGCGTGGCCACACGGC CAAATTCGTTTCGGAGGTTAGTTAATTTTGTGCTGGAGTTCTGGCTTTCGAG TTGCAGTCAATTGCCAATGTTTGCCCAACTGAGGGAATGAAGAACCGGC TAAAGATTGGAATTCAAAAAAGGATCCGCCATTGCCGCCAGGGGATTC TCTCATTAAACACAAAATTTTTGTCCGTAAACATTACAGTGTACAGGGCC AATTTCTGGCTTGTGCATAGGTTACGGCTGGAATTTTTGGGTTTAGATGG GAAAAGAGATATTTTGTAACTGCGGAAGTATTTACCAAGATGTTTAAAT TCCTTGCCAATAATTATTCACAATCTTTGGGGTAACTGCTTGCCTGGGG CTATTCACCTACTTGGCGATCGCCGTTCCAGTGGAAAGCCAGGGGCAA ATAGTTTTGAAAATTACCGTCAGCAATGCCTGCGTCCGGTGGAAACAGGC

G-block	DNA Sequence (5'→ 3')
	TGGCATTAAAGGGGGCGGGCGGCTCAGGAAATGTGCAACTGCACAATTAAT
	AAGTTCAAGCAAAAATATTCCCTGGCAGAA

Antibodies that were used in this study are described in previous studies: α CurT (Heinz *et al.*, 2016b), α D1 (Schottkowski *et al.*, 2009a), α D2 (Klinkert *et al.*, 2004). Antibodies purchased from Agrisera: α ATPase, α CP43, α CP47, α RcbL, α Rieske and α PsaD. Horseradish peroxidase (HRP) conjugated anti-rabbit antibody (Sigma-Aldrich, St. Louis, USA) served (1:10000) as a secondary antibody in western analysis. For immunofluorescence studies secondary antibody containing the fluorophore (Alexa Fluor™ 405 goat anti-rabbit IgG (H+L), diluted 1:300 (ThermoFisher Scientific, Waltham, USA) was used. A His probe HRP conjugate was used for detection of the His residue. Working dilutions of used primary antibodies are listed Table 6:

Table 6: Used Antibodies in this study.

Antibody	Dilution	size [kDa]	Host organism	Reference
6X His tag HRP	1:1000		Rabbit	Abcam (Cambridge, United Kingdom)
α ATPase α/β	1:2000	50	Rabbit	Gift from AG Soll
α CP43	1:2000	43	Rabbit	Agrisera AB, (Vännäs, Sweden)
α CP47	1:1000	47	Rabbit	this study
α CP47	1:2000	47	Rabbit	Agrisera AB, (Vännäs, Sweden)
α CurT	1:10000	17	Rabbit	(Heinz <i>et al.</i> , 2016b)
α D1	1:1000	30	Rabbit	(Schottkowski <i>et al.</i> 2009b)
α D2	1:1000	30	Rabbit	(Klinkert <i>et al.</i> , 2004)
α PsaD	1:1000	18	Rabbit	Agrisera AB, (Vännäs, Sweden)
α RcbL	1:1000	55	Rabbit	Agrisera AB, (Vännäs, Sweden)
α Rieske	1:2000	26	Rabbit	Agrisera AB, (Vännäs, Sweden)
α AncM	1:1000	32	Rabbit	this study
α Vipp1	1:1000	35	Rabbit	(Aseeva <i>et al.</i> , 2007)

2.2 Methods

2.2.1 Bioinformatic tools

In order to estimate the number and position of putative TMDs, protein sequences were analysed using following online tools: https://embnet.vital-it.ch/software/TMPRED_form.html and <http://www.cbs.dtu.dk/services/TMHMM/>. To predict a putative signal peptide the online

Material and Methods

tool <http://www.cbs.dtu.dk/services/SignalP/> was used. The webtool expasy (https://web.expasy.org/compute_pi) was used for calculation of the hypothetical mass weight. For co-expression patterns CyanoExpress 2.3 (<http://cyanoexpress.sysbiolab.eu>) was used (Hernandez-Prieto and Futschik, 2012). The presence of AncM homologues in other organisms was checked with NCBI/Blast (<https://blast.ncbi.nlm.nih.gov/Blast.cgi>).

2.2.2 Growth conditions

For subcloning *Escherichia Coli* (*E.Coli*) DH5 α and for overexpression *E.coli* BL21 (D3), strains were grown on solid or in liquid lysogeny broth (LB) medium (1% pepton, yeast extract, 1% NaCl) containing 100 $\mu\text{g/ml}$ ampicillin or 50 $\mu\text{g/ml}$ kanamycin at 37°C (Hanahan, 1983; Studier and Moffat, 1986). Optical density (OD) to track bacterial growth was measured at a wavelength of 600 nm. *Synechocystis* lines were grown at 30°C under continuous light at a photon irradiance of 30 $\mu\text{E m}^{-2} \text{s}^{-1}$ or for High Light Stress 200 $\mu\text{E m}^{-2} \text{s}^{-1}$ under cool white light (Osram, 18 W Lumilux[®] DE Luxe cool white). The cells were grown on solid or liquid BG11 medium with addition of 5 mM Glucose (Rippka *et al.*, 1979). The OD was measured at a wavelength of 750 nm. Doubling times were calculated after three days (with Glucose) or four days (without Glucose) by using following using the formula Doubling time = $\frac{\text{growth time} \cdot \log_{10}(2)}{\log_{10}(\text{final OD}_{750}) - \log_{10}(\text{start OD}_{750})}$. For counting the cell number, samples were set to OD₇₅₀ = 1 and counted by using a Neubauer counting chamber (Paul Marienfeld).

2.2.3 Molecular biology methods

DNA concentration was measured at a wavelength of 260 nm using an ultraviolet and visible (UV-Vis) spectrophotometer (implen). The purity was verified by the absorption ratio of 260/280 nm. If not otherwise stated, different plasmid DNA fragments from *Synechocystis* were amplified by polymerase chain reaction (PCR). The specific primers were designed using CLC Genomics Workbench 12. Annealing temperature of primer pairs were calculated using Tm calculator from New England Biolabs (<https://tmcaculator.neb.com/#!/main>). All primers used in this study were ordered from Sigma-Aldrich/Merck. PCR for strain generation was performed by using the proofreading Q5[®] High-Fidelity DNA Polymerase according to the company's manual. For segregation analysis of various strains a purified *Taq*-polymerase was used (Engelke *et al.*, 1990). PCR was performed in 20 mM Tris/HCl, pH 8.8, 50 mM KCl, 1.5 mM MgCl₂, 0.1% Tween-20. Resulting PCR fragments were separated on 1% or 2% Agarose gel buffered with Tris-acetate-EDTA (TAE), pH 8. The DNA fragments were stained by Midori Green and visualised with Fluorescence Gel Imager (Serva). The size of the fragments was analysed using 1 kb plus DNA Ladder (ThermoFisher Scientific, Waltham, USA). Purification of PCR products was performed by using NucleoSpin Gel and PCR clean-up kit (Table 2).

Material and Methods

For the ligation of DNA fragments T4 Ligase was used. Restriction digestion was performed by using FastDigest Restriction enzymes (Table 3)

2.2.3.1 Transformation of *E.coli* cells

For transformation heat shock competent cells were used. An overnight culture was diluted to OD₆₀₀ 0.1 and grown to an OD₆₀₀ of 0.45 – 0.6 at 37°C. Afterwards the culture was incubated for 15 min on ice. Following this, the cells were centrifuged at 4°C, 5000 g for 10 min and resuspended in 20 ml RF1 (100 mM RbCl, 50 mM MnCl₂, 30 mM Ka-acetate, 10 mM CaCl₂, 15% Glycerin, pH 5.8 with CH₃COOH). In the next step suspension was incubated for 2 h on ice. After centrifugation, the pellet was resuspended in 4 ml RF2 (10 mM 3-(*N*-Morpholino) propanesulfonacid (MOPS), 75 mM CaCl₂, 10 mM RbCl, 15% Glycerin). The suspension was incubated for 15 min on ice and aliquoted in 50 µl fractions. For long term storage, the cells were snap-frozen in liquid nitrogen. For transformation of plasmids, competent *E.coli* cells were used and incubated for 30 min with 1 µg plasmid DNA. A heat shock of cells at 42°C for 45 s was performed. Afterwards the cells were incubated on ice for 3 min. Subsequently, cells were spread on a LB-plate containing the selective antibiotic. The plate was incubated overnight at 37°C.

2.2.3.2 Plasmid isolation

For screening of colonies plasmids were isolated from overnight culture of cells that were harvested and resuspended in buffer P1 (50 mM Tris/HCl, pH 8, 10 mM EDTA, 100 µg/ml RNaseA). In the next step solution P2 (0.2 M NaOH, 1% SDS) was added to lyse the samples. Then 3.0 M K-acetate pH 5.5 was added and followed by further incubation on ice for 20 min. After centrifugation for 20 min at 20 000 g the supernatant was taken and the DNA was precipitated with 99.6% ethanol at 20 000 g, 4°C for 30 min. The pellet was washed with 70% ethanol and resuspend in *Aqua destillata* (*A.dest*). In order to increase purity and yield, plasmids were isolated using the NucleoBond Kit. Restriction enzyme digestion was performed using FastDigest Enzymes (Table 3).

2.2.4 Genetic screen

DNA from *curT* and *sucurT* *Synechocystis* mutants were extracted with Phenol/Chlorophorm. The cells were harvested and resuspended in DNA extraction buffer (100 mM Tris-HCl, pH 8, 1.4 M NaCl, 20 mM (Na-EDTA), 2% (v/v) β-Mercaptoethanol, 2% (w/v) CTAB). For cell lysis glass beads of Ø 0.5 mm (Carl Roth) were used. The samples were incubated for 60 min at 65°C and vortexed regularly. To extract the DNA, Phenol/Chloroform/Isomaylalcohol in the ratio 25:24:1 was added. After a centrifugation step the DNA was precipitated with Isopropanol. The DNA was sequenced at LMU genome sequence unit. For whole genome sequencing, library preparation was performed with 50 ng of genomic DNA each, as quantified on Qubit 2.0 Fluorometer (Thermo Fisher Scientific with ds HS Assay Kit), using the Nextera DNA Library Prep Kit (Illumina) according to

Material and Methods

manufacturer's instructions. Libraries were quality controlled with DNA High Sensitivity DNA Kit on Bioanalyser (Agilent) and quantified on Qubit 2.0 Fluorometer. Genome sequencing was performed on Illumina MiSeq with v2 chemistry (2x 200 bp and 2x 250 bp paired-end sequencing). The Data were analysed with CLC Genome Main Workbench 8.0.1 (Quiagen). The genome sequence of *Synechocystis* were obtained from (<http://genome.kazusa.or.jp/cyanobase/Synechocystis>).

2.2.5 Transformation of *Synechocystis*

In order to integrate external DNA into the genome of *Synechocystis* cells were grown to an OD₇₅₀ of 0.5, harvested and resuspended with BG11 to a final OD₇₅₀ of 2.5. To 400 µl cells 10 µg DNA was added and incubated for 3 h at 30 µE m⁻² s⁻¹ and 30°C without shaking. Afterwards cells were shaken at 120 (rounds per minute) rpm and incubated in addition of 1 ml BG11 overnight. The next day 200 µl cells were plated on BG11 plates containing the selective antibiotic.

2.2.5.1 Strain generation of *Synechocystis*

In order to generate a *fraH*, *cyt c_M*, *hik43* and *ancM* knock-out mutants the gene block fragments of *G-fraH*, *G-cytc_M*, *G-hik43* and *G-ancM* was used and cloned blunt end into pJet1.2/blunt (Table 5). In order to interrupt the corresponding ORF, a kanamycin cassette was inserted using the restriction sites EcoRI and BamHI (Alexeyev *et al.*, 1995). To verify the segregation level primer pairs fwd-seg-*fraH*/rev-seg-*fraH*, fwd-*cytc_M*-seg/rev-*cytc_M*-seg, fwd-*hik43*-seg/rev-*hik43*-seg and fwd-*ancM*-seg/rev-*ancM*-seg was used.

In order to generate *ancM*::*ancM* and *ancM*^{164STOP} strain DNA fragments was amplified by colony PCR with the Q5[®] High-Fidelity DNA Polymerase using WT and *sucurT* as template with the forward and reverse primer pair fwd-*ancMa* and rev-*ancMa* and fwd-*ancMb* and rev-*ancMb*, respectively. Resulting fragments were ligated into pJet1.2/blunt. For a positive selection a chloramphenicol cassette from pVZ321 was inserted after the *ancM* gene and transformed in *ancM* using the restriction interfaces *Sall*, *BamHI* (Zinchenko *et al.*, 1991). For *ancM*^{164His} a codon coding for a hexa histidine residue was inserted after the amino acid position 164 by PCR into the transformation plasmid of *ancM*^{164STOP} strain using the forward and reverse primer pair fwd-*ancM*^{164HisSTOP} and rev-*ancM*^{164HisSTOP}. This plasmid was then used to transform *ancM*. As mentioned before, a chloramphenicol resistance cassette was used for selection. Segregation level of *ancM* related strains were checked with the primer pair fwd-seg-*ancM* and rev-seg-*ancM*. To generate *ancM curT* line *curT* was disrupted in *ancM* by a chloramphenicol resistant cassette (Heinz *et al.*, 2016b). In order to verify the segregation level primer pair, fwd-*curT*-seg and rev-*curT*-seg was used. To interrupt *slr2071*, fragment a and b was amplified by colony PCR with the WT using the primer pair fwd-*slr2071a*/rev-*slr2071a* and fwd-*slr2071b*/rev-*slr2071b*. The restriction interfaces *BamHI* was used to insert the kanamycine resistant cassette (Alexeyev *et al.*, 1995).

Material and Methods

2.2.6 Microscopy

2.2.6.1 Immunofluorescence and fluorescence microscopy

Synechocystis cells were harvested in mid-log phase by centrifugation at 3000 g for 2 min and fixed with 3.7% (w/v) formaldehyde in phosphate buffered saline (PBS) (140 mM NaCl, 2.7 mM KCl, 10 mM Na₂HPO₄, 1.8 mM KH₂PO₄; pH 7.4). After 3 times washing with PBS the cells were permeabilised for 30 min with PBS-T (PBS supplemented with 0.5% Tween-20) followed by 1 h gentle shaking at 37°C in lysis buffer (50 mM Tris-HCl, 100 mM NaCl, 5 mg/ml Lysozyme). To neutralise any remaining aldehyde groups, the cells were incubated for 30 min in 0.1 M Glycine. In order to unspecific binding, the cells were incubated for 1 h at 30°C in blocking buffer (5% in PBS). The cells were incubated for 1 h at 30°C with the purified primary antibody α AncM diluted 1:100 in blocking buffer. After 3 times washing with blocking buffer, the cells were incubated in blocking buffer for 1 h at 30°C in dark with the secondary antibody linked to the fluorophore Alexa Fluor™ 405 diluted 1:300. To stain the plasma membrane the cells were treated for 10 min with FM 1-43 dye (Thermo Fisher Scientific) and washed three times in PBS. The sample was finally washed three times in PBS. Afterwards 20 μ l of the sample was dried overnight at room temperature (RT) on a glass slide (DWK Life Sciences GmbH) covered with a drop of Calbiochem FluorSave™ Reagent (Merck Millipore) and a high precision coverslip (Paul Marienfeld GmbH & Co. KG). The coverslip was sealed with nail polish (modified from (Rast *et al.*, 2016)). The micrographs were examined with an IX71 inverted microscope (Olympus Deutschland GmbH) combined with a Delta Vision Elite Filter Set (General Electric Company) and a CoolSNAP HQ2 camera (Photometrik GmbH).

2.2.6.2 Transmission electron microscopy (TEM) and correlative light-electron microscopy (CLEM)

Synechocystis cells were harvested in mid-log phase. After centrifugation at 3000 g for 5 min the supernatant was discarded. The TEM preparation was done by high pressure freezing with an EM HPM100 (Leica Microsystems GmbH) followed by a freeze substitution assay with A-O-U-H (0.2% OsO₄, 0.1% uranyl acetate and 9% (w/v) H₂O diluted in pure Acetone) in an EM AFS2 (Leica Microsystems GmbH) over 42 h (Peschke *et al.*, 2013). Finally, the samples were embedded in Epon 812 and polymerised at 63°C for 48 h. Ultrathin sections (thickness, 50 nm) were cut using a DiATOME ultra 35° diamond knife (Science Services GmbH) on a Ultracut-E ultramicrotome (formerly Reichert-Jung, now Leica Microsystems GmbH). Sections were mounted on collodium-coated copper grids with 400 mesh (Science Services GmbH), post-stained with 80 mM lead citrate/NaOH pH 13 and examined with an EM 912 transmission electron microscope (Zeiss) equipped with an integrated OMEGA energy filter operated in the zero-loss mode at 80 kV. Images were acquired using a 2k x 2k slow-scan CCD camera (Tröndle Restlichtverstärkersysteme).

Material and Methods

For correlative light-electron microscopy (CLEM) the *Synechocystis* cells were prepared according to TEM. Before post-staining, the ultrathin sections were subjected to widefield microscopy using the Delta Vision Elite microscope to detect the chlorophyll autofluorescence. Following this, the preparation and imaging for TEM as describe before was continued and the resulted micrographs from both microscopes were overlaid.

2.2.7 Measurement of chlorophyll and oxygen consumption/evolution

Chlorophyll *a* concentration was determined according to (Wellburn und Lichtenthaler; Wellburn und Lichtenthaler 1984). For oxygen evolution and consumption measurements, cells were grown in BG11 without adding glucose, harvested in the mid log phase and set to a chlorophyll concentration of 2.5 µg/ml. The oxygen consumption and evolution rate were measured in a volume of 2 ml without adding any electron acceptors or donors. The setup was performed with a Clark-type electrode (Hansatech Instruments). All measurements were performed after incubation of 5 min in darkness. The oxygen evolution rate was directly measured with a LED Lamp at 627 nm, 1000 µE m⁻² s⁻¹ (Hansatech instruments). The oxygen consumption rate was measured after an illumination of 30 µE m⁻² s⁻¹.

2.2.8 Fluorescence measurements

2.2.8.1 P₇₀₀⁺ reduction kinetics and relative electron transport rate

P₇₀₀⁺ absorption measurements and chlorophyll fluorescence measurements at different light intensities were performed at a chlorophyll concentration of 10 µg/ml with a Dual-PAM-100 instrument (Heinz Walz) in a Volume of 3 ml according to Heinz *et al.* (2016a). After 2 min of dark incubation P₇₀₀ RC were oxidised by a 50 ms multiple turnover saturating light pulse with an intensity of 10,000 µmol photons m⁻² s⁻¹. The experiments were also performed after addition of 50 µM DCMU. Ten technical replicates were averaged (Heinz *et al.*, 2016a). For calculation of the rate constant the data points were fitted with a single exponential function $y = y(0) + ae^{(-bx)}$ with the first data point being 1 ms after the saturating light pulse (Bernat *et al.*, 2009).

2.2.8.2 77 K Measurements

Cells were grown to the mid log phase and concentrated to a chlorophyll concentration of 10 µg/ml. 1 ml cells were transferred into thin glass tubes, dark adapted for 30 min and shock frozen in liquid nitrogen. In order to quantify the fluorescence, the samples were excited at 440 nm and emission was measured from 650 nm to 780 nm with a Jasco FP 6500 Spectrofluorometer (Jascon, Mary's Court, USA).

2.2.9 Protein analysis

2.2.9.1 SDS-PAGE

The protein concentration was determined according to the method of Bradford, (Bradford, Marion, M 1976) using RotiQuant (Carl Roth). Furthermore, for separation of denatured proteins according to their molecular weight SDS-PAGE (SDS-polyacrylamide gel electrophoresis) was performed (Table 7).

Table 7: SDS-Gel composition. SDS-Gel containing 10%, 12% or 15% acrylamide with a thickness of 1.5 mm and a size of 5 x 8 cm.

Components	Stacking gel [ml]	Resolving gel [ml]		
		10%	12%	15%
<i>A.dest</i>	3.3	4	3.6	3
Acrylamide/Bis Solution, 37.5:1 (40% (w/v))	0.5	2	2.4	3
4 x Tris-SDS, pH 8.8 (1.5 M Tris/HCl, pH 8.8, 0.4% (w/v) SDS)		2	2	2
4 x Tris-SDS, pH 6.8 (0.5 M Tris/HCl, pH 6.8, 0.4% (w/v) SDS)	1.25			
10% Ammoniumpersulfate (APS)	0.025	0.04	0.04	0.04
<i>N,N,N',N'</i> -Tetramethyl ethylenediamine (TEMED)	0.01	0.02	0.02	0.02
total volume [ml]	5	8	8	8

The gel was run in SDS running buffer (25 mM Tris, 192 mM Glycine, 1.5% SDS) at 40 V for 30 min, afterwards the voltage was increased to 70 V. Subsequently the gel was blotted (chapter 2.2.9.3 Western Blotting) or stained with Coomassie (0.2 w/v Coomassie brilliant blue R250, 10% acetic acid, 40% methanol) or silver nitrate (Chevallet *et al.*, 2006).

2.2.9.2 Blue Native (BN)-PAGE / 2D-PAGE

In order to separate big native protein complexes BN-PAGE was performed by casting an acrylamide gradient from 4.5% to 15% (Table 8). The gel run was performed overnight at 4°C at 40 V by using the running buffer blue cathode for the upper chamber (15 mM Bis-Tris, pH 7, 50 mM Tricine, 2% (w/v) Coomassie G-250) and running buffer anode for the lower box (50 mM Bis-Tris, pH 7). The next day, the voltage was increased to 300 V. After 1/3 gel run the running buffer blue cathode was exchanged with running buffer colorless cathode (15 mM Bis-Tris, pH 7, 50 mM Tricine).

Material and Methods

Table 8: Components of one BN-Gel.

Components	Stacking gel	Separating gel [ml]	
	[ml]	4%	15%
<i>A. dest</i>	5.85	8.36	1.25
Acrylamide/Bis Solution, 37.5:1 (40% (W/V))	1.05	1.87	6.25
3 x Gel buffer (150 mM Bis-Tris, pH 7, 1.5 M Aminocaproic acid)	3.5	5.5	5.5
Glycerin 50%			3
APS	0.01	0.01	0.01
TEMED	0.075	0.03	0.03
Total volume [ml]	10.485	16.4	16.4

For analysis of individual subunits, a second dimension was performed. The lane was cut out and solubilised by shaking for 15 min in solubilisation buffer (2% SDS (W/V), 66 mM Na₂CO₃, 0.67% β-mercaptoethanol). Afterwards the strip was placed on a 12% Acrylamid-Urea gel and fixed with 0.75% Agarose dissolved in SDS running buffer containing a few crystals of bromophenol blue. The composition of the urea gel is listed in Table 9.

Table 9: Composition of one Urea Gel.

Components	Stacking gel [ml]	Separation gel [ml]	
	4%	10%	12.5%
<i>A. dest</i>	1.85	15.4	12.6
Acrylamide	0.61	11.3	14.1
1.5 M Tris, pH 8.8		11.25	11.25
250 mM Tris, pH 6.8	2.54		
Urea		10.82	10.82
APS	0.075	0.04	0.04
TEMED	0.0075	0.18	0.18
Total volume [ml]	5.0825	38.17	38.13

2.2.9.3 Western Blotting

If not described otherwise, SDS or urea gel was blotted on a reprobe Nitrocellulose 0.45 µm membrane (AppliChem) by using the semi dry blotting method with a three blot buffer system Table 10.

Material and Methods

Table 10: Blot buffer composition.

Anode I	Anode II	Cathode
0.3 M Tris, pH 10.8	0.025 M Tris, pH 10.4	0.025 M Tris, pH 9.4
20% Methanol	20% Methanol	0.04 M Aminocaproic acid 20% Methanol

The nitrocellulose membrane was stained with Ponceau S solution (0.2% (W/V) Ponceau S, 2% (V/V) acetic acid). Afterwards the membrane was blocked with 5% (W/V) milk in Tris buffered saline with Tween-20 (TBS-T) (10 mM Tris/HCl, pH 7.5, 150 mM NaCl, 0.05% Tween-20). Antibodies were incubated overnight in TBS-T with 5% milk. Afterwards the membrane was washed with TBS-T. The secondary antibody was incubated for one hour at RT. For development solutions I and II were freshly prepared and mixed in a 1:1 ratio for the detection of protein bands Table 11.

Table 11: Western blot developing solutions.

Solution I	Volume [ml]	Solution II	Volume [ml]
100 mM Tris/HCl, pH 8.5	3	100 mM Tris/HCl, pH 8.5	3
90 mM <i>p</i> Coumaric acid	0.013	250 mM Luminol	0.03
H ₂ O ₂	0.00166		

Detection was performed with an electrochemiluminescence (ECL) Reader (ImageQuant LAS 4000, GE Healthcare, Chicago, Illinois, USA).

2.2.10 Protein purification

2.2.10.1 Maltose binding protein (MBP) Tagged Proteins

For overexpression of AncM the gene was amplified by colony PCR using the primer pair fwd-MBP-AncM and rev-MBP-AncM. For recombinant expression of PilQ, PilQ was fused to MBP. The *pilQ* sequence encodes for amino acids sequence 31-785 was amplified by PCR using the primer pair fwd-MBP-PilQ and rev-MBP-PilQ. Both PCR products were inserted into the vector pMAL-c5x via the restriction sites BamHI and PstI. Afterwards the constructs were expressed in BL21 (D3). Recombinant expression of MBP-AncM and MBP-PilQ was performed by induction with 1 mM IPTG overnight at 12°C. To purify the proteins the cells were harvest and disrupted by French Press using the buffer (30 mM Tris, pH 7.5, 300 mM NaCl, 1 mM DTT) in addition of a protease inhibitor tablet. After centrifugation at 20000 *g* supernatant (SN) was incubated overnight with amylose resin beads. To separate the beads, the lysate was filtered and washed with 25 ml buffer. Both proteins was eluted with 15 mM D(+)-Maltose in a volume of 5 ml. MBP-AncM was used as antiserum in a rabbit (Pineda Antikörper Service, Berlin, Germany).

Material and Methods

2.2.10.2 His Tagged Proteins

For antibody production of α CP47 the soluble loop of *psbB* (CP47) between TMD V and VI; was used for overexpression in *E. coli*. The fragment was obtained via colony PCR using the primer pair fwd-His-CP47 and rev-His-CP47 and inserted via restriction sites BamHI/Pst into pETSUMO28b (Bepperling *et al.*, 2012). For Prata, the coding sequence for amino acids 39-383 was cloned into the pET28b-Sumo plasmid (Bepperling *et al.*, 2012) by using the primer pair fwd-His-Prata and rev-His-Prata that include BamHI and PstI restriction sites. The plasmid was transformed into BL21 (DE3). The overexpression was performed at 12°C. For induction 1 mM IPTG was added. For purification the cells were disrupted with a French Press (50 mM NaH₂PO₄, pH 8, 300 mM NaCl, 10 mM Imidazol, Protease Inhibitor Tablet). For purification the protein was captured on Protino® Ni-NTA Agarose beads. After washing with 20 mM Imidazol the protein was eluted with 250 mM Imidazol. His-SUMO-CP47 was send to Pineda for immunisation in a rabbit. Cleavage of the His-Sumo tag was performed as described in Bepperling *et al.* (2012). Construction, overexpression and purification of the inactive form of HhoA-His, as well as His-DLA2, has been described in Huesgen *et al.* (2007) and Bohne *et al.* (2013).

2.2.11 Antibody purification

To avoid cross reactions α AncM was purified. Therefore 5 mg of the MBP-AncM was separated on SDS-PAGE and blotted on a nitrocellulose membrane. After staining the membrane with Ponceau the strip containing the antibody was cut out, blocked with milk overnight, and incubated with 2 ml α AncM Serum. After 3 times washing the antibody was eluted with 1 ml of 150 mM glycine, pH 2.5 and incubated for 10 min. The eluate was neutralised with 75 μ l 2 M Tris, pH 8. To stabilise the antibody 5.375 μ l of 1 M Natriumazid and 53.75 μ l BSA [20 mg/ml] was added. For long term storage the purified antibody was stored at -80°C.

2.2.12 Whole cell protein isolation

For whole cell Protein analysis cells were harvested and disrupted with glass beads \emptyset 0.5 mm (Carl Roth) and solubilised for 15 min in 50 mM Tris-HCl, pH 7, 20 mM MgCl₂, 20 mM KCl, 0.5% Triton X-100 and one Protease inhibitor Tablet per 15 ml (complete Tablets, Mini EDTA-free, Roche). After centrifugation at 10 000 *g* at 4°C the supernatant was denatured with ROTI®Load, 4x reducing (Carl Roth) over night at RT. Subsequently 30 μ g of whole cell Protein was analysed on an SDS-PAGE. Quantification of Western blot signal intensities was performed as described in (Rengstl *et al.*, 2011; Heinz *et al.*, 2016b).

Material and Methods

2.2.13 Analysis of cyanobacterial membrane complexes

According to Heinz *et al.* (2016b) and Schottkowski *et al.* (2009a) cells were harvested and resuspended in thylakoid buffer (50 mM Hepes/NaOH, pH7,5 mM MgCl₂, 25 mM CaCl₂, 10% Glycerin) after addition of a protease inhibitor tablet. Cells were opened with glass beads using a bead beater. Afterwards the supernatant was transferred into a new tube and centrifuged for 30 s at 1000 *g* at 4°C. The supernatant was centrifuged for 30 min, 20 000 *g* at 4 °C. After two washing steps, the membranes were suspended in thylakoid buffer.

2.2.13.1 Solubility Test

Solubility properties of AncM in isolated membranes was performed according Heinz *et al.* (2016b) and Schottkowski *et al.* (2009a). The membranes were incubated on ice for 30 min in 50 mM Hepes pH7.6 in addition with 0.1 M Na₂CO₃, 1 M NaCl, 4 M Urea, 1.3% β -DM, 0.1% NP-40, 0.5% Triton X-100 or DNaseI and containing 0.5% Triton. Membrane bound (M) and soluble (S) proteins were separated by centrifugation at 20 000 *g* at 4°C. Afterwards the pellet was washed twice with 50 mM Hepes pH 7.6. Samples were denaturated over night with Roti Load.

2.2.13.2 Analysis membrane complexes using 2D-PAGE

2D separation of cyanobacterial membrane complexes were performed as described in previous publications (Klinkert *et al.*, 2004; Schottkowski *et al.*, 2009b; Rengstl *et al.*, 2013; Heinz *et al.*, 2016b). The pellet membranes were resuspended in ACA Buffer (50 mM Bis-Tris, pH7, 750 mM aminocaproic acid (Merck), 0,5 mM Na-EDTA (Carl Roth). Afterwards 10 μ g chlorophyll of the isolated membranes was solubilised for 30 min on ice with 1.3% β -DM (Carl Roth). Subsequently the samples were centrifuged for 30 min, 20000 *g* at 4°C. The supernatant was taken, and loading buffer was added (750 mM aminocaproic acid, 5% Coomassie G-250 (AppliChem) The solubilised samples were separated on a BN-Gel (4.5%-15%). The second dimension were performed on a 10% acrylamide Urea-Gel PAGE.

2.2.13.3 Pulse-labeled Proteins

Cells were grown at 30 μ E m⁻² s⁻¹ and resuspended in fresh BG11 to reach a chlorophyll concentration of 0.3 μ g/ μ l. Afterwards ³⁵S-Met (Hartmann Analytic) >1000 Ci/mmol was added to a final activity of 750 μ Ci/ml according to (Klinkert *et al.*, 2004). The cells were incubated for 30 min at 60 μ E m⁻² s⁻¹. Afterwards the cells were harvested, and the cell wall was disrupted by glass beads with the buffer (10 mM Tris/HCl, pH 6.8, 10 mM MgCl₂, 20 mM KCl). Membranes were sedimented by centrifugation and washed with buffer. After centrifugation the samples were resuspend in ACA buffer (Klinkert *et al.*, 2004). For solubilisation 15 μ g chlorophyll was used and mixed with 1.3% β -DM and incubated for 30 min on ice. After centrifugation the supernatant was separated according to Heinz *et al.* (2016b) and Klinkert *et al.* (2004) by a 10% acrylamide Urea-Gel PAGE. The gel was stained with Coomassie-G250

and dried. For detection of the radioactivity the gel was exposed to phosphorimage films (Fuji Foto Film GmbH) and read out with Typhoon trio, Amersham.

2.2.13.4 Membrane fractionation

To separate membranes a two-step sucrose gradient method was used according to Schottkowski *et al.* (2009b); Rengstl *et al.* (2011); Heinz *et al.* (2016b). Cells from 1.5 l of a culture in the middle of exponential growth phase were harvested and washed with 5 mM Tris/HCl, pH 6.8. From cell lysis the peptidoglycane layered cells were incubated for 2 h, at 30°C and 30 $\mu\text{E m}^{-2} \text{ s}^{-1}$ with buffer I (10 mM Tris/HCl, pH 6.8, 600 mM sucrose, 1 mM phenylmethylsulfonyl fluoride (PMSF), 5 mM EDTA, 0.3% lysozyme). Following this, cell suspensions were washed with buffer II (20 mM Tris/HCl, pH 6.8, 1 mM PMSF, 600 mM sucrose). Afterwards, the cells were disrupted under pressure (15 000 PSI). The lysed cells were incubated with 20 units DNase for 15 min on ice to cleave genomic DNA. After centrifugation for 10 min at 5000 g, 4°C the supernatant was mixed with 0.83 vol. 80% sucrose solution. The first step gradient (10 ml sample, 8 ml 39% sucrose, 6 ml 30% and 8 ml 10%) was run 17 h at 135 536 g, 4°C. Afterwards the gradient was fractionated into V fractions (fraction I: 6 ml; fraction II: 7 ml; fraction III: 4 ml; fraction IV: 4 ml; fraction V: 9ml). Fractions I–IV were independently of each other concentrated to a volume of 250 μl in with Amicon® Ultra-15 centrifugation filter unit, cut-off 10 kDa. For the second gradient only fraction V was used and diluted in a 1:1 ratio with 10 mM Tris/HCl, pH 6.8 and separated in a linear sucrose gradient (30% - 60%) by ultracentrifugation for 17 h at 135 536 g, 4°C. The second gradient was divided into 14 fractions of 2.5 ml. All fractions were concentrated to a volume of 500 μl using Amicon® Ultra-15 centrifugal filter unit, cut-off 10 kDa. For SDS-PAGE and immunodetection the volume of 40 μg protein from fraction 7 were loaded for each fraction (1-14).

2.2.13.5 Co-Immunoprecipitation (Co-IP) of αCurT in PDM and TM

αCurT was cross linked to Protein A Agarose Beads (Roche). The antibodies were pre bound to the protein agarose beads overnight at 4°C. After washing with Co-IP buffer (100 mM Tris, pH 6.8, 150 mM NaCl) the antibodies were cross linked with 25 mM dimethyl pimelidate dihydrochloride to the beads for 45 min at RT. For the quenching step the beads were incubated with 100 mM ethanolamine for 30 min at RT. An elution step with 100 mM Glycine, pH 2.5 for 10 min removed the non-binding antibodies. The beads were washed with Co-IP buffer. For PDM fractions 1 to 6 and for TM fractions 8 and 9 were pooled. PDM and TM were concentrated with Amicon® Ultra Centrifugal Filter Units with a cut off size of 10 kDa (merckmillipore) and wash with Co-IP buffer. After solubilisation with 1.5% $\beta\text{-DM}$ for 45 min on ice the PDM and TM samples were incubated overnight with the cross linked protein A Agarose αCurT and αAncM beads. For mass spectrometry analysis the beads were washed with Co-IP buffer and eluate with 100 mM glycine, pH 2. The elution fraction was neutralised in the ratio 1:1 with 100 mM NH_4CO_3 .

Material and Methods

PratA complex Co-IP was performed on 50 µg isolated periplasmic proteins, which were incubated with the αPratA antibody linked to protein A agarose (Roche) for 90 min at RT. After five washing steps (50 mM Tris-HCl pH 8.0, 150 mM NaCl), bound proteins were eluted by incubation with Roti-Load 2x non reducing for 30 min at RT and SDS-PAGE was performed. Gels were either subjected to silver staining and mass spectrometry analysis.

2.2.14 Mass spectrometry (MS)

For MS samples were loaded on an SDS Gel. Gel run was stopped after samples entered the separation gel. Gels were stained afterwards with Coomassie-G250 blue. Sample or gel piece were cut out and incubated for 20 min in 200 ml with 50 mM NH₄CO₃. The pieces were de stained several times by 20 minutes of incubation in ABC25/ACN50 (25 mM 50%) solution until complete removal of the Coomassie. Thereafter, samples were incubated for 10 min with 200 µl 100% (V/V) acetonitrile and dried completely. For the tryptic digestion, gel pieces were incubated at 37°C overnight with Trypsin (0.125 µg/sample). Supernatants were transferred in new tubes and gel pieces were washed twice for 20 min with 50% (V/V) acetonitrile and formic acid 1% (V/V). Supernatant and wash fractions were combined and neutralised with 370 mM NH₄CO₃ and 0.67 mM EDTA. Samples were dried in a Speed-Vac (DNASpeed Vac DNA110 Savant, ThermoFisher Scientific, Waltham, USA). Samples were stored at -20°C.

Shortly before the measurement samples were resuspended with 0,1% (V/V) formic acid in a sonification bath. Protein separation was performed by reverse phase chromatography using an UPLC Symmetry C18 Trapping-column (5 µm, 180 µm, 20 mm) and an UPLC BEH C18 column (1.7 µm, 75 µm 150 µm Waters, Eschborn Germany) on a gradient pump system (nanoAcquity UPLC, Waters, Eschborn Germany) with the following gradient: 0.4 µl·min⁻¹ (0-5 min: 2% acetonitrile (ACN); 5-10 min: 5% ACN; 10-41 min: 30% ACN; 41-46 min: 85% ACN; 46-47 min: 95% ACN; 47-60 min: 2% ACN). The samples were analysed with a mass spectrometer Orbitrap Elite Hybrid Ion Trap-Orbitrap Mass Spectrometer (Thermo FisherScientific, Waltham, USA and emitted with PicoTip Emitter, SilicaTip, 30 µm, New Objective Woburn, USA). The temperature of the columns was kept constant at 45°C. The elution of the proteins happened stepwise with a flow rate of 0.4 µl/min. The electron spray ionisation was performed between 1.5 kV and 1.8 kV. The desolvation capillary was heat up to 275°C. Iontrap and Orbitrap were operated in parallel. Precursor ions were detected within a mass to charge ratio of 300-2000 m/z with a resolution of 60.000 in the orbitrap. The Tandem MS spectra of the 20 most intensive precursor ions (TOP 20) were taken. The relative collisions energy for collision induced dissociation (CID) was set to 35%. The dynamic exclusion of ions was enabled with a timeframe of one min and a repeat count of one. Single-charged ions were also excluded. Evaluation of Data was done using Thermo Proteome Discoverer Version

Material and Methods

1.3.0.339 using the proteomic dataset of *Synechocystis*, extended by typical human contaminations. Allowed Modifications: Methionin Oxidation

2.2.15 Protein interaction studies using microscale thermophoresis (MST)

The MST experiments were analysed by Monolith™ NT.115 instrument (NanoTemper Technologies GmbH, Munich, Germany). The Protein-protein interaction experiments were performed in MST buffer (50 mM Tris, pH 7.4, 150 mM NaCl, 10 mM MgCl₂, 0,05% Tween-20) using premium coated capillaries. All measurements were detected with a LED intensity by 30% and MST Power 40% or 80%. The proteins were fluorescent labeled by using the the Monolith™ NT.115 Protein Labeling Kit Red-NHS (Amine Reactive) according to manufacturer protocol. The concentration of fluorescence labeled proteins were kept constant by 10 nM or 40 nM. All experiments were performed three times and evaluated using the MO.Affinity Analysis Software 2.2.4 (NanoTemper Technologies GmbH, Munich, Germany).

2.2.16 Accession numbers

Sequence data were taken from EMBL/CyanoBase Gene Bank library.

3. RESULTS

3.1 PrtA complex

The manganese binding protein PrtA was found to be a part of a soluble complex in the PDM that interacts with PilQ and HhoA (Heinz *et al.* unpublished data (Schotchkowski *et al.*, 2009b). PilQ has a mass weight of about ~81 kDa and is part of the PilQ family. The other interaction partner HhoA has a mass weight of 41 kD and is part of an ATP-independent serine protease that is present in bacteria and eukaryotes (Clausen *et al.*, 2002; Huesgen *et al.*, 2007; Huesgen *et al.*, 2011).

To verify this complex, *in vitro* interaction studies were performed by MST. The method allows to verify potential interaction partners and characterisation of the interaction by calculation of a dissociation constant (K_D). The proteins PrtA, PilQ N-terminally fused to a MBP-tag, MBP, the inactive form of the DegA protease HhoA C-terminally fused to a His-tag and DLA2 N-terminally fused to a His-tag were recombinantly overexpressed in *E.coli* cells and purified (Huesgen *et al.*, 2011; Bohne *et al.*, 2013) (Figure 8).

Results

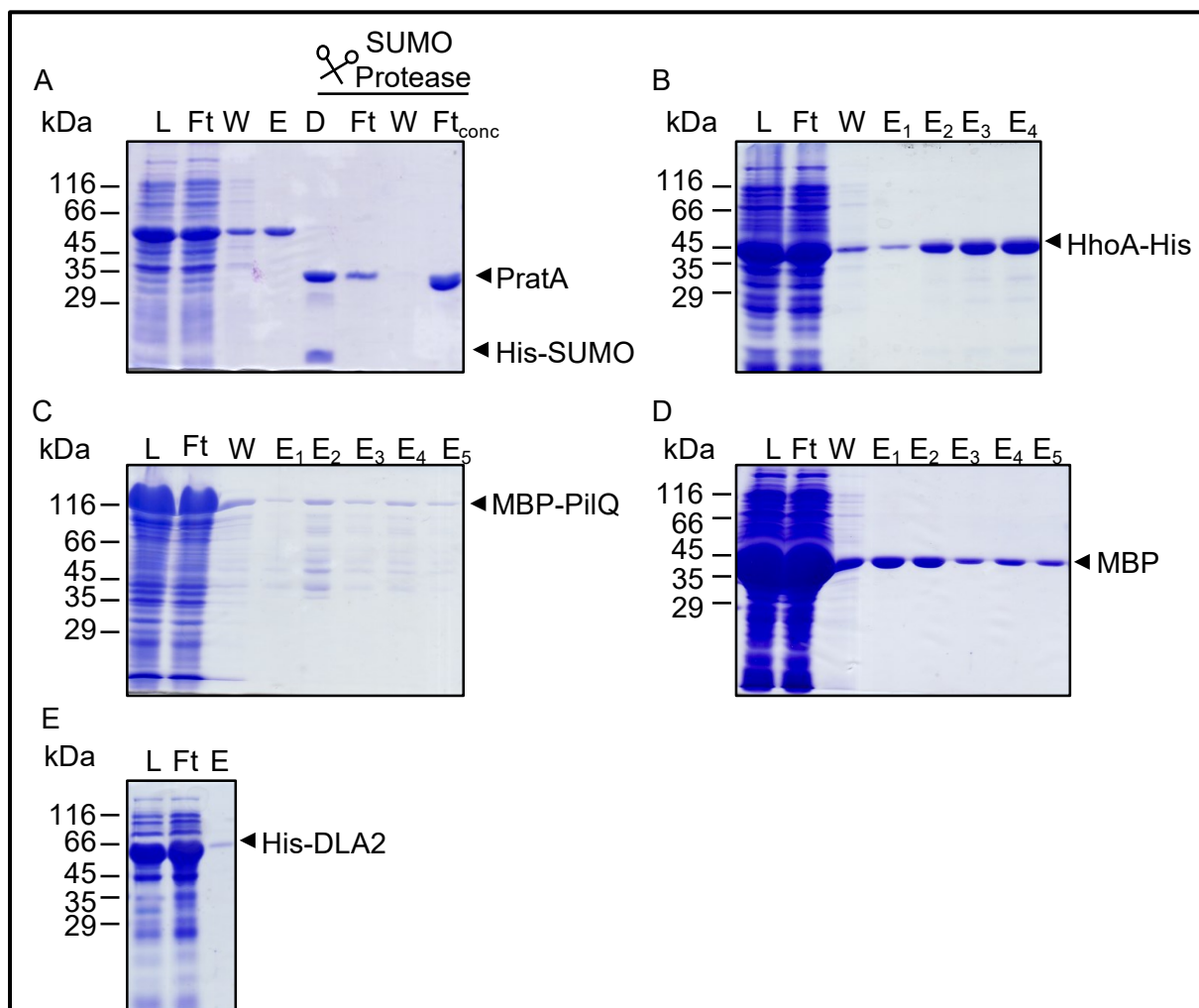


Figure 8: Purification of (A) PrtA, (B) HhoA-His, (C) MBP-PilQ, (D) MBP, (E) His-DLA2. The samples: Lysate (L), flow-through (Ft), wash (W), the digest of PrtA with the SUMO Protease (D) and eluate (E) was separated by SDS-PAGE. The Gels were subsequently stained with Coomassie brilliant blue G250.

The samples were loaded on an SDS Gel and separated by gel electrophoresis and subsequently stained with Coomassie (Figure 8). Figure 8 A shows the purification of the PrtA with Ni-NTA beads. A thick band is visible at 47 kDa in lysate, flow-through and wash fraction as well as in the eluate without treatment of the SUMO-protease. After cleavage by the SUMO-Protease the digest sample contains three bands: PrtA with a size of 35 kDa, the SUMO-Protease with a size of ~30 kDa and the His-SUMO Tag with a mass weight of 12 kDa. The Flow-through contains one band with the size of 35 kDa, this fraction was concentrated and separated in the last lane. To purify HhoA, an inactive variant of the DegA protease was used to enhance protein expression and stability (Huesgen et al., 2011). The recombinant HhoA was purified with a His-tag. The lysate as well as the flow-through has an intense band with a size of 45 kDa. Furthermore, the band is reduced in the wash fraction. The eluate fractions one to four increasing their intensity (Figure 8 B). Purification of MBP-Slr1277 is shown in Figure 8 C. The overexpressed MBP-PilQ has a size of 121 kDa that is evident in the flow-through and wash fractions. The eluate fractions one to five showing a clear more purified band

Results

of MBP-PilQ (Figure 8 C). As negative control for the MST measurements the MBP with a size of ~40 kDa was overexpressed and purified (Figure 8 D). As expected, the lysate and the flow-through reveals an intensive band with a size of 40 kDa. The wash fraction contains a 40 kDa band with some contamination. In contrast, the elution fraction contains only one band with the size of 40 kDa. The protein DLA2 from *Chlamydomonas reinhardtii* was purified by using the His-tag. The lysate and flow-through demonstrates a successful overexpression. The last band shows the purified eluate with one band at a size of 60 kD (Figure 8 E). For MST measurements the elution fractions were pooled and concentrated. Following this the recombinant purified proteins were labelled with the NT-647-NHS fluorophore before they were subjected to MST analysis (Figure 9).

Results

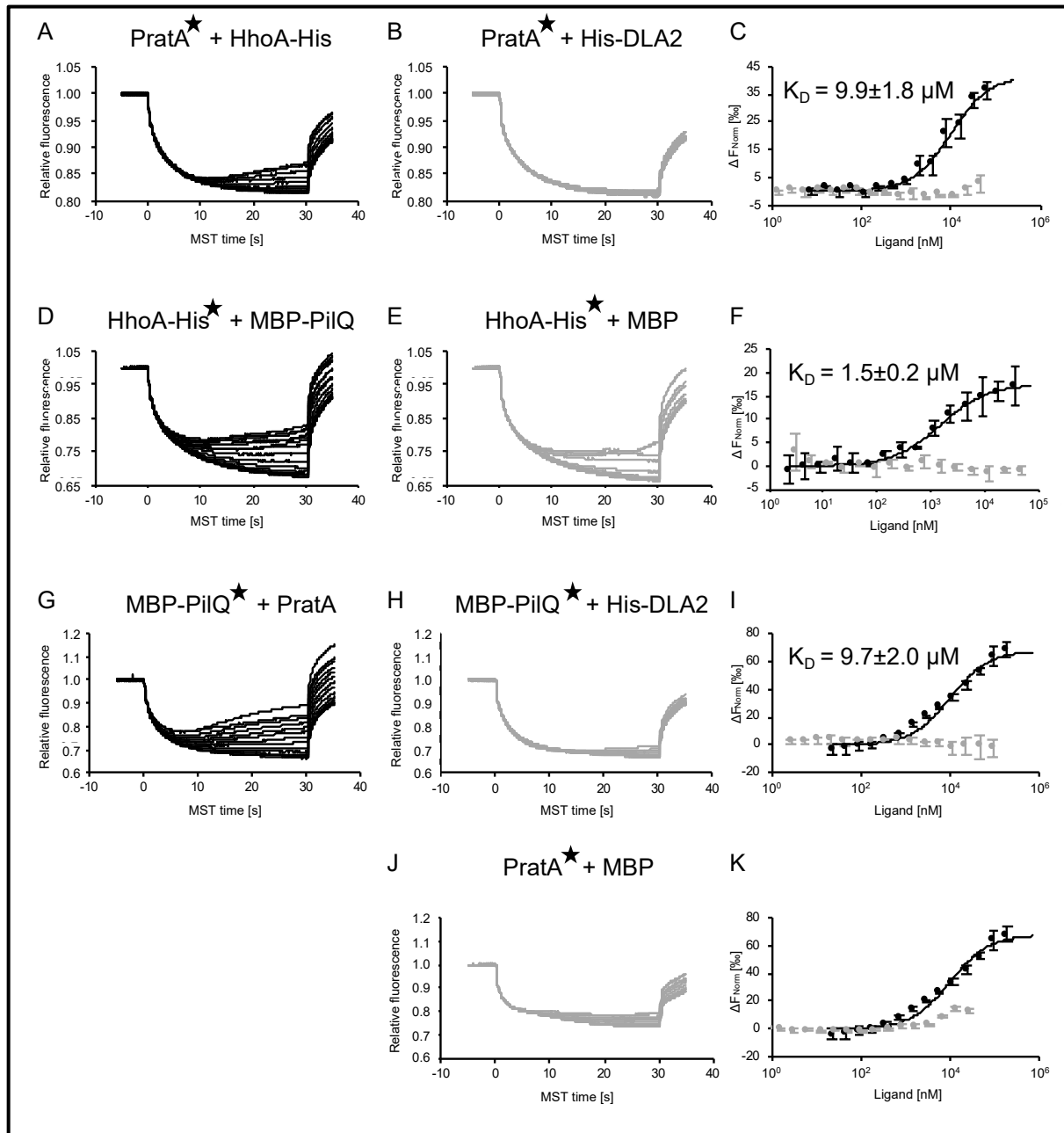


Figure 9: MST interaction studies of the PrataA interaction Partner. (A) A constant concentration of fluorescence-labeled PrataA (10 nM) was titrated with different concentrations of recombinant HhoA-His and (B) His-DLA2 (MST Power 40%, LED Power 30%). (C) The difference of the relative fluorescence (20 s MST time) was taken and plotted against the amount of ligand. (D) The fluorescence-labeled inactive recombinant form of HhoA-His (40 nM), was titrated with different concentrations recombinant Sir1277-MBP and (E) MBP concentrations (LED Power 30%, MST Power 80%). (F) The difference of the relative fluorescence (5 s MST time) was taken and plotted against the amount of ligand. (G) A constant concentration of fluorescence-labeled MBP-PilQ (40 nM) and PrataA (10 nM) was used to monitor changes in fluorescence at different concentrations of recombinant PrataA and (H) His-DLA2 (MST Power 40%, LED Power 30%). (I) The difference of the relative fluorescence (5 s MST Time) was taken and plotted against the amount of ligand. (J) In addition, 10 nM fluorescence labeled PrataA was titrated against MBP. (K) The resulting binding curve (MST time 5 s) was overlaid with the binding curve of MBP-PilQ and PrataA. Standard deviation was calculated from n=3 technical replicates.

Results

The interaction between an inactive form of HhoA-His and PrataA was first determined by MST. PrataA was fluorescence labeled and titrated with HhoA-His. His-DLA2 works as negative control. The fluorescence of data points shown in Figure 9. A and B were plotted against the ligand concentration in Figure 9 C. A fit across the datapoints demonstrates an interaction between HhoA-His and the labeled PrataA with a K_D value of $9.9 \pm 1.8 \mu\text{M}$. During negative control reveals no interaction between PrataA and His-DLA2. A similar approach was used to characterise the interaction of HhoA-His and PilQ fused to MBP. In this approach HhoA-His was fluorescent labeled and titrated against MBP-PilQ (Figure 9 D). As negative control MBP was titrated against the MBP (Figure 9 E). The plotted fluorescence against the MBP-PilQ concentration indicates a strong interaction with a K_D value of $1.5 \pm 0.2 \mu\text{M}$. The negative control demonstrates an unspecific increase of fluorescence after a long thermophoresis time but this does not affect the binding curve (Figure 9 F). To analyse the interaction between PrataA and PilQ, MBP-PilQ was fluorescence labeled and subjected to MST analysis (Figure 9 G). Interestingly, these two proteins demonstrate a binding affinity of $9.7 \pm 2.0 \mu\text{M}$ (Figure 9 I). To exclude unspecific binding, labeled MBP-PilQ and His-DLA2 was also analysed by MST (Figure 9 H). The resulting fitting curve shows no interaction (Figure 9 I). Additionally, the titration of MBP against labeled PrataA indicates no specific binding (Figure 9 J and K). In conclusion, all three proteins that have been identified as complex demonstrate a direct interaction in MST experiments.

3.2 Proteomic screen

In order to identify new PSII assembly factors, a proteomic screen based on the *prataA*⁻ mutant were performed. PrataA as marker for the PDM, allows to focus on candidates that might be involved in the early PSII assembly steps. Therefore, PDM and TM the fractions 2, 4, 6, 7 and 9 were isolated from WT and *prataA*⁻ by Dr. Steffen Heinz. To detect single peptides the particular fractions were analysed with LC-MS/MS performed by Dr. Sascha Rexroth, Ruhr-University Bochum (Figure 10).

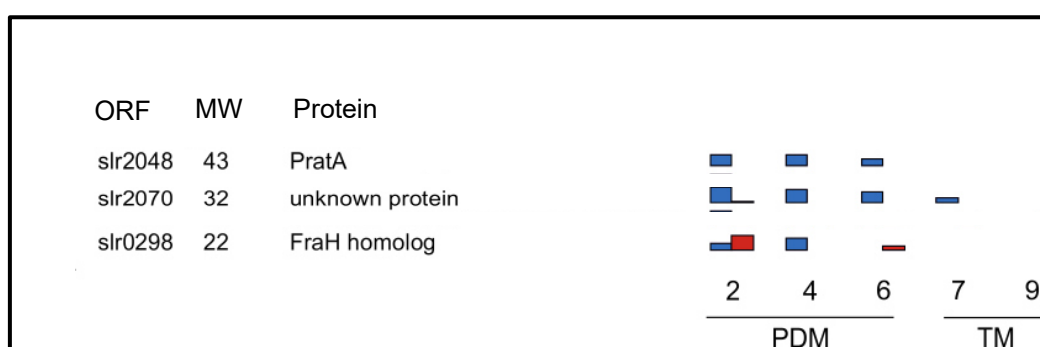


Figure 10: Mass Spectrometry analysis of PDM and TM fractions. The isolated PDM fractions 2, 4 and 6 and the TM 7 and 9 were analysed by LC-MS/MS in collaboration with the Ruhr- University Bochum. Blue barks WT and red barks *prataA*⁻.

Results

The distribution of the single detect peptides are displayed in blue balks for the WT and red balks for the strain *pratA*⁻. As negative control the ORF *slr2048*, which encodes for PrataA is shown in the first lane. The balks in the second lane reveal the distribution of the Slr2070. Based on the function that is reported in this work, the ORF *slr2070* is named anchoring of convergence membranes (*ancM*). Interestingly the peptides of AncM are only present in fraction 2 of the *pratA*⁻ mutant compared to the WT. On the other hand, the product of ORF *slr0298*, which encodes for FraH is shifted in *pratA*⁻ compared to the WT. Resulting in an increase of FraH in the PDMs in fraction 2 and the presence in fraction 6 in *pratA*⁻ compared to the WT. FraH has a mass weight of 22 kDa. Moreover, FraH is in *Anabaena* sp. Strain PCC 7120 required for heterocyst formation and has a mass weight of 22 kDa (Merino-Puerto *et al.*, 2011a).

In order to verify the reduced amount of membrane shift in the isolated fractions WT and *pratA*⁻ 2, 4, 6,7 and 9 were separated on a SAS-PAGE (Figure 11) performed by Dr. Steffen Heinz.

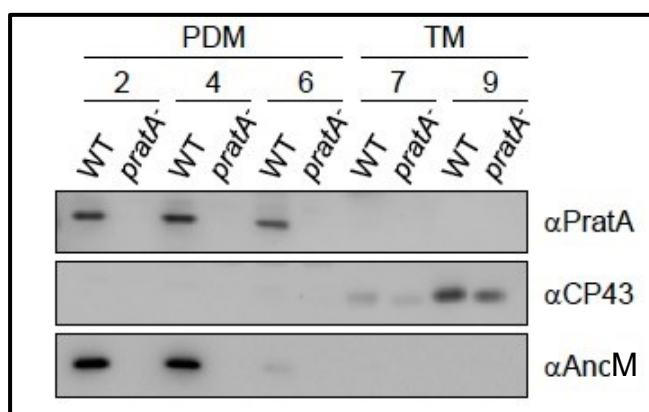


Figure 11: Membrane fractionation of WT and *pratA*⁻. The fractions 2, 4, 5, 7 and 9 of the two step sucrose gradient were separated on a SDS Page. Fractions 2, 4 and 6 represent the PDM and fractions 7 and 9 the thylakoid membranes (TM). For a comparison of the fractions the sample volume was normalised to the volume of fraction 7 containing 40 μ g protein.

As expected by mass spectrometry analysis the immunoblot demonstrates no detection of AncM in the PDM fractions in *pratA*⁻ compared to the WT. Interestingly PrataA is accompanied with AncM exclusively in the PDM. The PSII subunit CP43 is detected in WT and *pratA*⁻ at the TM (Rengstl *et al.*, 2011).

Based on this finding, a *fraH* and *ancM* knock-out mutants was created by interrupting the ORFs with a kanamycin resistant cassette (Figure 12).

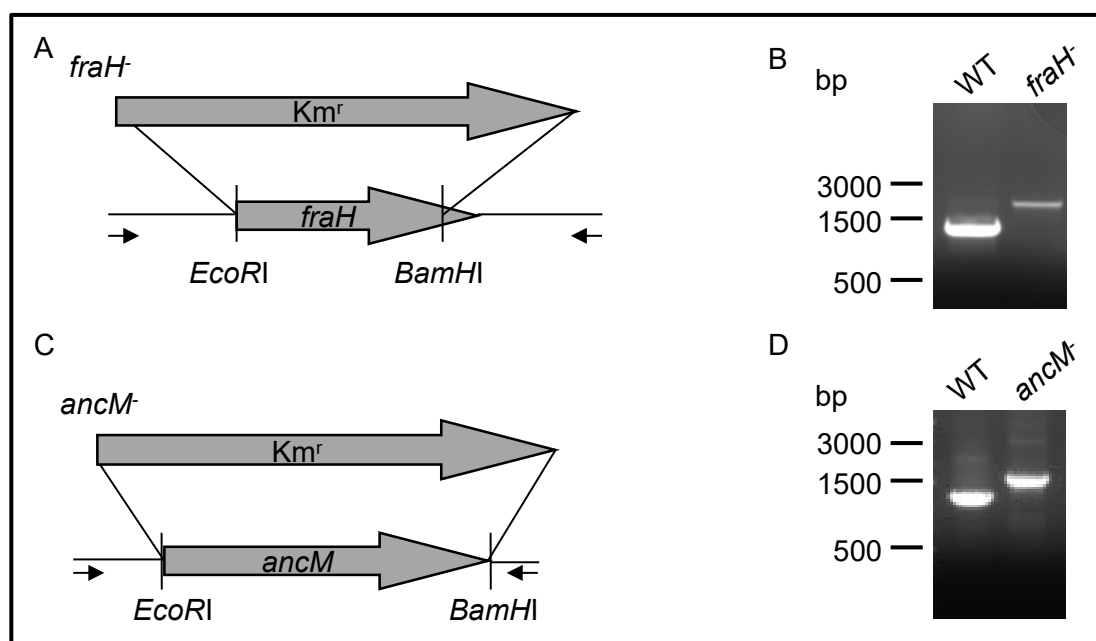


Figure 12: Strain generation of *fraH* and *ancM*⁻. (A) To interrupt *fraH* the ORF was replaced by a kanamycin resistance (Km^r) via the restriction enzymes *EcoRI* and *BamHI*. Arrows mark the position of segregation primer pair. (B) PCR segregation analysis of *fraH* with primer pair forw-*fraH*-seg / rev-*fraH*-seg. (C) Inactivation of *ancM*. The ORF was replaced by Km^r via the restriction sites *EcoRI* and *BamHI*. The arrows mark the position of the primer pair forw-*ancM*-seg / rev-*ancM*-seg. (D) PCR segregation of the WT and *ancM*.

The ORF *fraH* was interrupted by a kanamycin resistance cassette using the restriction sites *EcoRI* and *BamHI* (Figure 12 A). A complete segregation was verified by PCR analysis and was reached at a kanamycin concentration of 400 $\mu\text{g/ml}$. The PCR fragment of the WT has a size of 915 bp while the mutant fragment is 1988 bp long (Figure 12 B). The *ancM* gene was replaced by a kanamycin resistance cassette by using the restriction sites *EcoRI* and *BamHI* (Figure 12 C). The construct was transformed into *Synechocystis* WT strain by homologous recombination. Complete segregation was reached at a kanamycin concentration of 400 $\mu\text{g/ml}$. PCR analysis shows total segregation of *ancM*. As expected, the WT fragment has a size of 1217 bp in contrast to the 1579 bp of *ancM* (Figure 12 D)

In order to better understand the physiological properties of the new strains *fraH* and *ancM* the properties growth, chlorophyll amount and oxygen evolution were analysed. These physiological studies display possible effects on the photosynthetic performance (Table 12).

Results

Table 12: Strain characterisation of *fraH* and *ancM* compared to the WT.

Strain	Doubling time (h) ^a		Chlorophyll content ($\mu\text{g OD}_{750}^{-1}$) ^b	Oxygen evolution ($\mu\text{mol h}^{-1} \text{mg chlorophyll}^{-1}$) ^c
	+ glucose	- glucose		
WT	8.11 \pm 0.53	13.86 \pm 0.74	2.29 \pm 0.22	257.9 \pm 27.3
<i>fraH</i>	12.80 \pm 0.38*	14.08 \pm 0.34	2.54 \pm 0.12	180.13 \pm 5.40*
<i>ancM</i>	8.80 \pm 0.10	17.82 \pm 0.92*	2.35 \pm 0.12	^{c)} 262.52 \pm 24.03*

All data was taken from three independent biological replicates. WT was used as reference. Standard deviation was calculated, significant differences according to Student's *t* test, error probabilities of 5% are marked by one asterisks.

^{a)} Doubling time was calculated in the in presence and absence of glucose.

^{b)} The chlorophyll content is expressed in $\mu\text{g OD}_{750}^{-1}$.

^{c)} Oxygen evolution is expressed in $\mu\text{mol h}^{-1} \text{mg chlorophyll}^{-1}$, at 627 nm with a light intensity of 1000 $\mu\text{E m}^{-2} \text{s}^{-1}$.

Following this, the knock-out strain *fraH* shows a significant reduced heterotrophic growth compared to the WT. Whereas the chlorophyll content is not affected in *fraH*. This is in contrast to the oxygen evolution of *fraH* compared to the WT. However, the chlorophyll content is not affected. The loss of *ancM* cause a reduction of the photosynthetic performance apparent in photoautotrophic growth and oxygen evolution. However, the chlorophyll concentration does not differ from the WT. Hence, the oxygen evolution is halved *ancM* when compared with WT (Table 12).

3.3 Genetic screen

The loss of CurT causes a reduced photosynthetic performance. The phenotype can be suppressed by various spontaneous mutations during continues light irradiation at 30 $\mu\text{E m}^{-2}\text{s}^{-1}$. An initial genetic screen was performed by Anna Rast by whole genome sequencing of five different *sucurT* photosynthetic suppressor lines (Figure 13). The whole genome was compared with the DNA sequence of *curT* (Figure 13 A)

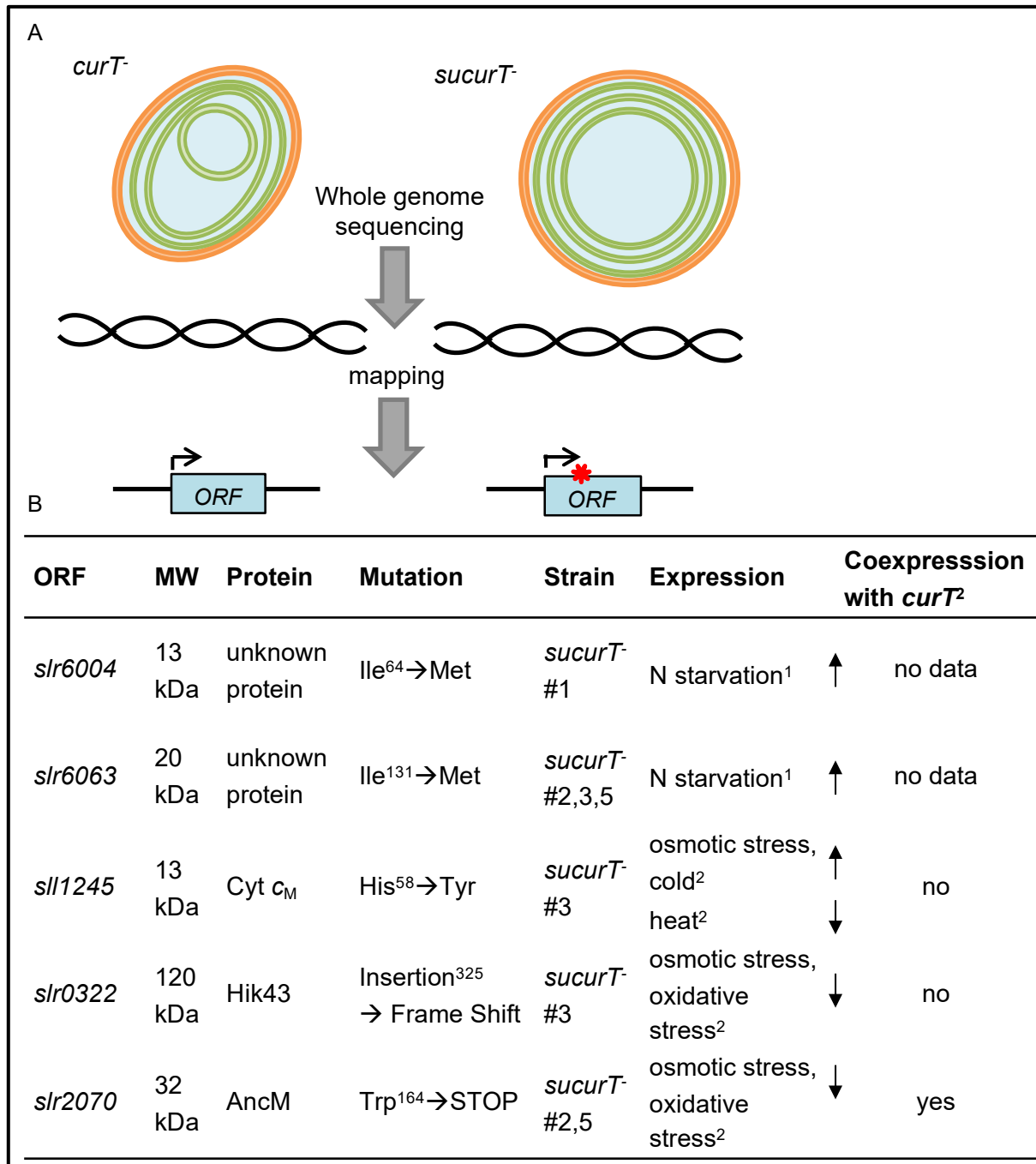


Figure 13: Genetic screen. (A) Schematic overview of the genetic suppressor screening. (B) Whole genome sequencing of suppressor strain *sucuT*⁻ #1-5. Expression of mRNA during stress conditions are listed based on transcriptomic data Kopf *et al.* 2014¹ and Hernandez-Prieto and Futschik, 2012². Co-expression data are listed based on Hernandez-Prieto and Futschik, 2012².

By mapping of the genome against each other, in total 147 mutations were observed. The mutations were ranked by frequency and effects on the translated protein, silent mutations were excluded. These critical procedures reduced the list to five candidates (Figure 13 B). The ORF *slr6004* and *slr6063* are located at the plasmid pSYSM of *Synechocystis*. Furthermore, the C-terminus of *slr6063* shows a high similarity to *slr6004*.

Results

Both ORFs contain the same point mutation in *sucurT* which leads to an amino acid exchange from isoleucine to methionine. The mutation is observed in different *sucurT* lines. The other candidates *sll1245*, *hik43* and *ancM* are on the main chromosomal encoded. The ORF *sll1245* encodes for Cytochrome c_M (Cyt c_M) with a size of 13 kDa, which contains one transmembrane domain (Cho *et al.*, 2000). Cyt c_M was first discovered by Malakhov *et al.* (1994). During stress Cyt c_M plays a role at the respiratory electron transport and replaced the electron carrier PC / cytochrome c_6 (Bernroitner *et al.*, 2009). The amino acid sequence of Cyt c_M exhibits a similarity of 35% to cytochrome c_6 and contains a hydrophobic N-terminus (Malakhov *et al.*, 1994). The ORF *slr0322* encodes for cytosolic protein Hik43 and has a size of 120 kDa (Matsusako *et al.*, 2017). The Protein prevents together with Hik35 and Rre6 autoaggregation but promotes biofilm formation under high salinity growth conditions (Kera *et al.*, 2020).

Co-expression analysis of Cyt c_M shows an increase of the expression level during osmotic stress, iron limitation and cold stress. A down-regulation of *cyt c_M* is observed during heat treatment (Hernandez-Prieto and Futschik, 2012). The ORF *hik43* demonstrates reduced expression level during osmotic stress like the treatment with sorbitol and oxidative stress (Hernandez-Prieto and Futschik, 2012). Both ORFs are affected in *sucurT* line number three. In ORF *cyt c_M* amino acid position 58 is affected by a point mutation that causes an in-amino acid exchange from histidin to tyrosine. The ORF *hik43* has a frameshift in the *sucurT* number three. Interestingly the ORF *ancM* that was also observed in the proteomic screen also popped up in the genetic screen. Furthermore, co-expression analysis reveals a down-regulation of the expression level of AncM during osmotic stress and long periods of oxidative stress. Furthermore, gene expression data indicates a co-expression of AncM together with CurT (Hernandez-Prieto and Futschik, 2012; Heinz *et al.*, 2016). A point mutation in *ancM* was observed in suppressor line number two and five. This nonsense mutation causes a STOP codon at position 164 instead of the amino acid tryptophan. *SucurT* line number two was chosen for further analysis.

Because of an easily genetic manipulation of chromosomal genes further analyses were focussed on the promising candidates *cyt c_M*, *hik43* and *ancM*.

Results

3.3.1 Primary analysis of the ORF *hik43* and *cyt c_M*

In order to characterise the ORF *hik43* and *cyt c_M* knock-out mutants were designed, and primary analyses were performed. To interrupt *hik43* and *cyt c_M* a kanamycin resistant cassette was inserted (

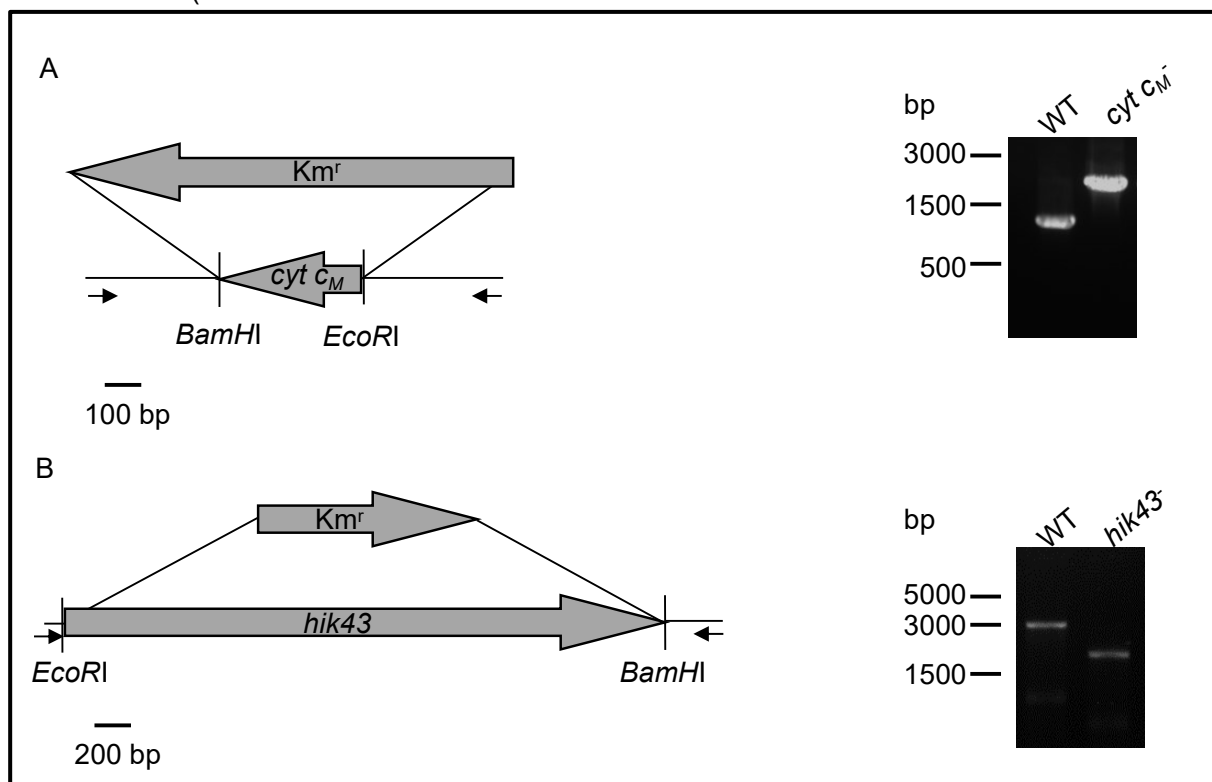


Figure 14).

Figure 14: Strain generation and PCR analysis of *hik43⁻* and *cyt c_M⁻*. (A) Cloning strategy for inactivation of ORF *cyt c_M*. (B) Segregation analysis of *cyt c_M⁻* using the primer pair forw-*cyt c_M*-seg / rev-*cyt c_M*-seg. (C) Inactivation of *hik43* with a kanamycin resistant cassette. (D) Segregation analysis of *hik43⁻* using the primer pair forw-*hik43*-seg / rev-*hik43*-seg.

As expected, the PCR fragment of the WT with the has a size of 1131 bp in contrast the single band *cyt c_M* has a size of 1961 bp (

Figure 14 B). The PCR product of *hik43⁻* has a single band with the size of 1839 bp while the WT has 966 bp more with a size of 2805 bp. Thus, PCR Segregation analysis reveals a complete segregation of *cyt c_M⁻* and *hik43⁻*. The Protein Cyt *c_M* contains one TMD at amino acid position 17 until 33. Furthermore, Cyt *c_M* has 128 amino acids, whereas Hik43 is predicted as a cytosolic protein and contains 1095 amino acids.

In order to characterise the new mutant strains the growth, the chlorophyll content and the oxygen evolution were determined from three independent biological replicates and the values are listed in Table 13.

Results

Table 13: Characterisation of *cyt c_M⁻* and *hik43⁻*.

Strain	Doubling time (h) ^a			Chlorophyll content ($\mu\text{g OD}_{750}^{-1}$) ^b	Oxygen evolution ($\mu\text{mol h}^{-1} \text{mg chlorophyll}^{-1}$) ^c
	+ glucose	- glucose	+ NaCl		
WT	8.11 \pm 0.53	13.86 \pm 0.74	13.42 \pm 0.36	2.29 \pm 0.22	257.9 \pm 27.3
<i>cyt c_M⁻</i>	7.23 \pm 0.07	17.01 \pm 0.23*	15.28 \pm 0.97*	2.13 \pm 0.11	213.9 \pm 30.1
<i>hik43⁻</i>	8.00 \pm 0.78	15.96 \pm 0.29	n.a	2.70 \pm 0.8	258.3 \pm 13.91

All data was taken from three independent biological replicates. WT was used as reference. Standard deviation was calculated, significant differences according to Student's *t* test, error probabilities of 5% are marked by one asterisks.

^aDoubling time was calculated in the in presence and absence of 5 mM glucose, as well as with 500 mM NaCl.

^bThe chlorophyll content is expressed in $\mu\text{g OD}_{750}^{-1}$.

^cOxygen evolution is expressed in $\mu\text{mol h}^{-1} \text{mg chlorophyll}^{-1}$, at 627 nm with a light intensity of 1000 $\mu\text{E m}^{-2}\text{s}^{-1}$.

Growth studies of *cyt c_M⁻* and *hik43⁻* knock-out mutants reveal no significant change compared to the WT during photoheterotrophic growth (Table 13). In contrast, the photoautotrophic growth is significantly reduced for *cyt c_M⁻*. The oxygen evolution is not significantly affected in either strains. In addition, *cyt c_M⁻* indicates an increase of the doubling time during osmotic stress (Table 13). In order to determine the oxygen consumption of WT and *cyt c_M⁻* the oxygen concentration was measured in dark after an illumination with different light intensities. The single values after the illumination with 30 μE and 120 μE were visualised in a balk diagram (Figure 15)

Results

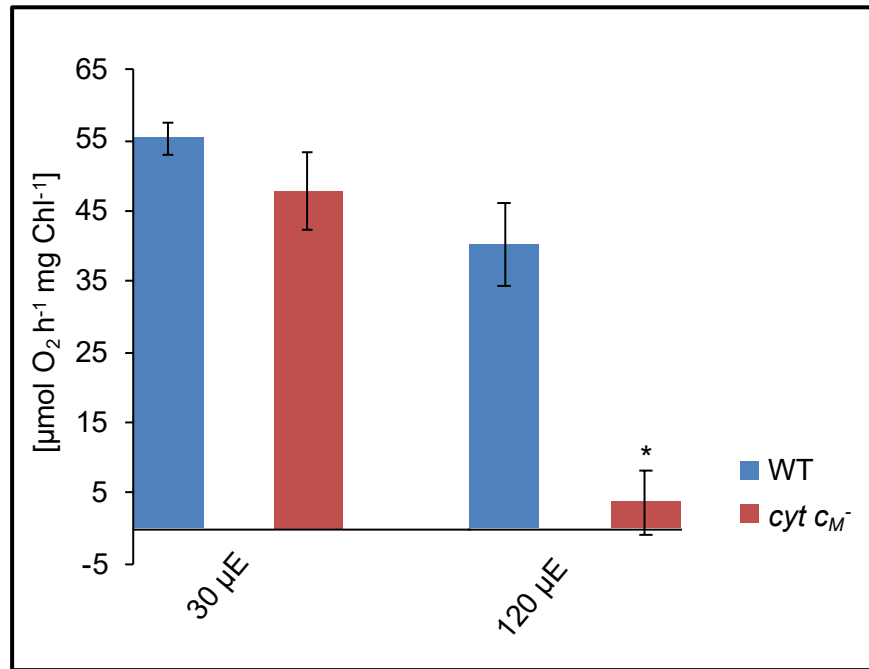


Figure 15: Oxygen consumption of WT (blue) and *cyt c_M^-* (red) after illumination with 30 $\mu\text{E m}^{-2}\text{s}^{-1}$ and 120 $\mu\text{E m}^{-2}\text{s}^{-1}$. Oxygen consumption was measured in dark after incubation for 5 min at 30 $\mu\text{E m}^{-2}\text{s}^{-1}$ / 120 $\mu\text{E m}^{-2}\text{s}^{-1}$, 627 nm. The data was tested with student's *t* test with error probabilities of 5%.

The oxygen consumption in *cyt c_M^-* with 47.77 $\mu\text{mol O}_2 \text{ h}^{-1}$ per mg chlorophyll is not affected compared to WT with 55.2 $\text{O}_2 \text{ h}^{-1}$ per mg chlorophyll at 30 $\mu\text{E m}^{-2}\text{s}^{-1}$. After illumination with 120 $\mu\text{E m}^{-2}\text{s}^{-1}$ a significant reduction of the oxygen consumption is observed for *cyt c_M^-* compared to the WT according to student's *t* Test (Figure 15).

3.4 Analysis of *ancM*

The ORF *ancM* which is coexpressed together with *curT* and was found independently in the genetic and proteomic screen. Based on these finding this work is focused on the function of AncM. AncM is expressed in a transcriptomic unit together with the ORF *slr2071* (Kopf *et al.*, 2014). AncM contains 284 amino acids with a theoretical mass weight of 31.87 kDa (Figure 16).

Results

```

MLNVRRLHPN SKLAIGTFSI CVREASVDDT YQGYINRVAP QTLAIAYEQQ LINAQGSPKF : 60
DQGQPVFPFG FSVVTFIAAD DPTNQSFYGH LTTVQGQVGE: ILGESFVAVP PESLHLTVAD: : 120
LIWDG:PYQAL RRHNPDFEQ LCNCLQHSFA DHQHSQSGPYS GCQWQVLGLL VLPRSLGVVL : 180
VPQREADYEP ILKVRRAIFQ NPTLIGLGIE QQYRYTAHIT LGYFDPAIEK LADSIGVSEQ : 240
LAAVNDRWIG HDPEILDIHS IELRYFSDMT QFTRQDYYPV LRAS : 284
  
```

Figure 16: Amino acid sequence of AncM. Position of transmembrane domains (TMD) marked in grey. AncM contains 284 amino acids with a mass weight of 31.87 kDa. DUF1868 marked with broken line box. The nonsense mutation in *sucurT* marked by one red asterisks.

The amino acid sequence has homologues in cyanobacteria (Altschul *et al.*, 1997). Following this, no hits in higher plants or algae were found. Moreover, AncM contains a domain of unknown function (DUF) 1868 region which is part of the 2H phosphoesterase superfamily (Mazumder *et al.*, 2002). Beside the DUF1868 domain, a putative TMD is predicted from the amino acid position 165 to 180. Furthermore, the amino acid sequence of AncM Protein contains in the *sucurT* a STOP codon instead of the amino acid tryptophan (see also Figure 13).

3.4.1 Recombinant overexpression of AncM for antibody production

In order to purify AncM for antibody production the whole gene/ORF of *ancM* was fused N-terminally to the MBP from *E.coli* with a size of 40 kDa (Guan *et al.*, 1988). The predicted size of MBP-AncM is ~72 kDa. The purification of the whole protein tagged MBP allows to keep the AncM in solution (Figure 17).

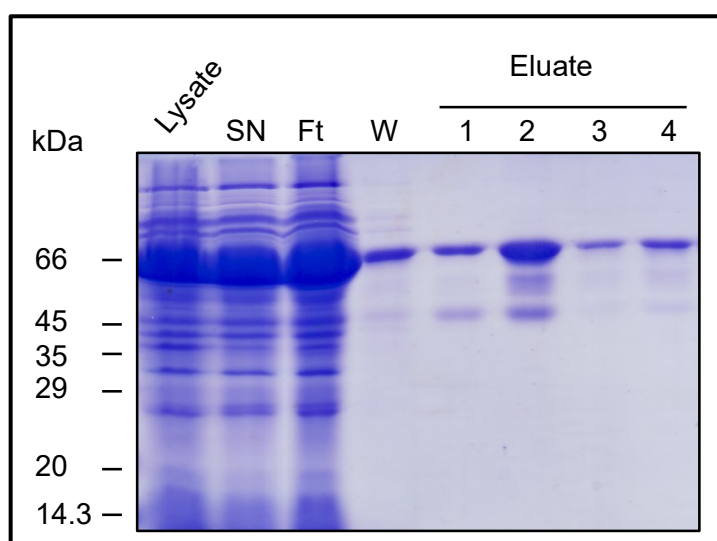


Figure 17: Purification of MBP-AncM. Coomassie blue stained SDS-Gel. Different samples of the purification steps were load on a SDS-Gel: 30 μ l of Lysate: (disrupted cells after induction with 1 M IPTG), 30 μ l of SN: supernatant, 30 μ l of Ft: Flow through, 30 μ l W: wash and 5 μ l eluted fractions 1-4.

Results

The tag binds to amylose and was eluted in four fractions with an excess of maltose. A successful overexpression is shown at the lysate. A high accumulation of MBP-AncM in the flow through and wash fractions indicates that a high amount of the protein is not bound to the amylose resin beads. The highest yield got eluted in fraction two. Following this, the elution fractions contains contamination bands at ~55 kDa and ~45 kDa. Degradation of MBP-AncM can't be excluded (Figure 17). For antibody production fractions 1 and 4 were concentrated to 1 mg/ml and sent to Pineda antibody service.

After 71 days of incubation in a rabbit the α AncM serum was tested on lysed *Synechocystis* WT and *ancM* cells as negative control. By comparison of WT with the mutant, a specific band around 28 kDa was found. Cross reactions with the cell lysate are visible at ~66 kDa (Figure 18 A). For determination of antibody titer from anti AncM purified MBP-AncM in various concentrations were analysed on an immunoblot. As shown in Figure 18 B the strongest signal is visible at a concentration of 1 μ g of recombinant protein. The lowest detectable protein concentration is 10 ng.

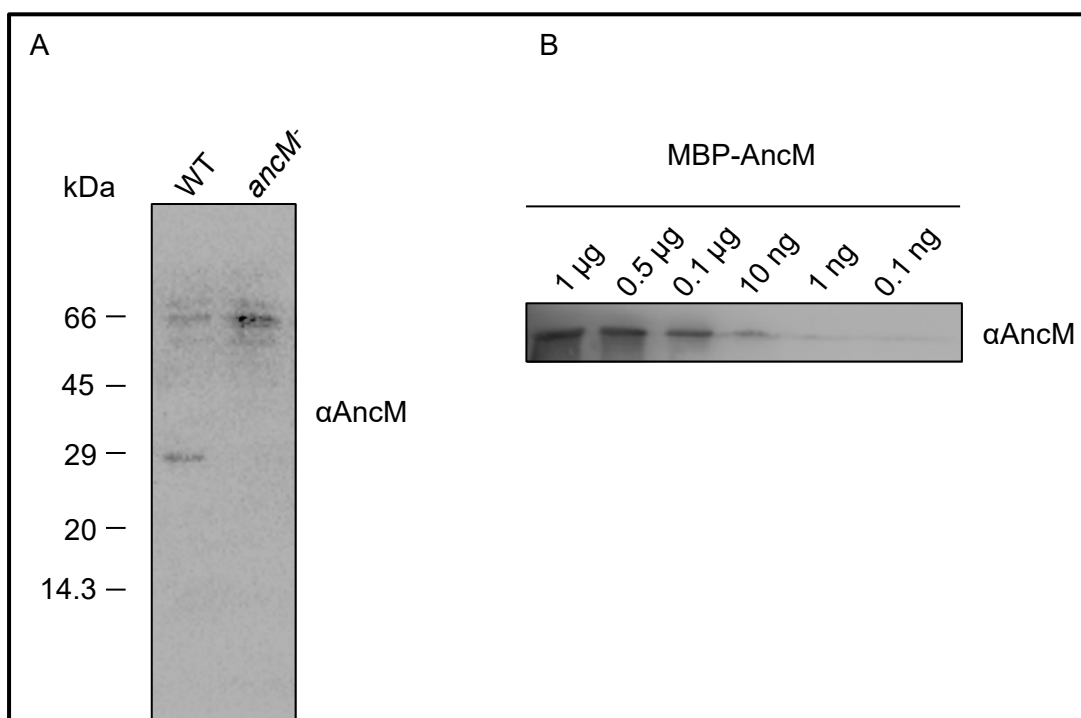


Figure 18: Analysis of anti AncM Serum. (A) Specificity of anti AncM Serum. 30 μ g extracted total proteins from WT and *ancM* *Synechocystis* cells were separated on a SDS Gel and blotted on a nitrocellulose membrane. α AncM were incubated 1:1000 overnight. Exposure time: 120s. (B) Titer determination of α AncM. Different concentrations of purified MBP-AncM were analysed by an immunoblot. α AncM Serum was used at 1:1000, exposure time: 10 s.

3.4.1 Generation of *ancM* related strains

To get a better knowledge of the suppressor mutation at amino acid position 164 the *ancM* related strains *ancM::ancM*, *ancM*^{W164STOP}, *ancM curT*, *ancM*^{W164HisSTOP} and *slr2071*⁻ were cloned by using different strategies (Figure 19). The resulting plasmids were integrated into

Results

the genome of *Synechocystis* by homologues recombination. In order to select the strains, antibiotic resistance cassettes kanamycin (or chloramphenicol) were used.

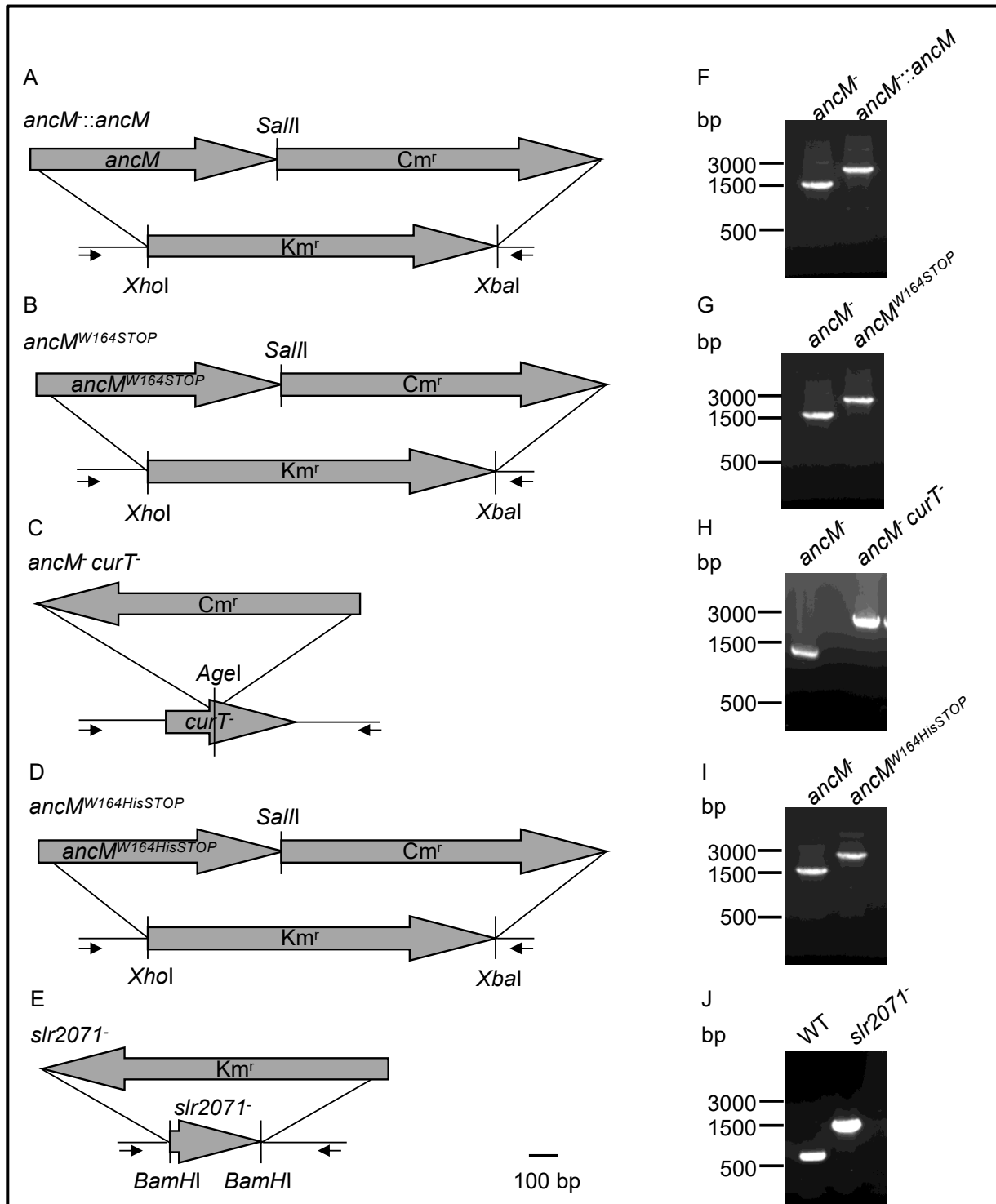


Figure 19: Construction of *ancM::ancM*, *ancM*^{W164STOP}, *ancM* *curT*⁻, *ancM*^{W164HisSTOP}, *slr2071*⁻. Strategy for inactivation of *ancM*, *curT*, *slr2071* or complementation of *ancM* including the exchange of STOP/HisSTOP instead of the tryptophan (W) mutation at amino acid position 164 by using the resistance cassettes for Kanamycin (Km^r) or Chloramphenicol (Cm^r). (F-J) Arrows mark the position of primers which were used for PCR segregation analysis of WT and mutant DNA. Bar 100 bp.

In order to create the complement line *ancM::ancM* and the *ancM*^{W164STOP} line the *ancM* was complemented with both the WT gene as well as with a truncated version of the gene

Results

harbouring a STOP codon instead of a tryptophan at the amino acid position 164 of the ORF *ancM*. To this end, a chloramphenicol resistant cassette was fused to the ORF *ancM* by using the restriction Enzyme *Sall*. Subsequently, the two constructs were integrated into the genome by replacing the kanamycin cassette in the *ancM* line (Figure 19 A and B). Total segregation was achieved at a chloramphenicol concentration of 8-10 µg/ml. Thereby the PCR fragment of the *ancM* was 1579 bp and those of the mutant strains *ancM::ancM* and *ancM^{W164STOP}* 2365 bp (Figure 19 F and G). In order to interrupt *curT* in *ancM* a chloramphenicol resistance cassette was inserted in 3'-'5 direction of *curT* (Figure 19 C) (Heinz *et al.*, 2016b). The strain *ancM curT⁻* was completely segregated at 10 µg/ml chloramphenicol and 400 µg/ml kanamycin. As demonstrated by PCR analysis, the mutant shows a PCR fragment size of 2211 bp and the WT a fragment size of 1025 bp (Figure 19 H). A hexa histidine-tag was inserted by PCR within the construct of *ancM^{W164STOP}* after the amino acid position 164 (Figure 19 D). The resulting plasmid was transformed into *ancM*. A complete segregation was reached at a chloramphenicol concentration of 10 µg/ml. As expected, the PCR fragment of *ancM^{W164HisSTOP}* has a size of 2389 bp and the *ancM* has a size of 1579 bp (Figure 19 I). In order to interrupt *slr2071* the ORF was replaced by a kanamycin resistance cassette in 3'-'5 direction (Figure 19 E). A total segregation was achieved at a kanamycin concentration of 400 µg/ml. As was calculated, the size of the mutant PCR fragment is 1541 bp in contrast to the WT size of 743 bp (Figure 19 J).

Western analysis of *ancM* and related strains demonstrated a successful knock-out of ORF *ancM* and *curT* in *ancM*, *curT⁻* and *ancM curT⁻* (Figure 20).

Results

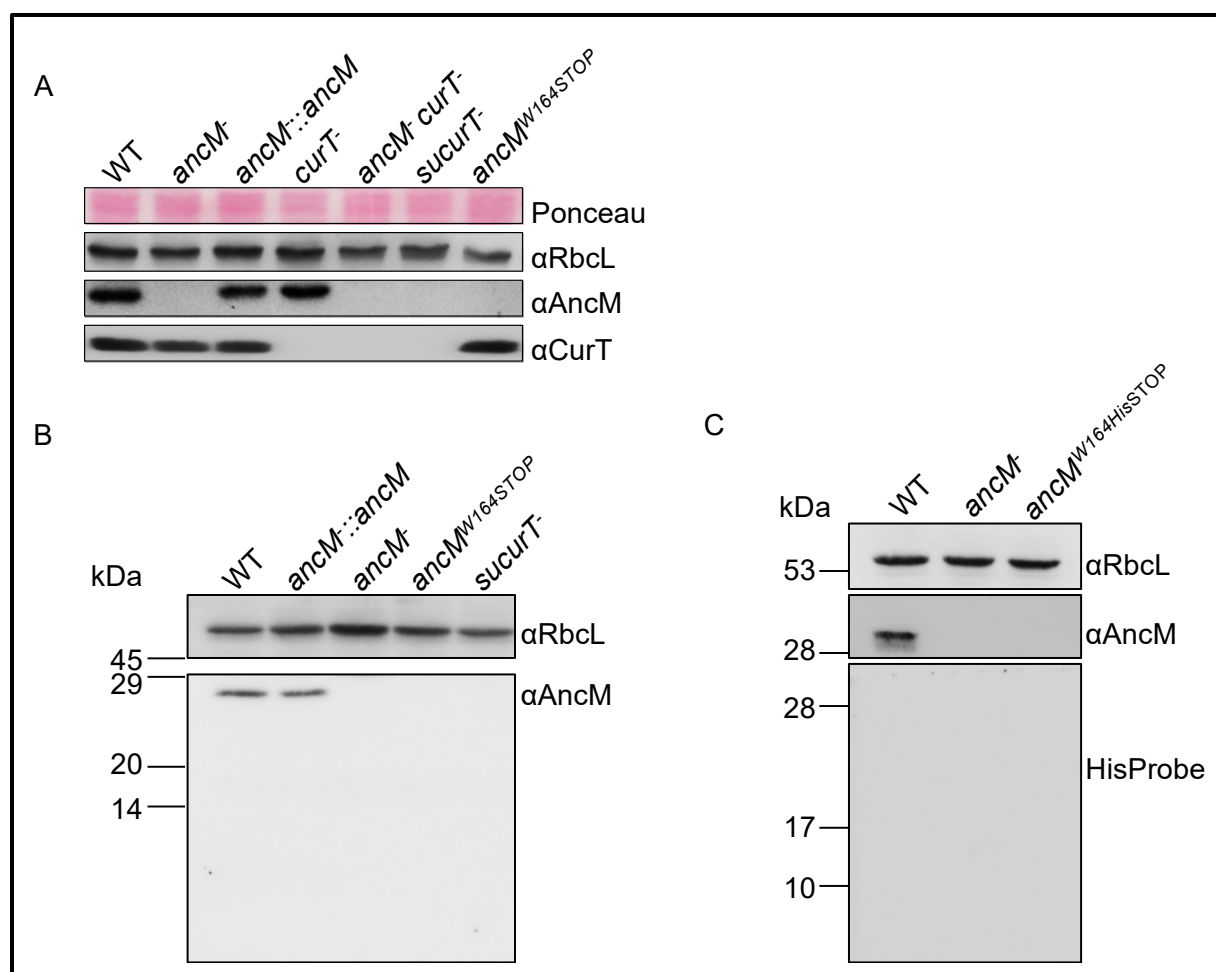


Figure 20: Accumulation of AncM in different strains. Proteins (30µg) were extracted and separated on a SDS-PAGE. (A) AncM, CurT and control large subunit of RubisCo (RbcL) were detected by an immunoblot. As a loading RbcL was visualised by staining with Ponceau. (B) Putative N-Terminus in *ancM^{W164STOP} sucuT-*. (C) Expression of putative N-terminus was detected in *ancM^{W164HisSTOP}* using a His HRP Konjugate (VWR)

The strain *sucuT-* displays no immunodetection of AncM and CurT. In addition, *ancM^{W164STOP}* has no signal of AncM but CurT still exist. An equal loading of all samples is shown by RubisCo stain with Ponceau and the immunosignal of the large subunit of RubisCo (RbcL) (Figure 20 A). In addition, the extended immunoblot (see Figure 20 B) reveals no immunosignal of α AncM in the strains *ancM*, *ancM^{W164STOP}* and *sucuT-*. Furthermore, a possible function of the N-Terminus of AncM was considered with a His tag line *ancM^{W164HisSTOP}*. Following this the His tag shows no signal via the His Probe (Figure 20 C)

3.4.2 *ancM* has a photosynthetic phenotype

In order to characterise the new mutant strains regarding to their physiological properties the heterotrophic and the photoautotrophic growth as well as the chlorophyll content and the oxygen evolution was measured. The average values and the standard deviation of each strain are listed in Table 14. The WT values were taken as a reference. See also Table 12 with the physiological characterisation of *ancM*. For better comparison by an

Results

affected chlorophyll content the oxygen evolution was also expressed in $\mu\text{mol h}^{-1} \text{mg chlorophyll}^{-1}$.

Table 14: Growth conditions and physiological characterisation of *ancM* related strains.

Strain	Doubling time (h) ^a		Chlorophyll content ($\mu\text{g OD}_{750}^{-1}$) ^b	Oxygen evolution ^{c,d}
	+ glucose	- glucose		
WT	8.54 ± 0.49	13.46 ± 0.67	2.40 ± 0.06	c) 495.62 ± 13.83 d) 212.42 ± 5.87
<i>ancM</i>	8.80 ± 0.10	17.82 ± 0.92*	2.35 ± 0.12	c) 262.52 ± 24.03* d) 116.85 ± 7.11*
<i>ancM::ancM</i>	9.27 ± 0.14	13.95 ± 0.55	2.55 ± 0.11	c) 527.49 ± 16.14 d) 217.28 ± 16.08
<i>sucurT</i> ⁻	13.55 ± 0.88*	18.58 ± 0.41*	1.63 ± 0.15*	c) 345.68 ± 41.22* d) 211.69 ± 9.65
<i>curT</i> ⁻	16.10 ± 0.65*	39.84 ± 1.83*	1.68 ± 0.03*	c) 147.65 ± 5.81* d) 81.60 ± 3.71*
<i>ancM</i> ^{W164STOP}	9.16 ± 0.52	15.56 ± 1.70	2.06 ± 0.10*	c) 348.17 ± 23.01* d) 179.10 ± 4.06*
<i>ancM curT</i> ⁻	10.94 ± 0.48*	14.20 ± 0.26	2.36 ± 0.13	c) 363.80 ± 2.29* d) 154.76 ± 9.05*

All data was taken from three independent biological replicates. WT was used as reference. Standard deviation was calculated, significant differences according to Student's *t* test, error probabilities of 5% are marked by one asterisks.

a) Doubling time was calculated in the in presence and absence of 5 mM glucose.

b) The chlorophyll content is expressed in $\mu\text{g OD}_{750}^{-1}$.

c) Oxygen evolution is expressed in $\text{nmol h}^{-1} \text{OD}_{750} \text{unit}^{-1}$.

d) Oxygen evolution is expressed in $\mu\text{mol h}^{-1} \text{mg chlorophyll}^{-1}$.

As a result, the photosynthetic phenotype of *ancM* can be reversed by complementation. The doubling time of *sucurT*⁻ in the absence of glucose is with 38% significantly slower compared to the WT and the chlorophyll concentration is reduced compared to the WT. Additionally, the oxygen evolution per OD_{750} is significantly reduced. Based on the reduced chlorophyll content in *sucurT*⁻, compared to the WT, the oxygen evolution per mg chlorophyll is not reduced. Taken together, the data *sucurT*⁻ displayed a moderate photosynthetic phenotype compared to *curT*⁻. However, the STOP mutation in *ancM*^{W164STOP} causes a slight, not significantly reduced growth rate in the absence of glucose compared to the WT. Following this, the chlorophyll content is significantly reduced compared

Results

to the WT. Beside the reduced chlorophyll content, the oxygen evolution is negatively affected by the nonsense mutation. Moreover, in comparison with the mutant strain *ancM* the photoautotrophic growth and the oxygen evolution of *ancM^{W164STOP}* is increased. For further analysis a double knock-out line *ancM curT* was created. Interestingly, the photoautotrophic growth and the chlorophyll concentration seem not affected in *ancM curT*. In contrast, the oxygen evolution and the heterotrophic growth is significantly reduced. Taken this data together, this suggests that the absence of AncM mitigates the photosynthetic phenotype of *curT*. On the other hand, the photosynthetic performance seems increased by the absence of CurT in *ancM* (Table 14).

The ORF *slr2071* is expressed in the same transcriptomic unit as *ancM* (Kopf *et al.*, 2014). In order to check if *slr2071* has a photosynthetic phenotype, growth studies with *slr2071⁻* was performed. The presence of AncM in *slr2071* was verified on an immunoblot (Figure 21)

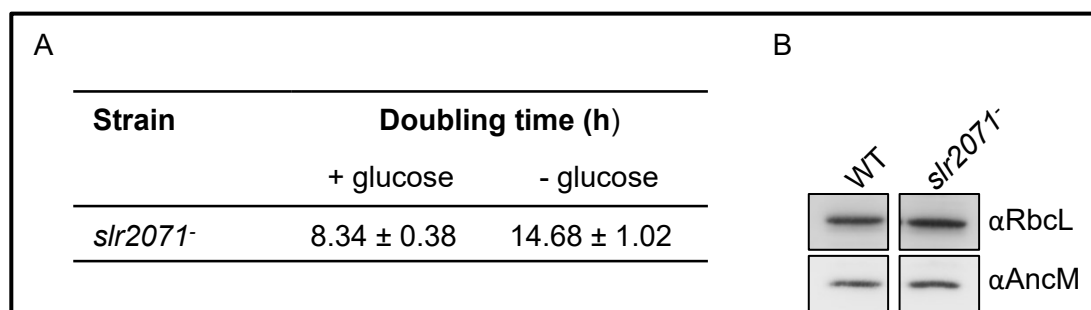


Figure 21: Analysis of *slr2071*. (A) Growth analysis of *slr2071⁻* in BG11 media in the presence and absence of 5 mM glucose, 30°C, 30 μ E. (B) Western analysis of *ancM*. Proteins of WT and *slr2071⁻* were extracted and separated on a SDS-PAGE. The Proteins RbcL and AncM were detected by an immunoblot.

Compared to WT (see Table 14) no significant changes in *slr2071⁻* heterotrophic and photoautotrophic growth were observed (Figure 21 A). In addition, Western blot analysis of the whole cell lysate from WT and *slr2071⁻* reveals a band detected by α AncM. As a loading control the subunit of RubisCo RbcL was used (Figure 21 A).

3.4.3 The effect of highlight treatment in *ancM* and related strains

In order to obtain better insight into the physiological properties, the cells were grown under highlight conditions for four days. The doubling was calculated for each strain and listed in (Table 15).

Results

Table 15: The effect of highlight stress on *ancM* related strains (*ancM::ancM*, *curT*⁻, *sucurT*⁻, *ancM*^{W164STOP}, *ancM curT*⁻, *slr2071*⁻). Cells were grown for 72 h under highlight 200 $\mu\text{E m}^{-2}\text{s}^{-1}$, 30°C doubling time of three independent replicates were calculated. Error probabilities ($p \leq 0.05$) were calculated using students *t* test and marked by one asterisk.

Strain	Doubling time (h)
WT	10.07 \pm 0.41
<i>ancM</i>	13.21 \pm 0.17*
<i>ancM::ancM</i>	10.23 \pm 0.18
<i>ancM</i> ^{W164STOP}	10.84 \pm 0.32
<i>sucurT</i> ⁻	11.58 \pm 0.24*
<i>curT</i> ⁻	13.37 \pm 0.06*
<i>curT ancM</i> ⁻	10.82 \pm 0.33
<i>slr2071</i> ⁻	10.32 \pm 0.55

By comparing the WT with *ancM* the growth rate of the mutant is significantly increased. Hence the doubling time of *curT*⁻, and the suppressor line is increased. Moreover, the complementation line, *ancM*^{W164STOP}, *curT ancM*⁻ and *slr2071*⁻ mutations shows no significant change of growth under high light conditions (Table 15).

In order to get an idea of a putative multimeric complex, the isolated MBP-AncM Protein and isolated PDM fractions were separated on a native gradient Gel. The several bands were stained by Coomassie blue (Figure 22 A). Furthermore, to detect a putative super complex *in vivo*, the isolated PDM fractions were separated on an BN-PAGE and α AncM got detected by an immunoblot (Figure 22 B).

Results

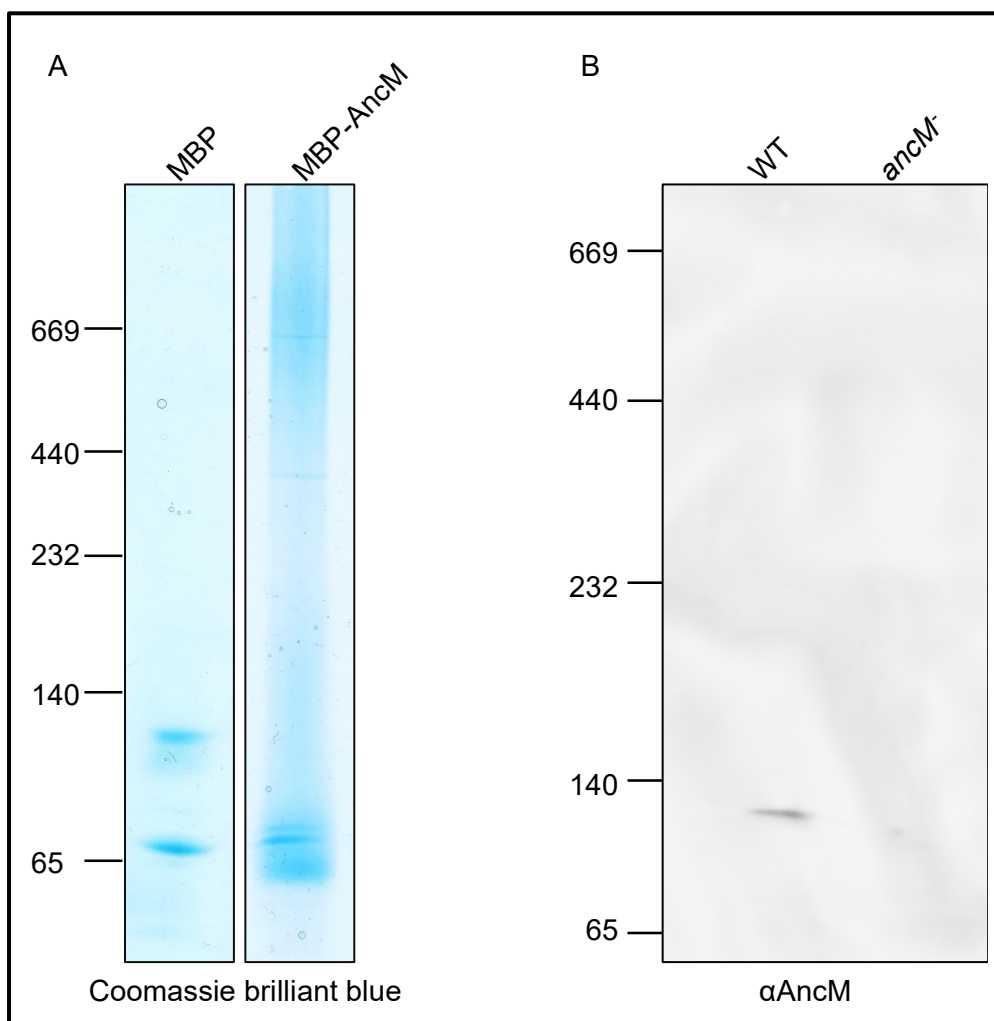


Figure 22: Super complex formation of AncM. (A) Recombinant MBP and MBP-AncM from *E.coli* was separated on a 4.5%-12% BN-Gel. Bands were stained with Coomassie R250 brilliant blue. Arrows mark the position of putative MBP-AncM complexes. (B) Isolated PDM fractions from WT and *ancM* 1-6 were pooled and 500 μ g was solubilised with 1.3% β -DM and subsequently separated on a 4.5%-12% BN-Gel. Afterwards the gel was directly blotted on nitrocellulose membrane and AncM detected by α AncM.

The stained bands indicate that recombinant MBP-AncM is able to form *in vitro* multimeric complexes. Based on the size of the stained bands and the mass weight, it is surmised that the formed complexes are higher molecular weight complexes like tetramers, pentamers, and nonamers. In addition, MBP alone forms aggregates with a size of 80 kDa and 120 kDa (Figure 22).

3.4.4 Molecular phenotype of *ancM*

In order to focus on the molecular phenotype of *ancM*, western blots with whole cell lysates were performed and the abundance of subunits from photosynthetic complexes and CurT were analysed (Figure 23 A)

Results

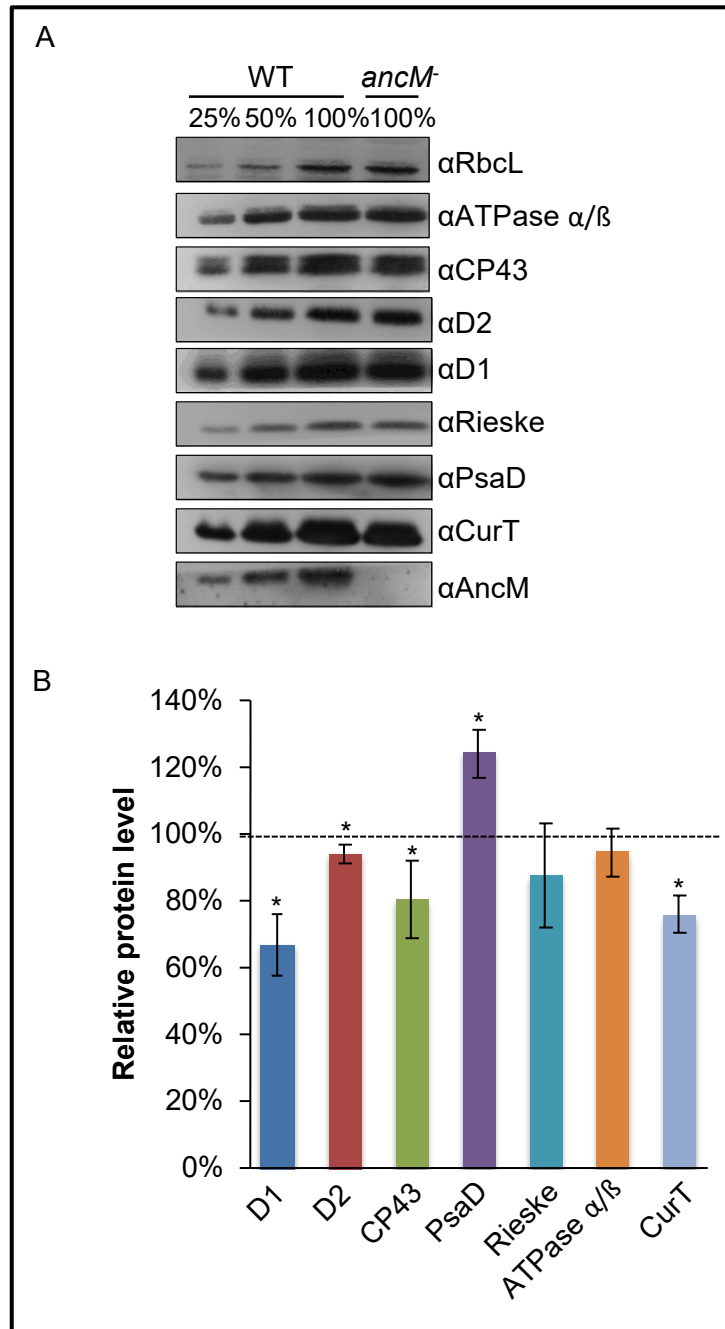


Figure 23: Accumulation of various proteins in *ancM*. (A) Whole cell extract Proteins (30µg) from WT and *ancM* were separated by SDS-PAGE and analysed on western blots using different antibodies. (B) Bar diagram illustrates the levels of different proteins compared to WT samples. Significant changes according to Students *t* test with error probabilities of 5% are marked by one asterisk.

PSII subunits show a significant reduction in *ancM*. The core subunits D1 and D2 are reduced with 33% and 6% in the mutant strain *ancM*. Moreover, the inner antenna protein CP43 of PSII is 20% reduced in *ancM*. The extrinsic subunit of PSI PsaD exhibits a significant increase of 24% compared to the WT (Figure 23 B). The membrane-bound protein CurT accumulates with 76% of the WT level in the mutant. The ATPase α/β subunits and Rieske protein are not affected (Figure 23 B).

Results

In order to confirm a reduced photosynthetic activity of *ancM* P_{700}^+ reduction and relative electron transport rate measurements were performed in collaboration with Ruhr-University Bochum, Prof. Dr. Marc Nowaczyk (Figure 24).

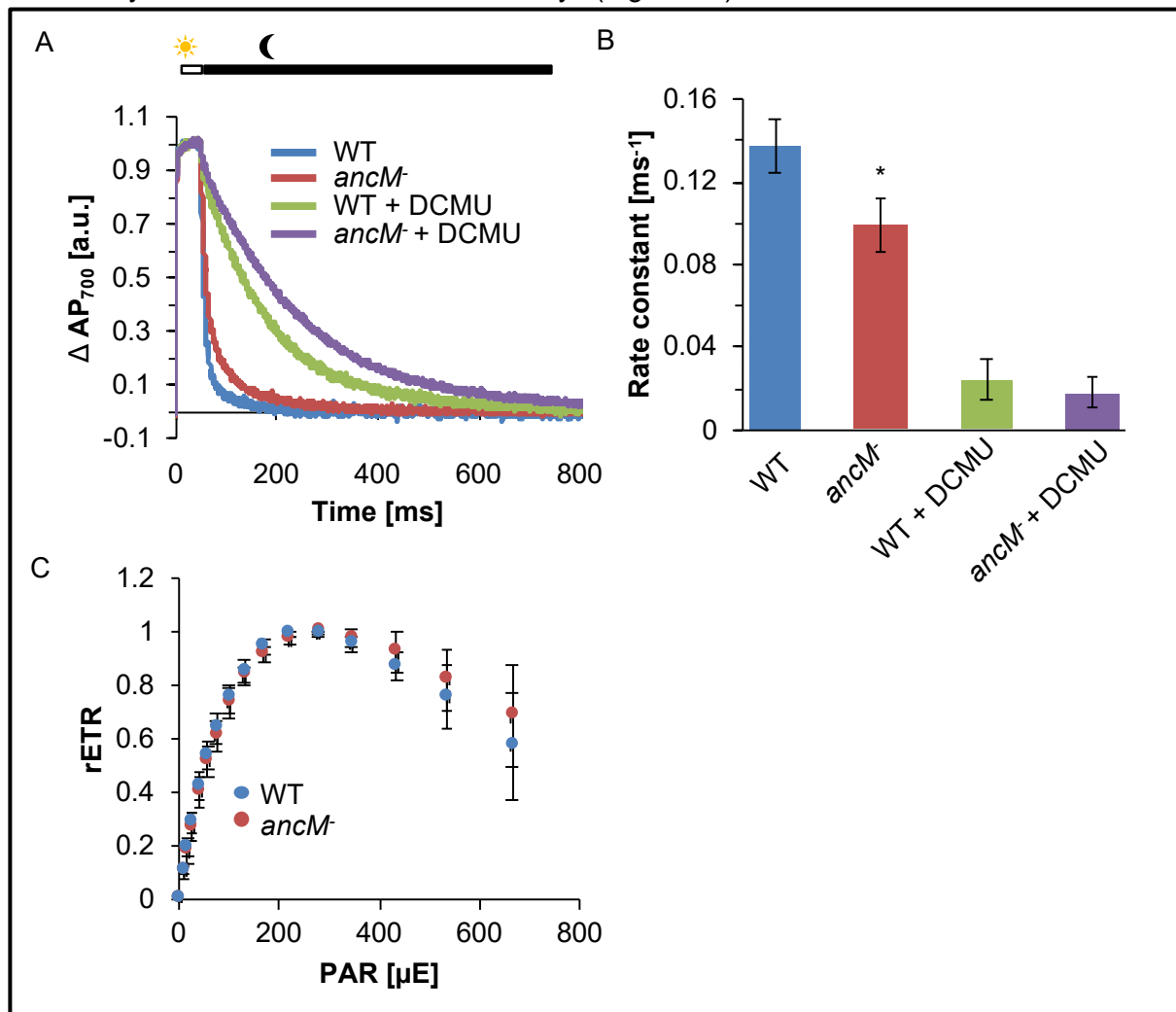


Figure 24: P_{700}^+ Reduction kinetics and relative electron transport rate. All measurements were performed in whole cells. (A) The absorption at 700 nm was measured after a 50 ms multiple turnover pulse ($10,000 \mu E m^{-2} s^{-1}$). The average of 10 traces in the presence and absence of DCMU was taken. (B) Bar diagram of the P_{700}^+ reduction rate constants. The rate was calculated by fitting the data with a single exponential function. According to students *t* test significant changes ($p \leq 0.05$) are marked by one asterisk. (C) Relative electron transport rate (rETR) was measured by increasing light intensity until the capacity limit was reached. PAR: light intensity in $\mu mol photons m^{-2} s^{-2}$.

The PSII driven reduction of the PSI reaction centre P_{700} indicates a significant $\sim 30\%$ reduction of the rate constant in *ancM* compared to the WT (Figure 24). In the presence of the PSII inhibitor DCMU, the cyclic electron flow between the Cyt b_6f and PSI shows no changes (Figure 24 B). Moreover, during PSII chlorophyll fluorescence measurements the light dependency of the electron flow is not shifted. Both strains reach the limit capacity at $\sim 278 \mu E m^{-2} s^{-1}$ (Figure 24 C).

Alteration of PSI and PSII ratio can be measured by low temperature fluorescence emission spectra of chlorophyll at a wavelength of 440 nm (77K). The maximum signal at 721 nm, corresponding to PSI, was normalised to 1 (Lamb *et al.*, 2018). The fluorescence

Results

signal at 685 nm and 695 nm originates from the chlorophylls bound in CP43/CP47 that are involved in light energy funneling to PSII (Sato, 1980; Shen and Vermaas, 1994). The ratio between PSII and PSI was calculated from the normalised absorption values at 690 nm and 721 nm (Figure 25).

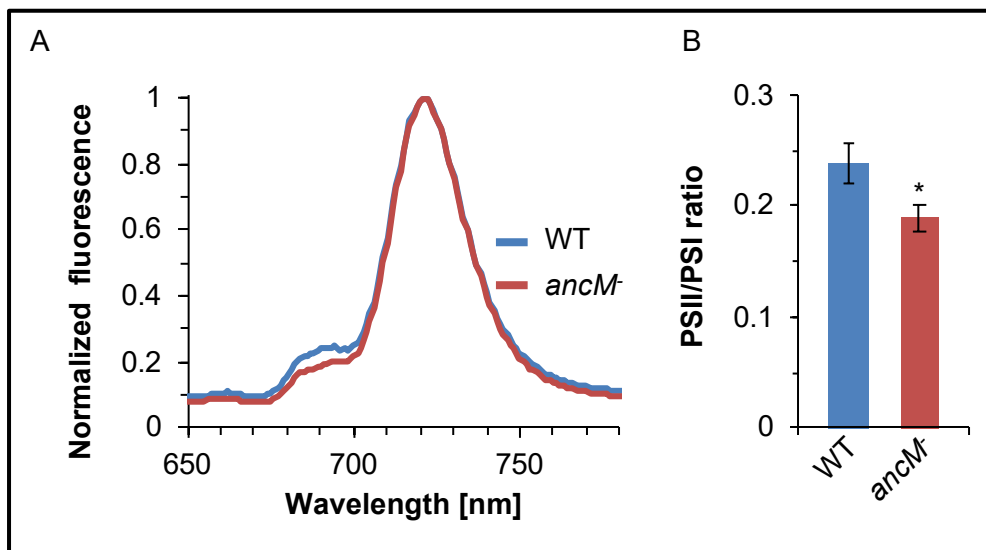


Figure 25: Low temperature measurements. (A) Fluorescence emission spectra of WT (blue) and *ancM* (red) at 77 K. The cells were excited at 440 nm. The graphs were normalised to 721 nm (Absorption maxima of PSI). (B) PSII/PSI ratio is shown in a bar diagram. According to students *t* test significant changes with error probabilities of 5% are marked by one asterisk.

The fluorescence emission spectra curve of WT (blue) and *ancM* (red) cells is shown in (Figure 25 A). The PSII related absorption peak at a wavelength of 690 nm differed in *ancM* from the WT. Following this the PSII/PSI ratio was significantly reduced in *ancM* compared to the WT (Figure 25 B). The data from the 77 K measurements suggests a PSII related phenotype and changes of PSI and PSII distribution in *ancM*.

3.4.5 Distribution of photosynthetic complexes

Different distribution of photosynthetic super-complexes was also observed in 2-D PAGE profiles by separation of membranes from WT and mutant strain. PSII subunits D1, D2, CP43, CP47 and PSI subunit PsaD were analysed by immunodetection (Figure 26).

Results

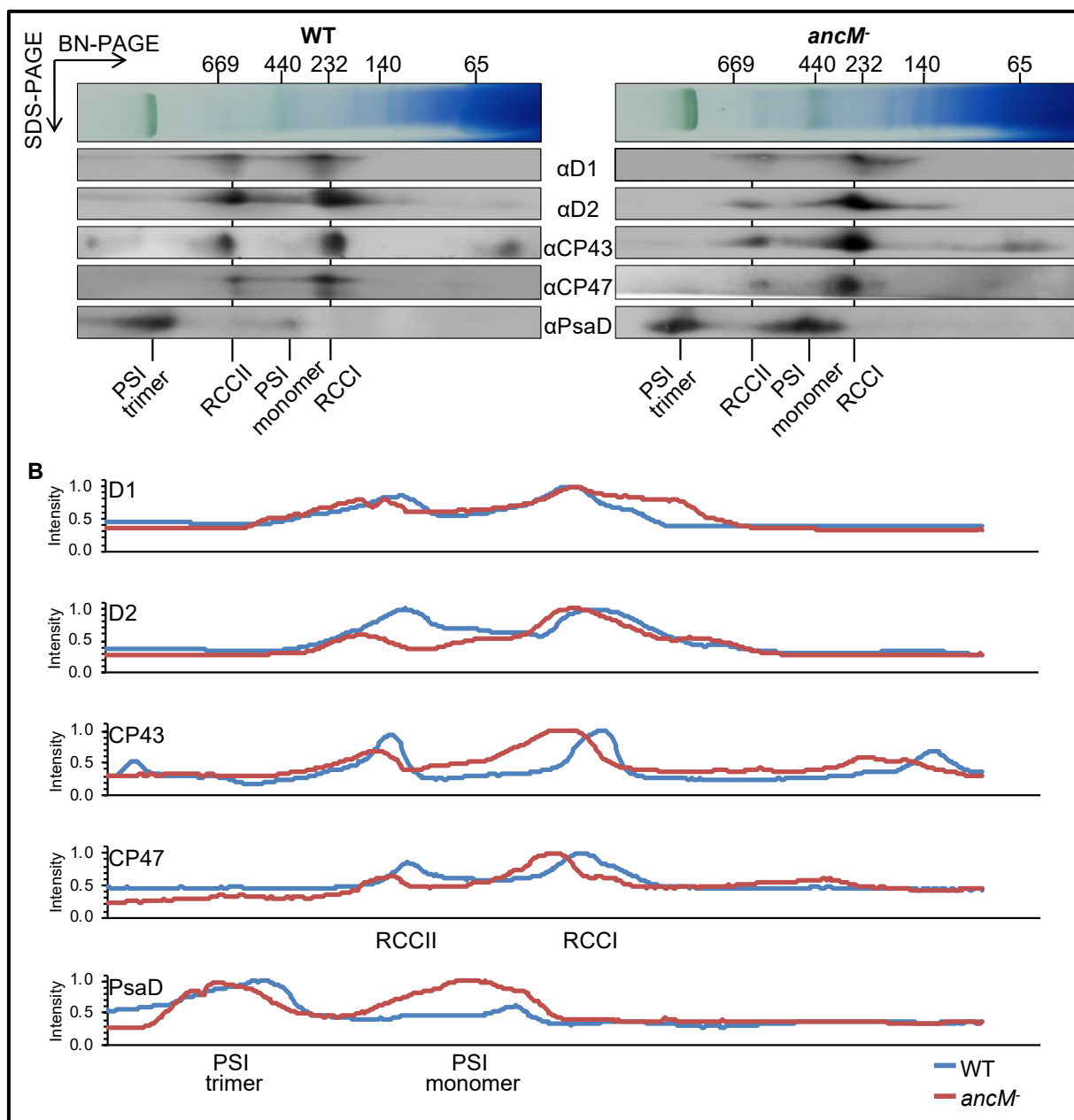


Figure 26: 2D-PAGE of thylakoid membranes from WT and *ancM* cells. (A) Membranes (10 μ g Chlorophyll) was solubilised with 1.3% β -DM and fractionated on a BN-PAGE. Afterwards the membranes were separated in a second dimension. Proteins from photosynthetic complexes were analysed by an immunoblot. α CP47 were purchased from Agrisera. (B) Intensity blot of photosynthetic membrane complexes were taken using Fiji: ImageJ. WT: blue line, *ancM* red line.

As can be seen in Figure 26 A, in both strains PSI trimer and monomer are accumulating at around 990 and 330 kDa, respectively the PSII dimer (RCCII) and monomer (RCCI) ~650 and 325 kDa. Beside the immunoblots, the band intensity plots demonstrate a distribution of the different PSI and PSII subunits (Figure 26 B). The immunoblot signal of D1 is shifted in *ancM* towards the PSII monomer. The subunit D2 in RCCII is less abundant in the mutant *ancM* compared to the WT. The antenna Proteins CP43 and CP47 are also shifted in *ancM* towards RCCI. CP43 is accumulating in the low molecular area. Furthermore, PsaD is present in the PSI trimer of the WT and *ancM* during in the monomer the PsaD level is

Results

increased in *ancM* compared to the WT. Taken all the data together the loss of *ancM* causes a shift of photosynthetic complexes from trimer/dimer to monomeric complexes.

In order to characterise the kinetics of PSII dimer formation ³⁵S-Methionin pulse labeling was performed *in vivo* in WT and *ancM* cells. The autoradiograph is shown in Figure 27.

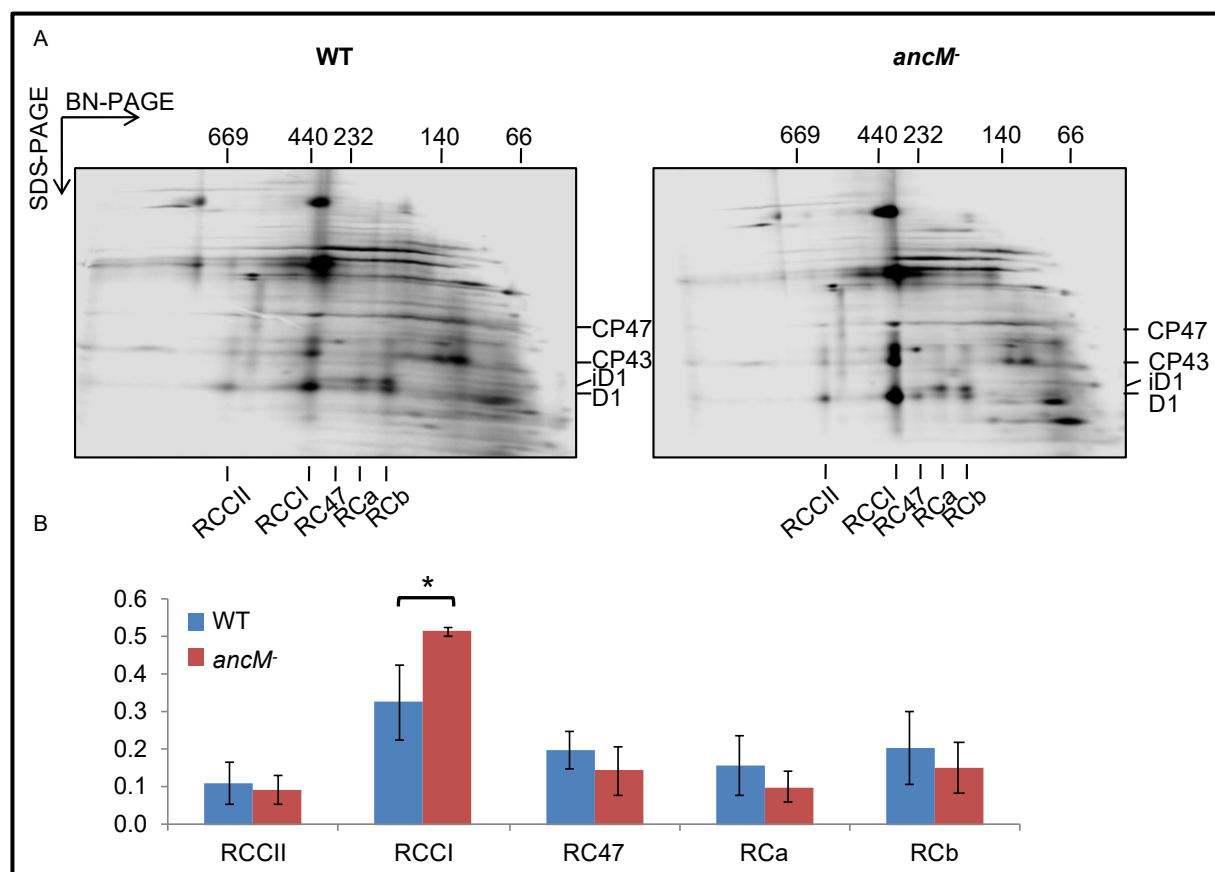


Figure 27: *In vivo* pulse labeling of membrane proteins from WT and *ancM* with ³⁵S-Met. (A) Autoradiograph of ³⁵S labeled Proteins from WT and *ancM*. Membrane fractions containing 15 µg chlorophyll of ³⁵S labeled Proteins were solubilised with 1.3% β-DM, separated with 2D-PAGE and visualised by autoradiograph. (B) Distribution of D1 signal in WT (blue) and *ancM* (red) through assembly intermediates in RCCII, RCCI, RC47, RCa and RCb performed by Dr. Steffen Heinz. Average and standard derivation were calculated from three independent replicates. According to students *t* test a significant change with error probabilities of 5% is marked by one asterisk, n=3. RCCII, PSII Dimer; RCCI, PSII monomer; RC47, reaction centre complex lacking CP43; RCa and RCb, reaction centre complex lacking CP47 and CP43.

The autoradiograph demonstrates that the radioactively labeled PSII subunits CP47, CP43, D1 and partially processed D1 (iD1) are visible in PSII related complexes. The RCCII, RCCI, the CP43-less RC47 complex as well as the RC complexes, RCb and RCa with iD1/ D1 are shown in the autoradiograph (Komenda *et al.*, 2004; Dobáková *et al.*, 2007; Komenda *et al.*, 2007b; Heinz *et al.*, 2016b) (Figure 27 A). However, the distribution of the D1 signal intensities are equal in both strains in the PSII dimer and assembly intermediates RC47, RCa and RCb. Interestingly, the PSII monomer signal is significantly enriched in *ancM* when compared to the WT (Figure 27 B).

Results

3.4.6 Localisation of AncM

In order to confirm if AncM is a membrane bound Protein the cells were exposed to different detergents like β -DM, Nonidet-40 (NP-40) and Triton. As a control for soluble or membrane attached proteins the isolated membranes were treated with Na_2CO_3 , NaCl and Urea. The integral membrane- proteins CP47 and CurT were used as a control (Figure 28).

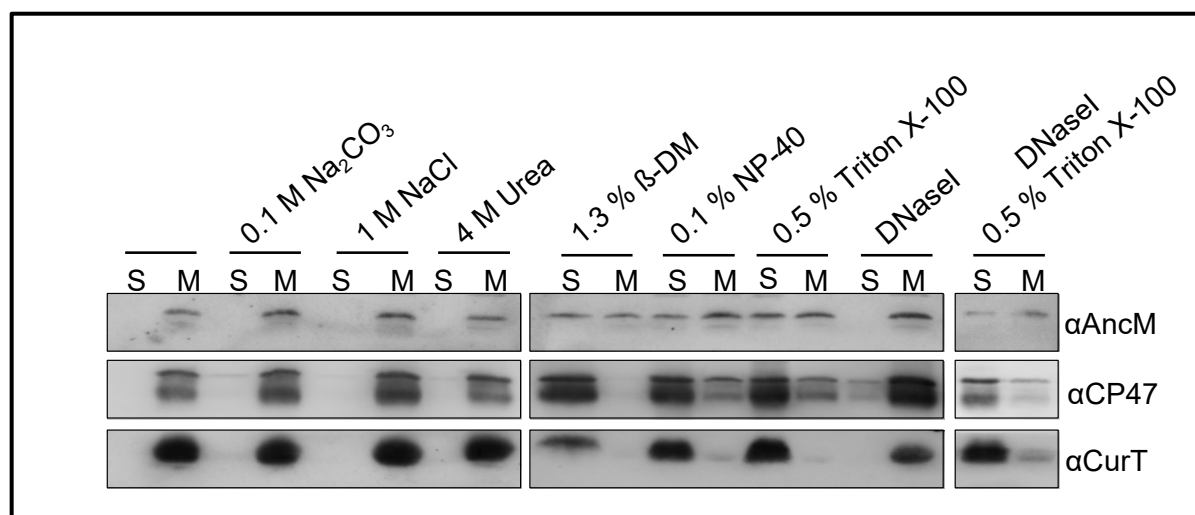


Figure 28: Solubility of AncM. Membranes from WT cells were extracted with 5 mM Hepes pH 7.6 afterwards treated with 0.1 M Na_2CO_3 , 1 M NaCl, 4 M Urea, 1.3% β -DM, 0.1% NP-40, 0.5% Triton X-100 or DNaseI and containing 0.5% Triton. Membrane bound (M) and soluble (S) proteins were separated by centrifugation. The fractions were analysed by SDS-PAGE. The proteins AncM, CP47 (Pineda) and CurT as control were detected by immunoblot.

Treatment of membranes with salts or urea reveals an immunoblot signal of α AncM together with the membrane proteins in the membrane bound fraction. By contrast solubilisation of membranes using different detergents lead to a partial release of AncM into the soluble fraction whereas CurT was completely solubilised. On the other hand, it was possible to solubilise CP47 with β -DM but treatment with NP-40 and Triton shows a weak signal in the membrane fraction. Thus, the data suggest that AncM is a membrane bound protein. Furthermore, in comparison with the membrane proteins CP47 and CurT the solubilisation assay revealed strong interaction in between AncM and the membrane. Moreover, the treatment with DNaseI in the presence and absence of Triton shows no effect on the solubility of AncM (Figure 28). It suggests that AncM is not bound to nucleic acids (Phinney and Thelen, 2005).

For a subcellular localisation of AncM membranes of WT cells were fractionated by a two-step sucrose density gradient centrifugation. The first gradient centrifugation led to five fractions in different concentrations of sucrose. Fraction II represents the plasma membrane and fraction V contains TM and PDM proteins (Schottkowski *et al.*, 2009b; Heinz *et al.*, 2016b). Whether AncM is bound to the plasma membrane or TM western analysis of fraction II and V were performed (Figure 29).

Results

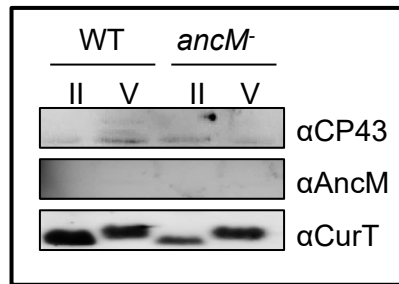


Figure 29: Analysis of fractions II and V. The first sucrose density step-gradient was separated into five fractions. 5 µg protein of fraction II and V were analysed by immunoblot using different antibodies.

However, western blot analysis demonstrates a clear immune signal of AncM in fraction V of the WT during in fraction II no band appears. As control the integral membrane Protein CP43 is exclusively present in fraction V. In addition, CurT, which is known to be present in plasma membrane and TM and PDM, has a band in fraction II and V. Moreover, in the mutant line *ancM* the amount of CurT in fraction II is slightly reduced compared to the WT.

Because of the localisation of AncM in fraction V we focused on the second gradient and performed western blot analysis on the particular fractions 1-14. Figure 30 shows the membrane compartmentalisation from WT and the mutant lines *ancM* and *curT*. These density centrifugations allow the separation of TM from PDM marked by the Mn²⁺ delivery factor PrtA (Schottkowski *et al.*, 2009b; Rengstl *et al.*, 2011; Stengel *et al.*, 2012).

Results

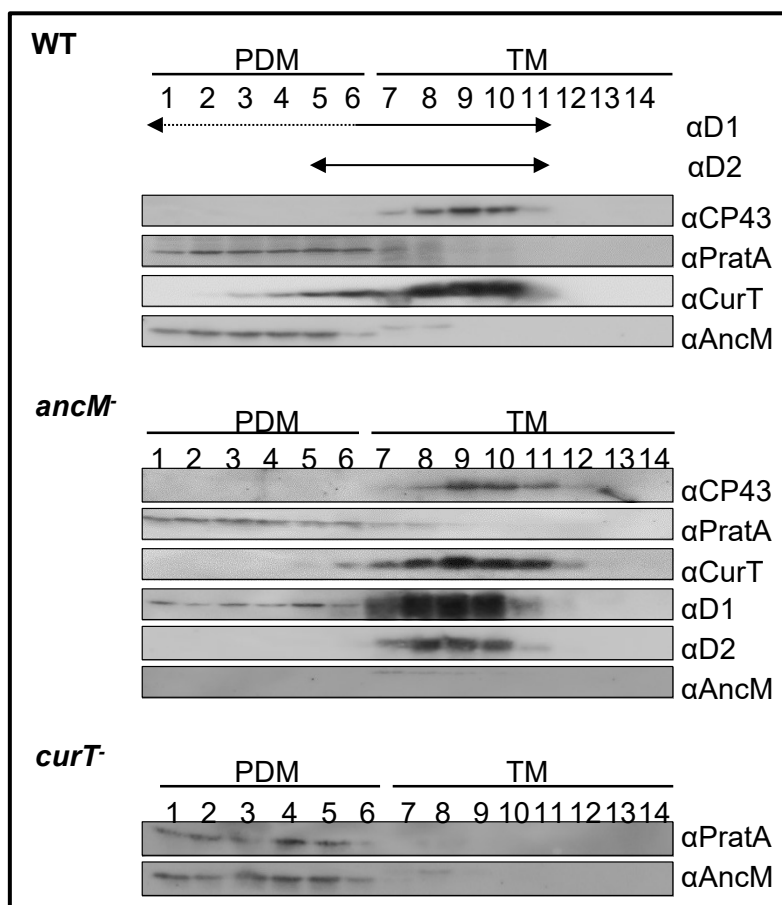


Figure 30: Membrane fraction V of photosynthetic membranes from WT, *ancM*⁻ and *curT*⁻ were separated by a second sucrose density gradient centrifugation. The second gradient (20-60%) was fractionated into 14 samples. Fraction 1-6 represent the PDM and fraction 7 until 14 the thylakoid membranes (TM). For a comparison of the fractions the sample volume was normalised to the volume of fraction 7 containing 40 µg protein.

As expected, the fractionation of WT membranes shows that proteins PratA and CurT are present in PDM (Schottkowski *et al.*, 2009b; Heinz *et al.*, 2016b). AncM is colocalised with PratA in the PDM. Furthermore, the immunoblot shows that AncM is similar to WT and *curT*⁻ located in PDM (Schottkowski *et al.*, 2009b; Heinz *et al.*, 2016b). Furthermore membrane fractionation of *ancM*⁻ shows a shift of the D2 towards the TM. In contrast to the PSII related proteins CP43, D1 and the PSII assembly factor PratA no pattern changes observed in *ancM*⁻. Interestingly, in *ancM*⁻ the distribution of CurT is shifted towards the TM.

In order to identify putative interaction, partners of AncM in the PDM a Co-IP were performed. Therefore, the PDM of WT and *curT*⁻ cells were pulled down using αCurT (Figure 31).

Results

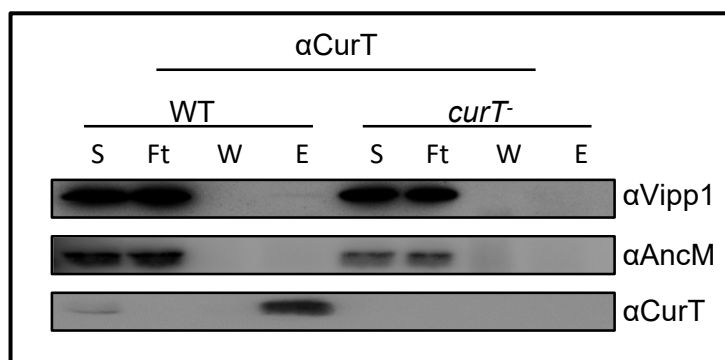


Figure 31: CoIP with α CurT on WT and *curT*⁻ on PDMs. Fraction 1 to 6 were pooled and concentrated. α CurT was chemically crosslinked to Protein A Agarose Beads. CoIP was performed with 500 μ g Protein overnight and eluted with 100 mM Glycine, pH 2. 20 μ l of pooled fractions (S), Flow through (Ft), second wash fraction and the whole eluate (E) was separated on a SDS-PAGE and analysed by an immunoblot.

The Immunoblot shows the signals of α Vipp1, α AncM and α CurT. The immunosignal of Vipp1 is present in the sample and flow through of WT and the negative control *curT*⁻. Furthermore, a weak band is visible in the eluate of WT. In contrast, the band is missing in *curT*⁻ cells. Moreover, the immunosignal of AncM is exclusively visible in sample and flow-through of WT and *curT*⁻. The detection of CurT shows a small band in the sample fraction and a strong band in the eluate of the WT. As expected, CurT is not present in *curT*⁻ (Figure 31).

The eluate fractions of the CoIP were analysed by mass spectrometry analysis in collaboration with the Ruhr-University Bochum, Prof. Dr. Marc Nowaczyk for. The detected candidates were sort after the score and the first 10 are listed in Table 16. See also the complete Table 18 with hits in the Annex.

Table 16: Top 10 of mass spectrometry analysis of the Co-IP with α CurT on PDM fractions. As negative control the strain *ancM curT*⁻ was used. Ten of the potential ORF was listed after highest abundance in mass spectrometry analysis.

Bioinformatical analysis are shown in column 3-5. The hits are listed after the score.

ORF	Function	Mass weight [kDa] ^a	Predicted TM helices ^b	Co-expression with CurT/AncM ^c	Score ^d
<i>ancM</i>	Slr2070	31.87	1	CurT	24.85
<i>slr0193</i>	RNA-binding protein, Rbp3	16.62	0	CurT	19.86
<i>sll0617</i>	VIPP1	28.90	2	no	16.79
<i>sll0822</i>	hypothetical protein	13.96	0	CurT	15.84
<i>sll1244</i>	50S ribosomal protein L9	16.64	1	no	8.7
<i>sll1028</i>	carbon dioxide concentrating mechanism protein CcmK	11.13	0	no	8.52

Results

ORF	Function	Mass weight [kDa] ^a	Predicted TM helices ^b	Co-expression with CurT/AncM ^c	Score ^d
<i>slr1034</i>	hypothetical protein YCF41	14.41	0	no	7.94
<i>sll0359</i>	hypothetical protein	17.22	0	no	7.82
<i>slr0952</i>	fructose-1.6-bisphosphatase	38.26	3	no	7.36
<i>sll1837</i>	periplasmic protein, function unknown	15.47	1	AncM	5.87

^a) Theoretical mass weight was calculated using https://web.expasy.org/compute_pi/

^b) Transmembrane domains theoretical analysed using the tools https://embnet.vital-it.ch/software/TMPRED_form.html and <http://www.cbs.dtu.dk/services/TMHMM/>

^c) Co-expression data was analysed using <http://cyanoexpress.sysbiolab.eu>

^d) The score value is calculated for each peptide by matching the predicted ions to the ions observed in the mass spectrum (Eng *et al.*, 1994).

The preliminary analysis confirms Vipp1 with a score of 16.79 as an interaction partner of CurT in the PDM. Interestingly the eluate contains beside Vipp1 the cyanobacterial protein AncM with the highest score of 24.85. As expected, the eluate contains CurT (see Annex, Table 19). Beside these proteins this approach contains a lot of ribosomal proteins and the RNA binding protein Slr0193 which is also known as Rbp3 with a score 19.86. Rbp3 is predicted to be cytosolic and it is co-expressed with CurT (Hernandez-Prieto and Futschik, 2012). In addition, the hypothetical protein Sll0822 and the ORF *slr1329* which encodes for the ATP synthase beta subunit is co-expressed with CurT (Hernandez-Prieto and Futschik, 2012). The periplasmic protein Sll1837 displays a co-expression with AncM in Expression analysis (Table 16) (Hernandez-Prieto and Futschik, 2012).

In addition, the Co-IP was performed on TM fraction 8 and 9 with α CurT with the WT and *ancM curT* as negative control. The eluates were sent for mass spectrometry analysis to Ruhr-University Bochum, Prof. Marc Nowaczyk. The ten hits with the highest score are listed in Table 17. The candidates with a score lower 8.73 are listed in Table 19.

Results

Table 17: Top 10 of mass spectrometry analysis of the Co-IP with α CurT on the TM fraction 8-9. As negative control the strain *ancM curT*⁻ was used. Potential ORF was listed after abundance in mass spectrometry analysis. Bioinformatical analysis are shown in column 3-5.

ORF	Function	Mass weight [kDa] ^a	Predicted TM helices ^b	Co-expression with CurT/AncM ^c	Score ^d
<i>sll1808</i>	50S ribosomal protein L5	20.23	0	no	25.71
<i>slr1128</i>	hypothetical protein	35.73	1	no	21.61
<i>sll0469</i>	ribose-phosphate pyrophosphokinase	36.40	2	no	16.47
<i>slr0404</i>	hypothetical protein	34.87	3	no	15.72
<i>slr1537</i>	unknown protein	32.42	1	no	13.76
<i>slr1238</i>	glutathione synthetase	35.07	4	no	10.33
<i>sll1837</i>	periplasmic protein, function unknown	15.47	1	AncM	9.88
<i>slr0012</i>	ribulose biphosphate carboxylase small subunit	13.24	1	no	9.58
<i>slr0543</i>	tryptophan synthase beta subunit	45.07	3	no	8.75
<i>sll0891</i>	malate dehydrogenase	34.35	4	no	8.73

^aTheoretical mass weight was calculated using https://web.expasy.org/compute_pi/

^bTransmembrane domains theoretical analysed using the tools https://embnet.vital-it.ch/software/TMPRED_form.html and <http://www.cbs.dtu.dk/services/TMHMM/>

^cCo-expression data was analysed using <http://cyanoexpress.sysbiolab.eu>

^dThe score value is calculated for each peptide by matching the predicted ions to the ions observed in the mass spectrum (Eng *et al.*, 1994).

The ribosomal protein Sll1808 is the candidate with the highest score of 27.71 followed by ORF *slr1128* and ORF *sll0469*, which encodes for the ribose-phosphate pyrophosphokinase. Interestingly the ORF *sll1837* that is coexpressed with AncM, was also found with a score of 9.88 in the eluate of the TM fractions. Sll1837 a periplasmic protein with an unknown function. In addition, two proteins are co-expressed with CurT: Fructose-biphosphate aldolase and Slr1719, a DrgA protein homolog (Hernandez-Prieto and Futschik, 2012). The theoretical calculated mass weight and putative TM helices are listed in columns three and four (Table 18).

Results

In order to further analyse the localisation of AncM at a cellular level a widefield immunofluorescence was performed by Matthias Ostermeier. To this end, the purified antibodies against AncM and CurT were labeled with a secondary antibody containing the Alexa Fluorophore that absorbs at a wavelength of 405 nm (Figure 32).

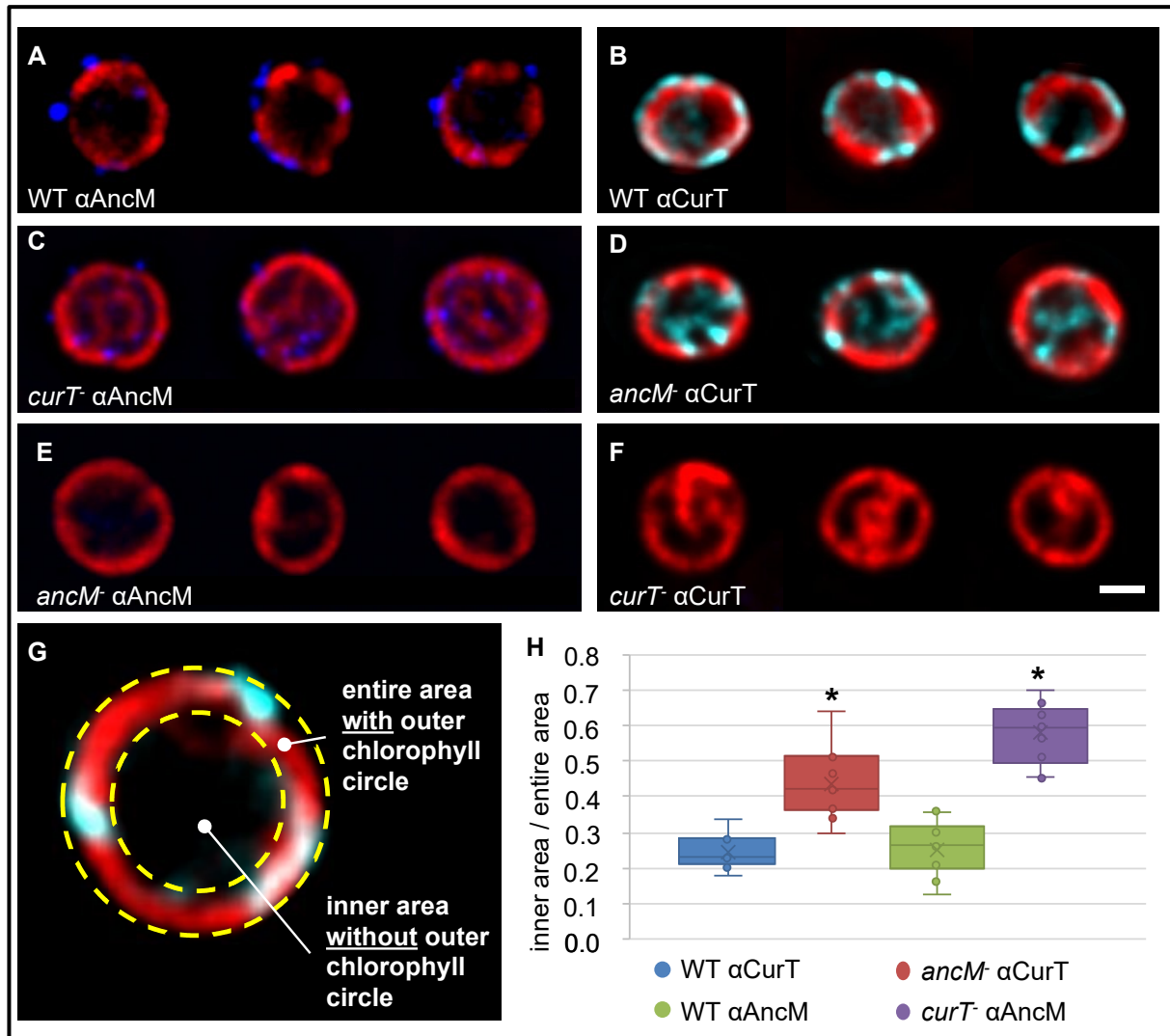


Figure 32: Widefield immunofluorescence micrographs. (A) WT α AncM, (B) WT α CurT, (C) *curT*⁻ α AncM, (D) *ancM*⁻ α CurT, (E) *ancM*⁻ α AncM and (F) *curT*⁻ α CurT *Synechocystis* cells. All lines were incubated with a primary α AncM (A, C and E) or a primary α CurT (B, D and F) and a secondary Alexa Fluor™ 405 antibody. (H) The ratio of the immunofluorescence signal from the cell interior vs. periphery (example shown in G) using CurT or AncM primary antibodies. Images (example shown in G) were measured 10 times for each line. Error probabilities according to students *t*-test the asterisks show a significance level below 0.01. Bar = 1 μ m. All immunofluorescence micrographs were performed by Matthias Ostermeier.

The immunofluorescence signal of AncM (blue) shows selective spots located in external areas of WT *Synechocystis* cell. These the strong blue spots are visible in regions without chlorophyll fluorescence, which is visualised in red (Figure 32 A). CurT build-up in the WT a network like pattern, visualised in turquoise (Figure 32 B). In *curT*⁻ a shift in the signal distribution of AncM is observed. The strong blue spots around the cell are reduced and are located mostly in the centre of the cell (Figure 32 C). Also, the distribution of the chlorophyll signal is more random, which correlates with the loss of converging zones in *curT*⁻ (Heinz *et al.*, 2016b). These

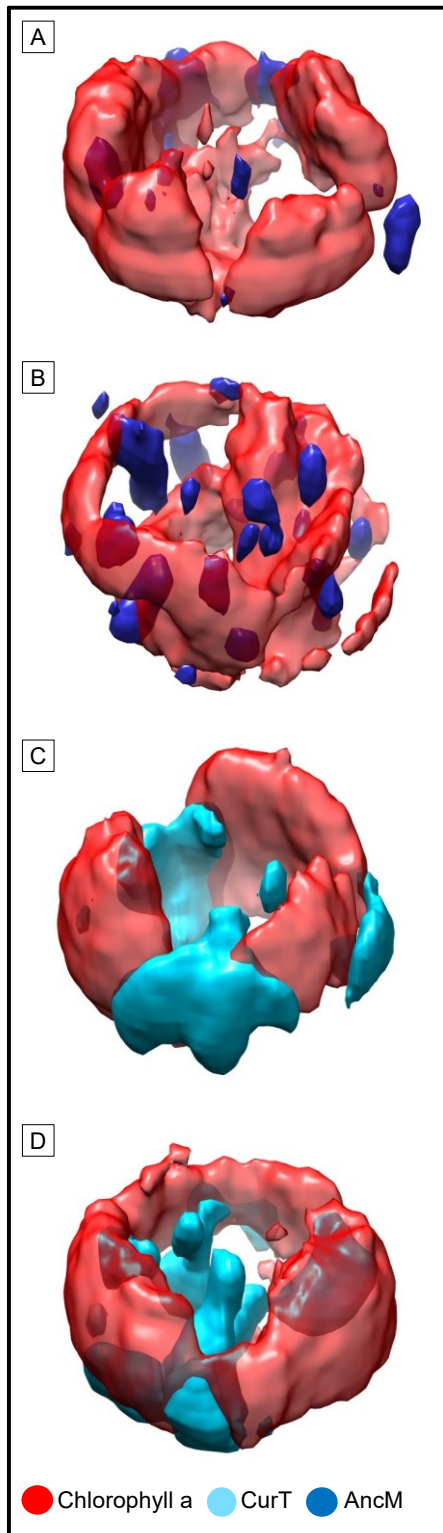


Figure 33: 3D reconstructions of *Synechocystis* cells. Z-axis stacks of cells shown in Figure 32 were used to create 3-D models. Immunolocalisation of AncM in (A) WT and (B) *curT* treated with α AncM and Alexa Fluor™ 405 (blue). (C) CurT immunofluorescence signal in WT and (D) *ancM*. All 3D reconstructions were performed by Matthias Ostermeier

changes of distribution confirm the shift from AncM directed to the TM as observed in the sucrose density gradients. Performing immunofluorescence in *ancM* with CurT show that the network-like structure of CurT is shifted inside the *Synechocystis* cell (Figure 32 D). The shift of CurT was also observed in the membrane fractions of *ancM* cells. No immunofluorescence signal was observed in *ancM* or *curT* by using α AncM and α CurT, respectively (Figure 32 E and F). To clarify the shift of AncM and CurT in the mutants *curT* and *ancM* the ratio of the immunofluorescence signal intensities of the outer chlorophyll circle and the inner area without the outer chlorophyll circle were taken and visualised in a balk diagram (Figure 32 G and H). Following this, it could be demonstrated that the shift of the observed immunofluorescence signals of CurT and AncM in the corresponding mutant strains is significant (Figure 32 H).

3D reconstruction of WT, *curT* and *ancM* with the chlorophyll autofluorescence in red and AncM immunofluorescence in blue and signal in turquoise. In WT, the AncM signal is located at the outside of chlorophyll circle in spots and mainly in the areas without chlorophyll fluorescence (Figure 33 A). The loss of CurT triggers a shift of the AncM spots from this location to the inner side of the chlorophyll ring (Figure 33 B). The immune fluorescence signal of CurT in WT background is arranged in a network structure as observed in (Figure 34 C). The loss of AncM causes a movement of the signal into the inner area of the cell (Figure 33 D).

Results

As marker for convergence zones the CFP-tagged CurT strain was used for a co-localisation with AncM by immunofluorescence (Figure 34).

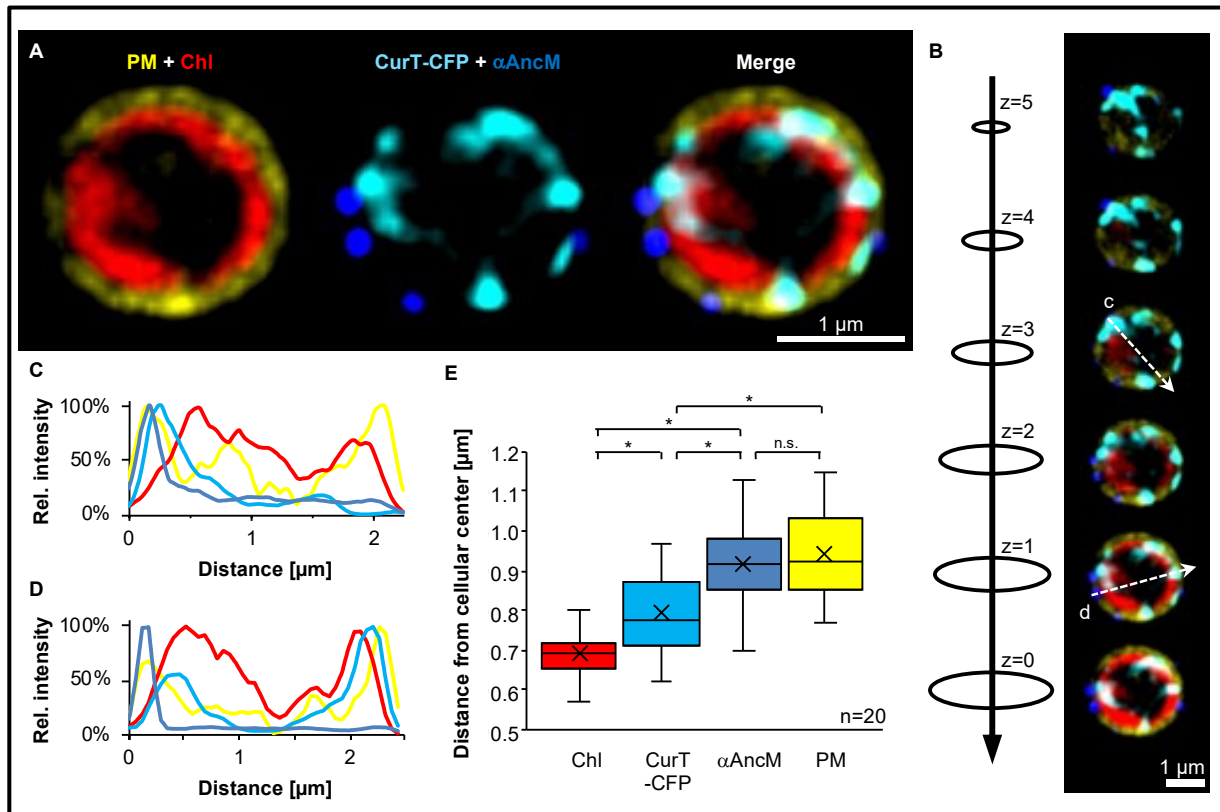


Figure 34: Co-localisation of AncM and CurT close to the plasma membrane. The autofluorescence of chlorophyll *a* (red) is measured at 680 nm. CurT is genetically tagged with mTurquoise2 (cyan) (Heinz *et al.*, 2016b), AncM is immunofluorescence tagged with Alexa Fluor™ 405 (blue) using α AncM. To stain the plasma membrane the cells were treated with FM 1-43 (A) Four channel fluorescence micrographs. (B) Fluorescence signals through the z-axis of the cell shown in A. Several slices with 200 nm spacing from top (z=5) to the mid-cell plane (z=0) (C, D) Fluorescence intensity profiles. Relative intensities of the plasma membrane (yellow), chlorophyll autofluorescence (red), CurT-CFP (cyan) and α AncM (blue) indicates in lines and were plotted against the diameter of the z axis plane. (E) Quantification of the intensity profiles. The intensity profiles (shown in C, D) of n=20 from mid-cell planes were taken and the distances of fluorescence peaks to the centre of the cell were determined for each fluorescence channel. Significant changes are marked by asterisks according to Student's *t* test with an error probability of $\leq 1\%$. Performed by Matthias Ostermeier.

Again, AncM is located in the outer region of the cell; CurT develops a network structure and the chlorophyll builds a ring around the cell which is surrounded by the plasma membrane (Figure 34 A). In order to clarify this, the fluorescence signals through the z-axis slices from the top (z=5) to the mid cell plane (z=0) of the same cell is shown in Figure 34 B. Furthermore, the fluorescence intensity profiles show close to the plasma membrane an overlay of CurT and the AncM signal (Figure 34 C and D). The quantification of the intensity profiles taken from the mid cell plane and the distances of the fluorescence peaks to the centre of cell were determined and visualised in a box diagram (Figure 34 E). With respect to this, it could be demonstrated that the overlay of the fluorescence signals of CurT, AncM and the plasma membrane is significant. Taking the data together, the fluorescence micrographs revealed a co-localisation between AncM and CurT close to the plasma membrane (Figure 34 E).

Results

3.4.7 The loss of AncM affects the thylakoid membrane structure

To verify if the loss of AncM affects the cellular ultrastructure different *Synechocystis* lines were examined by TEM (Figure 35).

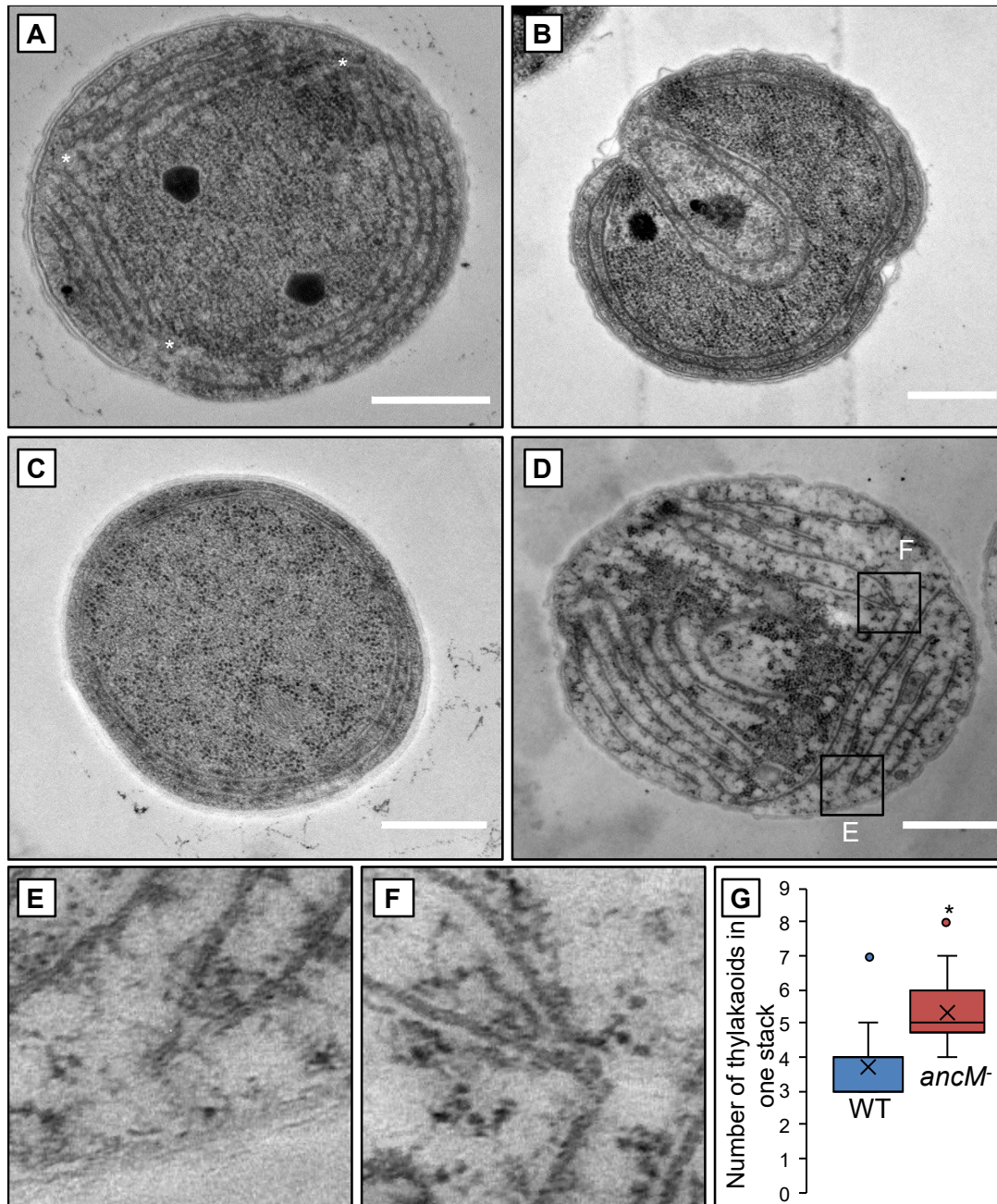


Figure 35: TEM micrographs of *Synechocystis* cells. (A) WT, (B) *curT*, (C) *sucrT* and (D) *ancM* *Synechocystis* cells, taken at 12,500x magnification. The enlarged sections (E and F) show converged thylakoids at a great distance to the plasma membrane in *ancM*. White asterisks (A) reveal a thylakoid converging zones close to the plasma membrane. Ultrathin sections (50 nm) of cryo fixed samples were stained with osmium tetroxide and post stained using lead citrate. Bars = 0.5 μ m. Performed by Matthias Ostermeier.

The thylakoid membranes form an ordered stack in a WT cell and they are curved towards the plasma membrane to form convergence zones marked by white asterisk (Figure 35 A, G). The thylakoids in *curT* cells are randomly ordered and not arranged towards the

Results

plasma membrane, convergence zones are completely absent (Heinz *et al.*, 2016b) (Figure 35 B). In contrast to *curT*, in *sucurT* the thylakoids are ordered but not shaped towards the plasma membrane and convergence zones are missing (Figure 35 C). The loss of AncM causes a detach of thylakoids from the plasma membrane. In addition, *ancM* contains an average of five thylakoids in one stack, which is significantly more compared to the WT with usually 3 to 4 thylakoids in one stack (Figure 35 G). Thereby the thylakoids are able to form some connections but nevertheless it seems that they have lost a fixing point with the plasma membrane (Figure 35 D, E and F).

CLEM was used to detect the chlorophyll autofluorescence on ultrathin sections that were subjected to TEM analysis afterwards. This technique allows one to distinguish between photosynthetic active areas containing the chlorophyll autofluorescence and non photosynthetic active regions such as the convergence zones (Figure 36).

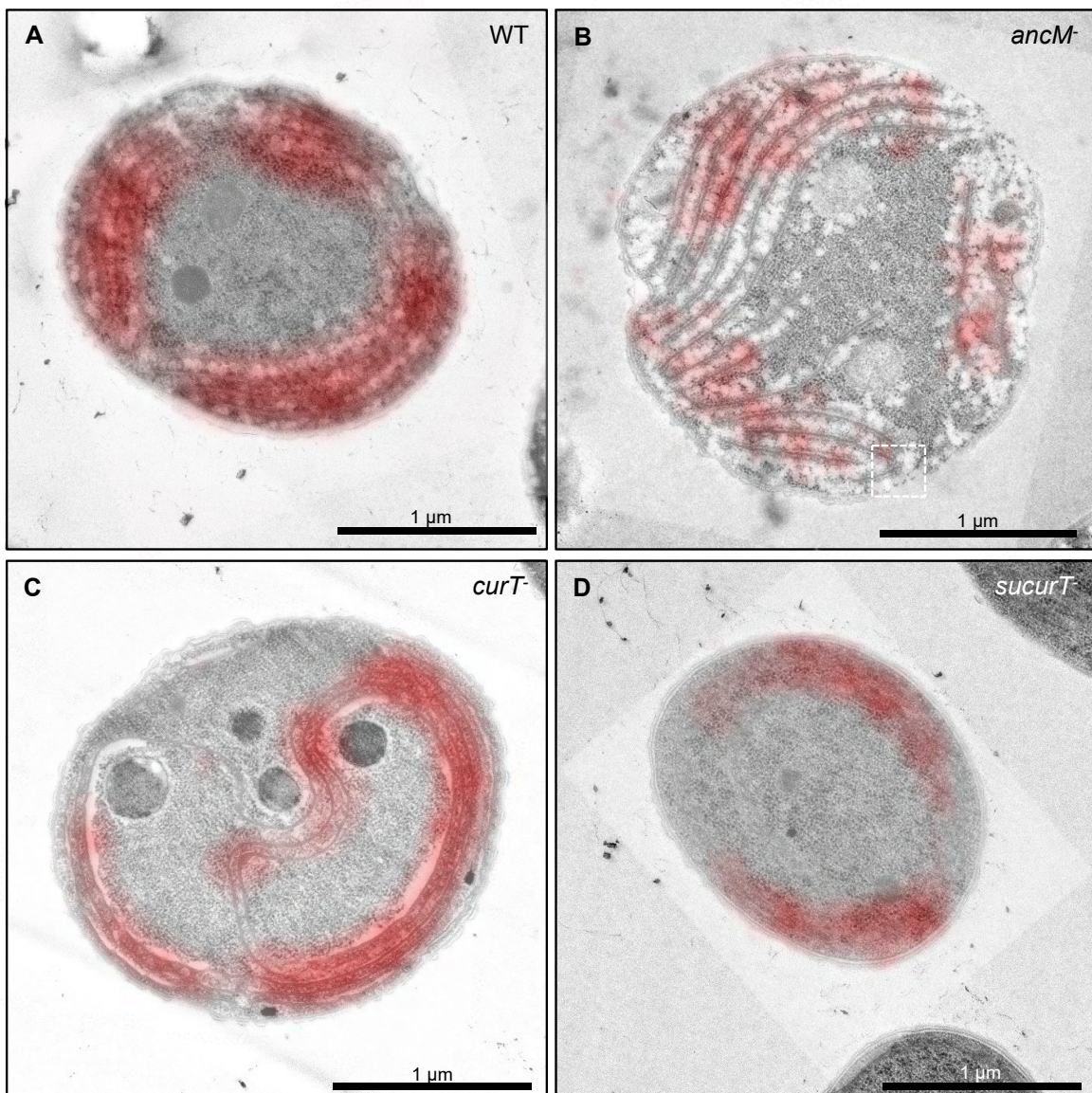


Figure 36: Correlative light electron micrographs (CLEM) of *Synechocystis* cells. (A) WT, (B) *ancM*, (C) *curT* of *Synechocystis* cells. The transmission electron micrographs were taken at 10,000 x magnification, superimposed by fluorescence micrographs of the chlorophyll autofluorescence (red). Performed by Matthias Ostermeier.

Results

The correlative micrograph of a WT *Synechocystis* cell shows the red chlorophyll autofluorescence signal at the thylakoids, which are located at the cell periphery. Thereby several spots are visible without the autofluorescence of chlorophyll at the converging zones (Figure 36 A). The chlorophyll autofluorescence of *ancM* is less intense and more dispersed, as opposed to the WT *curT* cells. Like in the WT the converged thylakoids don't exhibit a chlorophyll signal (Figure 36 B). In *curT* the chlorophyll signal is distributed through the thylakoids excepted two spots. Thereby the thylakoids are disorganised and also extends to the interior of the cell (Figure 36 C). During the chlorophyll autofluorescence in *sucurT* seems uneven distributed over the stacked thylakoids (Figure 36 D)

4. DISCUSSION

4.1 PrataA Complex

Co-IP studies and the following mass spectrometry analysis have shown that PrataA interacts *in vivo* in the periplasm of *Synechocystis* with a soluble form of PilQ and the DegA protease HhoA. Based on *in vitro* MST experiments, it could be confirmed that PrataA interacts with a high affinity with PilQ and HhoA and forms a complex (Schottkowski *et al.*, 2009b). Furthermore this biophysical approach allows the determination of the K_D between protein interactions (Wienken *et al.*, 2010; Chen *et al.*, 2017). Bartoschik *et al.* (2018) demonstrate that this technique can be applied to calculate interaction K_D in bacterial lysate samples which revealed that contaminations or degradations of proteins are negligible. Thus, it can be assumed that similar side effects of the MBP or Histidine tag will not affect the interaction studies. It is known that MBP is able to form aggregates with itself (Richarme, 1983). Therefore, a long exposure with infra-red laser can accelerate the formation of such aggregates leading to an increase of fluorescence during titration. These side effects can be excluded by using the MBP Tag as negative control. The observed high affinity ($1.5 \pm 0.2 \mu\text{M}$) between His-HhoA and MBP-PilQ allows to speculate if the interaction is separated in time. A possible explanation could be a successive binding HhoA to PilQ followed by a complex formation with PrataA. The results also confirm a possible complex formation stabilising PrataA, which is important for the preloading of pD1 with manganese and forms an important step of the PSII assembly machinery (Figure 37). Taken together, these aspects of the MST measurements offer a direct interaction in between the recombinant proteins PrataA, MBP-PilQ and His-HhoA. Moreover, this method allows to calculate K_D values of protein interactions. So it was demonstrated that all three proteins interact with affinity $< 10 \mu\text{M}$, revealing a strong interaction of the PrataA complex.

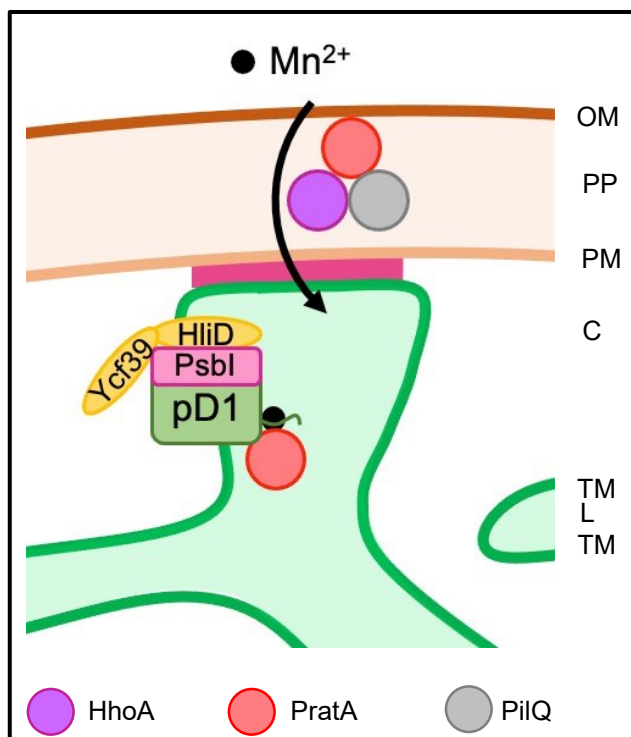


Figure 37: Model of the PrataA complex. PrataA (red circle) binds Mn^{2+} and preloads pD1, the precursor form of D1. *In vivo* and *in vitro* studies suggest a complex of PrataA (red circle) HhoA (purple circle) and PilQ (grey circle) in the periplasm (PP). Plasma membrane (PM), cytoplasm (C), thylakoid membrane (TM), lumen (L).

4.2 Proteomic screen

Proteomic analysis could show an increase of FraH in PDM fractions in *pratA*⁻ (Figure 10). A negative influence on heterotrophic growth in *fraH* studies might suggest that FraH is involved in the carbohydrate metabolism. Following this, co-expression analysis shows a potential connection with the assembly proteins of glucose-6-phosphate-dehydrogenase, which catalyzes the first step of the oxidative-pentose-phosphate pathway, OpcA and FraH (Hernandez-Prieto and Futschik, 2012; Ge *et al.*, 2018). Thereby, the loss of FraH may have a negative effect on the expression level of *opcA*, which reduces the activity of the glucose-6-phosphate-dehydrogenase (Özkul and Karakaya, 2015). A reduced in the oxygen evolution of *fraH* is in contrast to a normal photoautotrophic growth rate (Table 12). It can be speculated, if an increase of the cyclic electron results by a decrease of the electron flow through PSII, which is observed in *Pisum sativum* L. (Sukhov *et al.*, 2015). This might reveal in a reduced oxygen evolution without any effect on the photoautotrophic growth of *fraH*. In *Anabaena* sp. it has been shown that *fraH* gets induced by nitrogen deprivation (Merino-Puerto *et al.*, 2010). Structural analysis demonstrates also, that FraH is required for heterocyst formation in *Anabaena* sp. (Merino-Puerto *et al.*, 2011b). For further experiments it can be interested to perform growth studies of *fraH* under nitrogen limitation including ultra-structure analysis.

Beside FraH also the candidate AncM was identified in the proteomic screen. The reduced amount of AncM observed in the PDM was confirmed by Western blot analysis (Figure 11).

4.3 Genetic Screen

The genetic screen based on photosynthetic suppressor of *curT*⁻ provides an opportunity to identify potential candidates that may have an influence on the architecture of convergence zones or the PSII assembly machinery. Following this, five candidates: *slr6004*, *slr6063*, *cyt c_M*, *hik43* and *ancM* were found. The amino acid exchange from isoleucine to methionine in the ORFs *slr6004* and *slr6063* can suggest a transcription start point. The similarity of the putative peptides reveals the same function of this small transcripts. However, for further experimental analysis, this work focusses on the chromosomal ORFs *cyt c_M*, *hik43* and *ancM*.

Primary studies with the candidate *cyt c_M* show a reduced photoautotrophic growth rate (Table 13). This is in contradiction to the reported cell counting method using a Goryaev camera in Malakhov *et al.* (Malakhov *et al.*, 1994). It should be mentioned that the reported growth conditions with 34°C and a gas exposure of 1% CO₂ in the presence of oxygen differs from the growth condition used in this study (Malakhov *et al.*, 1994). Recent studies observed that the Cyt c_M plays a role under photomixotrophy conditions (Solymosi *et al.*, 2019). Based on that knowledge, it can be interesting for further experiments to increase the glucose concentration of growth studies. Based on the knowledge that the expression level of *cyt c_M* encoding protein Cyt c_M is induced during stress conditions (Shuvalov *et al.*, 2001), it could be demonstrated that the respiration in *cyt c_M*⁻ is negatively affected after high light (Figure 15) (Malakhov *et al.*, 1999). Expression analysis data of *cyt c_M* showed an increase of *cyt c_M* expression during salt stress (Hernandez-Prieto and Futschik, 2012). The loss of Cyt c_M might affect the growth under salt stress. Based on these experiments and the literature, this suggests that during stress, the respiratory electron transport carrier PC / cytochrome c₆ is replaced by Cyt c_M (Bernroither *et al.*, 2009). Stress can be induced by increased radiation (high light) or osmotically demanding conditions.

Based on the knowledge that Hik43 is involved in Pilus biogenesis, investigating the phenotype of a *hik43* in motile variant of *Synechocystis* like the PCC-Moscow sub strain WT (Yoshihara *et al.*, 2002; Ding *et al.*, 2015; Morris *et al.*, 2016) would be advisable. With respect to CurT, the connection between Hik43 and CurT proteins has to be determined.

Taking this data together, the candidates *cyt c_M* and *hik43* might not participate in the PSII biogenesis. Concerning that fact, the co-expression with CurT and that AncM was found in both independent screens, the main part of this work deals with the candidate *ancM* (Hernandez-Prieto and Futschik, 2012).

4.3.1 Characterisation of AncM

4.3.1.1 Properties of recombinant AncM

A separation by Blue-Native PAGE allows characterisation of native protein complexes. This suggests that MBP-AncM is able to form *in vitro* high molecular weight complexes with a size of ~290/650 kDa (Figure 22 A). Beside the self-aggregation of MBP, AncM might be involved in the formation of this complexes. Separation experiments of MBP on a Native Gel indicate that MBP forms a dimer/trimer (Ganesh *et al.*, 2001). Based on the known ability of self-aggregation of the MBP tag, this suggests that the formed Tetramer/Nonamer of AncM is independent of MBP.

Furthermore, it should be mentioned that the expected mass weight with 32 kDa of AncM differs from the specific band with ~28 kDa. Basically, this difference can be caused by signal peptides which gets cleaved off like the N-terminal processing of D1 (Komenda *et al.*, 2007a). However, bioinformatical studies suggest that AncM is free of signal peptides. The difference of 4 kDa can be affected by a different running behavior during electrophoresis.

4.3.1.2 *ancM* and the phenotypes of the related strains

The photosynthetic phenotype of *ancM* is caused by the loss of *ancM*, which was verified by complementation of the gene (Table 14). In addition, a possible role of *slr2071*, which is expressed in one transcriptomic unit with *ancM* (Kopf *et al.*, 2014) could be excluded by growth studies of the strain *slr2071*⁻ (Figure 21). The reported reduced photosynthetic performance of *curT*⁻ was confirmed by Heinz *et al.* (Heinz *et al.*, 2016b). The significant reduction in growth of *ancM* during highlight illumination point to a possible defect during PSII repair cycle.

The resulting photosynthetic suppressor line *sucurT* demonstrates a partial suppression of the *curT*⁻ phenotype (Heinz *et al.*, 2016b). Structural comparison of *sucurT*⁻ and *curT*⁻ shows an organised arrangement of thylakoid in *sucurT*⁻ (Figure 35). In contrast to WT, the thylakoids in *sucurT*⁻ are arranged at the outside of the cell. This order of thylakoids might allow *sucurT*⁻ to harvest light in an efficient way to perform photosynthesis in the absence of convergence zones. For further experiments it could be interesting to verify if PSII gets easily damaged in *sucurT*⁻ by high light. This could perhaps be an explanation for a reduced chlorophyll content during the oxygen evolution of *sucurT*⁻'s comparable to the WT.

A reduced photosynthetic performance is also observed in *ancM*^{W164STOP}. It is interesting that the strains *sucurT*⁻ and *ancM*^{W164STOP} have the same oxygen evolution per OD₇₅₀. A possible role of the soluble N-terminus of AncM needs to be discussed. The potential expression of N-terminal AncM might explain the positive effect on the photosynthetic performance on the strain *ancM*^{W164STOP} in contrast to *ancM*⁻. Western blot analysis shows no detection in the lines *sucurT*⁻ and *ancM*^{W164STOP} of a putative N-terminus, not even N-terminal detection of a His Tag by using a HisHRP conjugate (Figure 20). A possible option is the

degradation of the N-terminus by the proteases after expression. Additionally, the detection limit of the HisHRP conjugate is also conceivable.

Another aspect is the reduced chlorophyll content in *ancM*^{W164STOP} compared to the WT and *ancM*. It is well known that PSI is the protein complex with the most chlorophyll molecules (Jordan *et al.*, 2001). It remains to be studied if *ancM*^{W164STOP} has less PSI trimers, which would result in a reduced photosynthetic performance.

In contrast, the double knock-out line *ancM* *curT* has a reduced light dependent oxygen evolution during normal photoautotrophic growth and a chlorophyll content like the WT. The reduced oxygen evolution can be based on the loss of the PSII convergence zones in the double mutant, which can be observed in *curT* (Heinz *et al.*, 2016b). This moderate photosynthetic phenotype of the double knock-out line suggests that AncM is the antagonist of CurT. This theory may be supported by the fact that high light has no effect on the growth of the double knock-out mutant *ancM* *curT* in contrast to the single knock-out strains (Table 15).

4.3.1.3 *ancM* has a molecular photosynthetic phenotype

The reduction of photoautotrophic growth and oxygen evolution as well as the PSII driven reduction of the PSI reaction centre P₇₀₀ in *ancM* could be the result of the significant decrease in the amount of PSII, as judged by the reduced abundance of the core proteins D1, D2 and CP43 (Figure 23). In addition, the P₇₀₀⁺ absorption measurements showed that the cyclic electron flow is not affected in *ancM*. However, the relative electron transfer rate measurements suggest that the electrons get inside PSII, transferred like the WT (Figure 24). Moreover, a non-affected electron transfer rate was also observed in *curT* (Heinz *et al.*, 2016b).

As opposed to the decrease in PSII, the stromal subunit of PSI PsaD is increased in the *ancM* mutant strain. An imbalance of the PSII and PSI ratio could be confirmed by low temperature fluorescence measurements (Figure 25). A decreased oxygen evolution in *ancM* is observed in the presence of a constant chlorophyll concentration, which might be the result of an imbalance of the photosynthetic complexes (Table 14). Interestingly, the distribution of the photosynthetic super-complexes is shifted in *ancM* to monomeric PSI and RCCI. An increase of monomeric PSII can be the reason for the reduced photosynthetic performance of *ancM*. The low molecular subunits PsbI and PsbM are the key proteins to form PSII super complexes in cyanobacteria like *Thermosynechococcus elongatus* (Kawakami *et al.*, 2011). Thus, it can be speculated that the amount of the low molecular mass subunits PsbI and PsbM are reduced in the AncM lacking strain.

However, the high turnover of the PSII assembly allows to follow *de novo* synthesis of PSII over a short time using radio-labelled methionine (Komenda *et al.*, 2004; Dobáková *et al.*, 2007; Komenda *et al.*, 2007b; Heinz *et al.*, 2016b). Following this, the PSII monomer formation

is retarded in *ancM* compared to the WT (Figure 28). The shift of the photosynthetic complexes towards PSII and PSI monomer might also link to the PSII assembly machinery.

4.3.1.4 AncM is localised at the PDM

Primary bioinformatic analysis predicts a transmembrane domain from amino acid position 164 until position 180 (Figure 16). This could be confirmed by solubilising of the membrane proteins with various detergents and salts (Figure 28). AncM is identified as a membrane protein, like the well characterised membrane proteins CP43 and CurT (Umena *et al.*, 2011; Heinz *et al.*, 2016b). A localisation at the plasma membrane can be excluded by an one step sucrose density gradient (Figure 29) (Schottkowski *et al.*, 2009b).

In detail, membrane fractionation shows a localisation of AncM and PrataA at the PDM (Rengstl *et al.*, 2011; Stengel *et al.*, 2012) (Figure 30). The correlation of localisation with PrataA allows to use AncM as marker for PDM regions (Stengel *et al.*, 2012). Based on the high cross reactivity of anti PrataA, the detection of PrataA via immunolocalisation studies has been unsuccessful (Klinkert *et al.*, 2004; Schottkowski *et al.*, 2009b). In contrast, the high specificity of α AncM that was produced in this work allows the detection of AncM by immunofluorescence.

The distinguished blue immunofluorescence spots resulting from incubation with α AncM and WT cells reveals AncM at the periphery of the cyanobacterial cell (Figure 32 - Figure 34). The precise arrangement of the signal dots localised at the entire area at the WT cell in combination with the sub-localisation at the PDM lead to the hypothesis that the blue spots could represent the PDM (Rengstl *et al.*, 2011). Moreover, this specialised region including the convergence zones within the thylakoids is the place where the PSII assembly takes place (Rengstl *et al.*, 2011; Rast *et al.*, 2015; Heinz *et al.*, 2016b; Rast *et al.*, 2019). The loss of AncM results in a structural change of the convergence zones caused by the loss of fixing points from the PDM with PM. As secondary effect, it is conceivable that the structural change of the PDM revealed an increase of RCCI, as is observed in *ancM* (Figure 26).

Beside the PSII assembly machinery the location of the PSI assembly machinery is still under discussion. One possibility is that this process takes place at the active thylakoids. Concerning that possibility, this suggests that the PSI assembly machinery is in *ancM* not primarily affected (Dühring *et al.*, 2006; Rengstl *et al.*, 2011).

As already indicated by immunofluorescence studies with α CurT, it was possible to confirm that CurT protein forms tubular structures (Heinz *et al.*, 2016b). Moreover, CLEM studies revealed that CurT is accumulating at the area without chlorophyll autofluorescence are the convergence zones (Heinz *et al.*, 2016b). In addition, a movement of the outer chlorophyll circle into the insight of the *curT*⁻ cell was confirmed by CLEM (Figure 36).

Interestingly, membrane fractionation demonstrates a shift of CurT in *ancM* towards the active TM (Figure 30). Such a movement of CurT into the inner area of the cell was also observed in immunofluorescence studies in *ancM* (Figure 32 H). This movement was also

observed in the vice versa experiment, which might lead to an imbalance during the formation of thylakoids.

The movement of the AncM immunofluorescence signal in *curT* indicates a shift of the PDM into the inner area. Considering this fact, the data suggest that the incomplete PSII assembly in *curT* might take place inside the cell.

Colocalisation studies with genetically fluorescence-tagged CurT as a marker for biogenic regions allows an overlay with the immunofluorescence signal of AncM. The overlay of the fluorescence displays a partial co-localisation of AncM and CurT (Figure 34). The co-localisation in the regions without chlorophyll autofluorescence suggests that the proteins accumulate at the convergence zones (Rengstl *et al.*, 2011; Rast *et al.*, 2015; Heinz *et al.*, 2016b; Rast *et al.*, 2019).

4.3.1.5 The relationship of CurT and AncM

The genetic screen points out to a relationship between the proteins AncM and CurT. This connection could be confirmed by bioinformatic co-expression analysis (Hernandez-Prieto and Futschik, 2012) and various experiments:

- Decreased PSII activity if one partner is missing (Table 14, Figure 24, Figure 25), (Heinz *et al.*, 2016b)
- Reduced amount of CurT in *ancM* (Figure 20)
- Partial colocalisation of CurT and AncM at the convergence zones (Figure 34).
- Shift of one partner during the absence of the other one (Figure 32).

An interaction between AncM and CurT is suggested based on the co-localisation studies (Figure 34). This was confirmed by mass spectrometry at the PDM (Table 16). Thus, it can be speculated that AncM forms a complex with CurT. However, western blot analysis with the immuno-precipitation eluate did not confirm a possible interaction (Figure 31). It should be mentioned that the mass spectrometry approach has to be repeated by two independent biological replicates. Additionally, it is possible that the amount of bound AncM is below the detection limit of α AncM (Figure 18).

4.3.1.6 Comparison of PDM and TM

A mass spectrometric analysis of the PDM as well as the TM allows to get a better understanding of putative interaction partners of CurT. (Table 16 and Table 17). CurT, which is present in both fractions, could be established as a good candidate for further analysis of possible interaction partners. In addition to AncM, which is well characterised in this study, Vipp1 was identified as possible interaction partner of CurT in the PDM by mass spectrometry and western blot analysis (Table 16, Figure 31). The presence of Vipp1 at the PDM is suggested by localisation studies of GFP tagged Vipp1 performed by Bryan *et al.* (2014). This previous fluorescence study shows a localisation of Vipp1 inside the cytoplasm and at the outer periphery of the cyanobacterial cell. This suggests an interaction between CurT and

Vipp1 at PDM. It should be mentioned that the protein level of Vipp1 is not affected in *curT* (Heinz *et al.*, 2016b). Based on the interaction of CurT and Vipp1, it can be speculated if this complex is involved in structural formation of the thylapse (Heinz *et al.*, 2016b; Rast *et al.*, 2019; Siebenaller *et al.*, 2019).

As a novel putative interaction partner of CurT at the PDM the RNA binding protein Rbp3 was identified (Tang *et al.*, 2010). Interestingly, a possible relationship between CurT and Rbp3 was shown by co-expression studies (Hernandez-Prieto and Futschik, 2012). The loss of Rbp3 is accompanied by a reduction of membrane lipids (Tang *et al.*, 2010). Moreover, recent Fish experiments performed by Mahbub *et al.* (2020) reported that Rbp3 is bound to *psbA2* and *psaA* mRNA. Furthermore, these studies indicate that the *psbA* mRNA is located at the inner thylakoids of the cell, which revealed that the D1 synthesis takes place at the interior of the cell (Mahbub *et al.* (2020). These results are in line with the studies of Rast *et al.* (2019), which located the ribosomes at the cytosol-facing inner thylakoids by cryo-electron tomograms. In addition, these studies reported also from the thylakoid convergence membrane, which is decorated with ribosomes. However, these findings match to the idea that only sub fractions of the *psbA* mRNA is part of the PSII *de novo* biogenesis whereas the major part takes place to spatial separated PSII repair synthesis like the situation observed in chloroplast (Uniacke and Zerges, 2007). This data confirms the important function of CurT in the early steps of PSII assembly (Rengstl *et al.*, 2011; Stengel *et al.*, 2012; Heinz *et al.*, 2016b).

A possible co-expression with CurT was also demonstrated for ORF *sll0822*, a hypothetical protein and *slr1329*, which encodes for the ATPase β subunit (Hernandez-Prieto and Futschik, 2012). Contrary, the ORF *sll1837* is known as a periplasmatic protein that displays a co-expression with AncM and was found at PDM and TM. A possible role of AncM in the periplasm and TM was excluded by sucrose step gradient (Table 16).

A possible interaction of CurT with FtsH and CP43 might link to the PSII repair machinery (Komenda *et al.*, 2006; Heinz *et al.*, 2016b). This also explains the resulting increase of D1 turnover in the CurT lacking strain (Heinz *et al.*, 2016b). For further experiments this putative interaction partner of CurT should be verified by biological replicates and western blot analysis.

4.3.1.7 AncM - The membrane anchor.

Electron microscopy studies revealed an unordered organisation of thylakoids in a *Synechocystis* cell caused by the loss of AncM. In contrast to *curT* and *sucurT*, the thylakoids in *ancM* are fused but didn't get converged towards the plasma membrane (Heinz *et al.*, 2016b). Following this, AncM has significantly more thylakoids in one stack compared to the WT (Figure 32). This suggests that AncM is involved in the regulation of thylakoid organisation and biogenesis.

Discussion

Moreover, CLEM offers as a powerful method to obtain a better understanding of the chlorophyll and thylakoid distribution (Figure 36). The arrangement of thylakoids in combination with the localisation of chlorophyll autofluorescence allows to detect the active membrane layers inside the cell. Correlative micrographs show that the distribution of chlorophyll molecules is not shifted in *ancM*. This contrasts with the chlorophyll distribution observed in *curT*. Based on the unordered thylakoids the chlorophyll is distributed to the thylakoids inside the cell (Heinz *et al.*, 2016b).

The correlative micrographs allow to identify the convergence zones by the absence of the chlorophyll auto fluorescence in WT (Rengstl *et al.*, 2011). The architecture of the convergence zones in *ancM* and *sucurT* differ to WT. Interestingly, it can be speculated that the chlorophyll less spots in *curT* and *sucurT* are the location of PSII assembly. In the WT these spots are located close to the plasma membrane at the thylakoids converging zone (Stengel *et al.*, 2012; Heinz *et al.*, 2016b). This fits to the converging zones reported in Rast *et al.* (2019) that are decorated with ribosomes but not with phycobilisomes. The detachment of thylakoids converging tubule observed in *ancM* and *sucurT* revealed that AncM is needed to fix the thylakoid converging tubule with the plasma membrane (CLEM). Based on the position of the TMD, this suggests that the N-terminus of AncM is connecting the plasma membrane across the cytosol. The localisation of AncM and the altered organisation of thylakoids in *ancM* allow to speculate if AncM is responsible for the connection between the thylakoids and the plasma membrane, which is also called the thylapse (Rast *et al.*, 2019). This theory is supported by the presence of the DUF168 domain, which encodes for 2H phosphodiesterase protein family (Mazumder *et al.*, 2002). This region is responsible for anchoring of tubulin in brain tissue (Bifulco *et al.*, 2002). It is thus possible that AncM is anchoring the thylakoids with the plasma membrane (Figure 38). It is hypothesised that AncM is located at the thylapse, a structuring region of the thylakoids and is responsible for anchoring the thylakoids with the plasma membrane (Rast *et al.*, 2019). Moreover, based on the reported gap in Rast *et al.* (2019) of 2-4 nm in between the thylakoid converging membrane and the plasma membrane, this suggests that AncM is part of the electron dense material that connects the plasma membrane with the TM.

Discussion

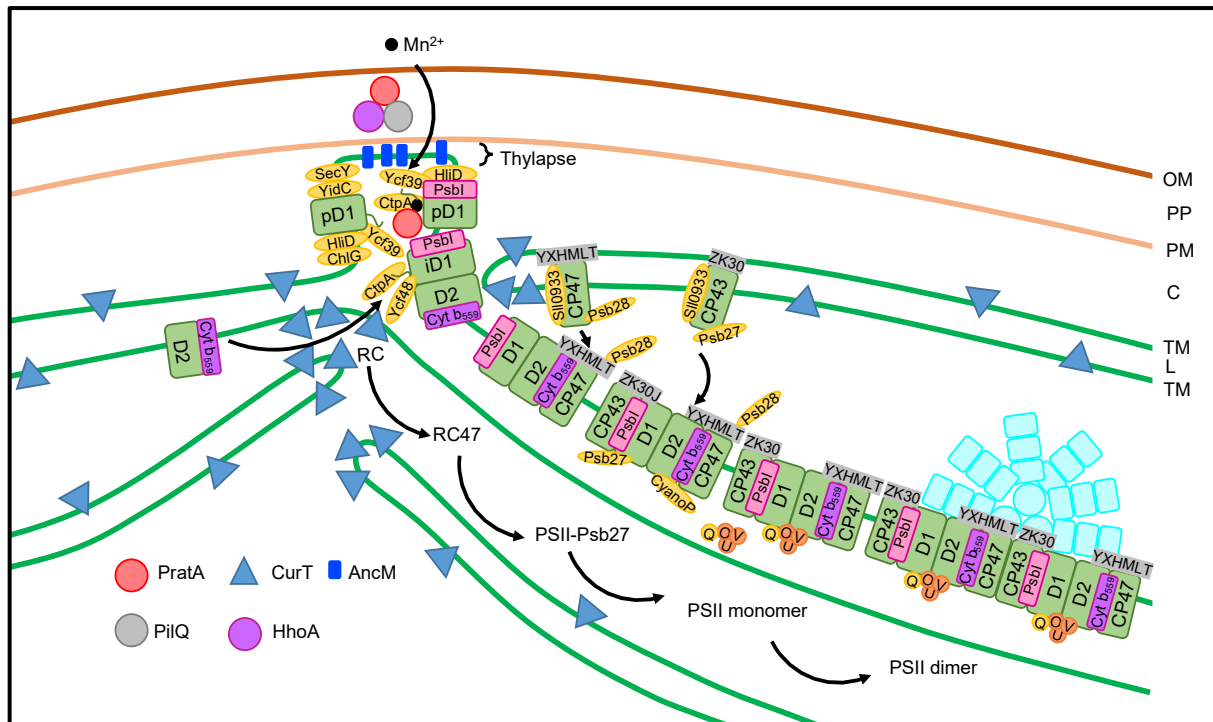


Figure 38: Is AncM the membrane anchor for thylakoids? Updated working model. CurT curvature the thylakoids towards the plasma membrane and form the convergence zones. AncM is located at thylapase and fix the thylakoids with the plasma membrane (PM). pD1 gets preloaded by PratA with Mn^{2+} and followed by further PSII assembly step. Red circle: PratA, grey circle: PilQ, purple circle: HhoA, blue triangle: CurT, blue balk: AncM, yellow: PSII assembly factors, green: intrinsic subunits D1, D2 and the chlorophyll binding proteins CP43 and CP47, pink: PsbI, purple: Cyt b_{559} , grey: low mass subunits, orange: extrinsic subunits, turquoise: phycobilisomes.

BIBLIOGRAPHY

- Acuña, A.M., van Alphen, P., van Grondelle, R., and van Stokkum, I.H.M.** (2018). The phycobilisome terminal emitter transfers its energy with a rate of $(20 \text{ ps})^{-1}$ to photosystem II. *Photosynthetica* **56**, 265-274.
- Alexeyev, M.F., Shokolenko, I.N., and Croughan, T.P.** (1995). Improved antibiotic-resistance gene cassettes and omega elements for *Escherichia coli* vector construction and in vitro deletion/insertion mutagenesis. *Gene* **160**, 63-67.
- Allen, F., and Good, P.** (1971). Acyl lipids in photosynthetic systems. *Methods in Enzymology* **23**, 523-547.
- Altschul, S.F., Madden, T.L., Schäffer, A.A., Zhang, J., Zhang, Z., Miller, W., and Lipman, D.J.** (1997). Gapped BLAST and PSI-BLAST: a new generation of protein database search programs. *Nucleic Acids Res* **25**, 3389–3402.
- Ananyev, G.M., and Dismukes, C.G.** (1997). Calcium induces binding and formation of a spin-coupled dimanganese (II,II) center in the apo-water oxidation complex of photosystem II as precursor to the functional Tetra-Mn/Ca Cluster. *Biochemistry* **36**, 11342-11450.
- Anbudurai, P.R., Mor, T.S., Ohad, I., Shestakov, S.V., and Pakrasi, H.B.** (1994). The *ctpA* gene encodes the C-terminal processing protease for the D1 of the photosystem II reaction center complex. *Proc Natl Acad Sci U S A* **91**, 8082-8086.
- Apel, K., and Hirt, H.** (2004). Reactive oxygen species: metabolism, oxidative stress, and signal transduction. *Annu Rev Plant Biol* **55**, 373-399.
- Armbruster, U., Zühlke, J., Rengstl, B., Kreller, R., Makarenko, E., Rühle, T., Schünemann, D., Jahns, P., Weisshaar, B., Nickelsen, J., and Leister, D.** (2010). The *Arabidopsis* thylakoid protein PAM68 is required for efficient D1 biogenesis and photosystem II assembly. *Plant Cell* **22**, 3439-3460.
- Armbruster, U., Labs, M., Pribil, M., Viola, S., Xu, W., Scharfenberg, M., Hertle, A.P., Rojahn, U., Jensen, P.E., Rappaport, F., Joliot, P., Dormann, P., Wanner, G., and Leister, D.** (2013). *Arabidopsis* CURVATURE THYLAKOID1 proteins modify thylakoid architecture by inducing membrane curvature. *Plant Cell* **25**, 2661-2678.
- Arteni, A.A., Ajlani, G., and Boekema, E.J.** (2009). Structural organisation of phycobilisomes from *Synechocystis* sp. strain PCC6803 and their interaction with the membrane. *Biochim Biophys Acta* **1787**, 272-279.
- Aseeva, E., Ossenbühl, F., Sippel, C., Cho, W.K., Stein, B., Eichacker, L., Meurer, J., Wanner, G., Westhoff, P., Soll, J., and Voithknecht, U.C.** (2007). Vipp1 is required for basic thylakoid membrane formation but for the assembly of protein complexes. *Plant Physiol Biochem.* **45**, 119-128.

Bibliography

- Bandyopadhyay, A., Elvitigala, T., Welsh, E., Stockel, J., Liberton, M., Min, H., Sherman, L.A., and Pakrasi, H.B.** (2011). Novel metabolic attributes of the genus *Cyanothece*, comprising a group of unicellular nitrogen-fixing *Cyanothece*. *mBio* **2**.
- Barber, J., and De Las Rivas, J.** (1993). A functional model for the role cytochrome b559 in the protection against donor and acceptor side photoinhibition. *Proc Natl Acad Sci U S A* **90**, 10942-10946.
- Bartoschik, T., Galinec, S., Kleusch, C., Walkiewicz, K., Breitsprecher, D., Weiter, S., Muller, Y.A., You, C., Piehler, J., Vercruyssen, T., Daelemaes, D., and Tschammer, N.** (2018). Near-native, site-specific and purification-free protein labeling for quantitative protein interaction analysis by MicroScale Thermophoresis. *Scientific Reports* **8**, 1-10.
- Benning, C., Beatty, J.T., Prince, R.C., and Somerville, C.R.** (1993). The sulfolipid sulfoquinovosyldiacylglycerol is not required for photosynthetic electron transport in *Rhodobacter sphaeroides* but enhances growth under phosphate limitation. *Proc Natl Acad Sci U S A* **90**, 1561-1565.
- Benson, A., and Calvin, M.** (1947). The dark reactions of photosynthesis *Science* **105**, 648-649.
- Bepperling, A., Alte, F., Kriehuber, T., Braun, N., Weinkauff, S., Groll, M., Haslbeck, M., and Buchner, J.** (2012). Alternative bacterial two-component small heat shock protein systems. *Proc Natl Acad Sci U S A* **109**, 20407-20412.
- Bernat, G., Waschewski, N., and Rögner, M.** (2009). Towards efficient hydrogen production: the impact of antenna size and external factors on electron transport dynamics in *Synechocystis* PCC 6803. *Photosynth Res* **99**, 205-216.
- Bernroither, M., Tangl, D., Lucini, C., Furtmüller, P.G., Peschek, G.A., and Obinger, C.** (2009). Cyanobacterial cytochrome c(M): probing its role as electron donor for Cu(A) of cytochrome c oxidase. *Biochim Biophys Acta* **1787**, 135-143.
- Bifulco, M., Laezza, C., Stingo, S., and Wolff, J.** (2002). 2',3'-Cyclic nucleotide 3'-phosphodiesterase: a membrane-bound, microtubule-associated protein and membrane anchor for tubulin. *Proc Natl Acad Sci U S A* **99**, 1807-1812.
- Blankenship, R.E.** (1992). Origin and early evolution of photosynthesis. *Photosynth Res* **33**, 91-111.
- Boehm, M., Romero, E., Reisinger, V., Jianfeng, Y., Komenda, J., Eichacker, L., Dekker, J.P., and Nixon, P.J.** (2011). Investigating the early stage of photosystem II assembly in *Synechocystis* sp. PCC 6803: Isolation of CP47 and CP43 complexes. *Journal of biological chemistry* **286**, 1412-1419.
- Boehm, M., Yu, J., Reisinger, V., Beckova, M., Eichacker, L.A., Schlodder, E., Komenda, J., and Nixon, P.J.** (2012a). Subunit composition of CP43-less photosystem II complexes of *Synechocystis* sp. PCC 6803: implications for the assembly and repair of photosystem II. *Philos Trans R Soc Lond B Biol Sci* **367**, 3444-3454.

Bibliography

- Boehm, M., Yu, J., Krynicka, V., Barker, M., Tichý, M., Komenda, J., Nixon, P.J., and Nield, J.** (2012b). Subunit organization of a *Synechocystis* hetero-oligomeric thylakoid FtsH complex involved in photosystem II repair. *Plant Cell* **24**, 3669-3683.
- Bohne, A.V., Schwarz, C., Schottkowski, M., Lidschreiber, M., Piotrowski, M., Zerges, W., and Nickelsen, J.** (2013). Reciprocal regulation of protein synthesis and carbon metabolism for thylakoid membrane biogenesis. *PLoS Biol* **11**, e1001482.
- Bottier, C., Géan, J., Artzner, F., Desbat, B., Pézolet, M., Renault, A., Marion, D., and Vié, V.** (2007). Galactosyl headgroup interactions control the molecular packing of wheat lipids in langmuir films and in hydrated liquid-crystalline mesophases. *Biochimica et Biophysica Acta (BBA) - Biomembranes* **1768**, 1526-1540.
- Boudière, L., Michaud, M., Petroutsos, D., Rébeillé, F., Falconet, D., Bastien, O., Roy, S., Finazzi, G., Rolland, N., Jouhet, J., Block, M.A., and Maréchal, E.** (2014). Glycerolipids in photosynthesis: composition, synthesis and trafficking. *Biochim Biophys Acta* **1837**, 470-480.
- Brocks, J.J., Love, G.D., Summons, R.E., Knoll, A.H., Logan, G.A., and Bowden, S.A.** (2005). Biomarker evidence for green and purple sulphur bacteria in a stratified Palaeoproterozoic sea. *Nature* **437**, 866-870.
- Bryan, S.J., Nigel, B.J., Shevela, D., Jianfeng, Y., Rupprecht, E., Liu, L., Mastroianni, G., Xue, Q., Liorente-Garcia, I., Leake, M.C., Eichacker, L., Schneider, D., Nixon, P.J., and Mullineaux, C.W.** (2014). Localisation and interactions of the Vipp1 protein in cyanobacteria. *Molecular Microbiology* **94**, 1179-1195.
- Campbell, E.L., Summers, M.L., Christman, H., Martin, M.E., and Meeks, J.C.** (2007). Global gene expression patterns of *Nostoc punctiforme* in steady-state dinitrogen-grown heterocyst-containing cultures and at single time points during the differentiation of akinetes and hormogonia. *J Bacteriol* **189**, 5247-5256.
- Chen, S., He, N., Chen, J., and Guo, F.** (2017). Identification of core subunits of photosystem II as action sites of HSP21, which is activated by the GUN5-mediated retrograde pathway in *Arabidopsis*. *the plant journal* **89**, 1106-1118.
- Cheregi, O., Wagner, R., and Funk, C.** (2016). Insights into the Cyanobacterial Deg/HtrA Proteases. *Frontiers in Plant Science* **7**.
- Chevallet, M., Luche, S., and Rabilloud, T.** (2006). Silver staining of proteins in polyacrylamid gels. *Nature Protocols* **1**, 1852-1856.
- Chidgey, J.W., Linhartova, M., Komenda, J., Jackson, P.J., Dickman, M.J., Canniffe, D.P., Konik, P., Pilny, J., Hunter, C.N., and Sobotka, R.** (2014). A cyanobacterial chlorophyll synthase-HliD complex associates with the Ycf39 protein and the YidC/Alb3 insertase. *Plant Cell* **26**, 1267-1279.
- Chitnis, V.P., and Chitnis, P.R.** (1993). PsaL subunit required for the formation of photosystem I trimers in the cyanobacterium *Synechocystis* sp. PCC 6803. *FEBS Letters* **336**, 330-334.

Bibliography

- Cho, Y.S., Pakrasi, H.B., and Whitmarsh, J.** (2000). Cytochrome c_M from *Synechocystis* 6803. Detection in cells, expression in *Escherichia coli*, purification and physical characterization. *European Journal of Biochemistry* **267**, 1068-1074.
- Chrysina, M., Heyno, E., Kutin, Y., Reus, M., Nilsson, H., Nowaczyk, M.M., DeBeer, S., Neese, F., Messinger, J., Lubitz, W., and Cox, N.** (2019). Five-coordinate Mn(IV) intermediate in the activation of nature's water splitting cofactor. *Proc Natl Acad Sci U S A* **116**, 16841-16846.
- Chu, H.A., and Chiu, Y.F.** (2015). The roles of cytochrome *b* 559 in assembly and photoprotection of photosystem II revealed by site-directed mutagenesis studies. *Front Plant Sci* **6**, 1261.
- Clausen, T., Southan, C., and Ehrmann, M.** (2002). The HtrA Family of Proteases. *Molecular Cell* **10**, 443-455.
- Cormann, K.U., Bartsch, M., Rögner, M., and Nowaczyk, M.M.** (2014). Localization of the CyanoP binding site on photosystem II by surface plasmon resonance spectroscopy. *Front Plant Sci* **5**, 595.
- Cormann, K.U., Bangert, J.A., Ikeuchi, M., Rögner, M., Stoll, R., and Nowaczyk, M.M.** (2009). Structure of Psb27 in solution: implications for transient binding to photosystem II during biogenesis and repair. *Biochemistry* **48**, 8768-8770.
- Cox, N., Retegan, M., Neese, F., Pantazis, D.A., Bousac, A., and Lubitz, W.** (2014). Electronic structure of the oxygen-evolving complex in photosystem prior to O-O bond formation. *Photosynthesis* **345**, 804-808.
- Ding, Q., Chen, G., Wang, Y., and Wei, D.** (2015). Identification of specific variations in a non-motile strain of cyanobacterium *Synechocystis* sp. originated from ATCC 27184 by whole genome resequencing. *Int J Mol Sci* **16**, 24081-24093.
- Dobáková, M., Tichý, M., and Komenda, J.** (2007). Role of the PsbI protein in photosystem II assembly and repair in the cyanobacterium *Synechocystis* sp. PCC 6803. *Plant Physiol* **145**, 1681-1691.
- Dobáková, M., Sobotka, R., Tichý, M., and Komenda, J.** (2009). Psb28 protein is involved in the biogenesis of the photosystem II inner antenna CP47 (PsbB) in the cyanobacterium *Synechocystis* sp. PCC 6803. *Plant Physiol* **149**, 1076-1086.
- Dolganov, N.A., Bhaya, D., and Grossman, A.R.** (1995). Cyanobacterial proteins with similarity to the chlorophyll *a* / *b* binding proteins of higher plants: Evolution and regulation. *PNAS* **92**, 636-640.
- Dühring, U., Irrgang, K.D., Lünser, K., Kehr, J., and Wilde, A.** (2006). Analysis of photosynthetic complexes from a cyanobacterial *ycf37* mutant. *Bioenergetics* **1757**, 3-1.
- Edelman, M., and Mattoo, A.K.** (2008). D1-protein dynamics in photosystem II: the lingering enigma. *Photosynth Res* **98**, 609-620.

Bibliography

- Eng, J.K., McCormack, A.L., and Yates, J.R.** (1994). An approach to correlate tandem mass spectral data of peptides with amino acid sequence in a protein database. *Journal of the American Society for Mass Spectrometry* **5**, 976-989.
- Engelke, D.R., Krikos, A., Bruck, M.E., and Ginsburg, D.** (1990). Purification of *Thermus aquaticus* DNA Polymerase expressed in *Escherichia coli*. *Analytical Biochemistry* **191**, 396-400.
- Falcon, L.I., Magallon, S., and Castillo, A.** (2010). Dating the cyanobacterial ancestor of the chloroplast. *ISME J* **4**, 777-783.
- Ferreira, K., Iverson, T.M., Maghlaoui, K., Barber, J., and Iwata, S.** (2004). Architecture of the photosynthetic oxygen-evolving center. *Science* **303**, 1831-1838.
- Fischer, N., Sétif, P., and Rochaix, J.-D.** (1999). Site-directed mutagenesis of the PsaC subunit photosystem I. F_B is the cluster interacting with soluble ferredoxin. *The Journal of Biological Chemistry* **274**, 23333-22340.
- Fish, L.E., Kück, U., and Bogorad, L.** (1985). Two partially homologues adjacent light-inducible Maize chloroplast genes encoding polypeptides of the P700 chlorophyll a-Protein complex of photosystem I. *The Journal of Biological Chemistry* **260**, 1413-1421.
- Fromme, P., Jordan, P., and Krauß, N.** (2001). Structure of photosystem I. *Biochimica et Biophysica Acta (BBA) - Bioenergetics* **1507**, 5-31.
- Ganesh, C., Zaidi, F.N., Udgaonkar, J.B., and Varadarajan, R.** (2001). Reversible formation of on-pathway macroscopic aggregates during the folding of maltose binding protein. *Protein Science* **10**, 1635-1644.
- Gathmann, S., Rupprecht, E., Kahmann, U., and Schneider, D.** (2008). A conserved structure and function of the YidC homologous protein Slr1471 from *Synechocystis* sp. PCC 6803. *Journal of Microbiology and Biotechnology* **18**, 1090-1094.
- Ge, H., Fang, L., Huang, X., Wang, J., Chen, W., Zhan, Y., Wang, X., Sui, N., He, Q., and Wang, Y.** (2018). Activation of the Oxidative Pentose Phosphate Pathway is Critical for Photomixotrophic Growth of a hik33-Deletion Mutant of *Synechocystis* sp. PCC 6803. *Proteomics* **18**, 1-31.
- Göhre, V., Ossenbühl, F., Crevecoeur, M., Eichacker, L.A., and Rochaix, J.D.** (2006). One of two Alb3 proteins is essential for the assembly of the photosystems and for cell survival in *Chlamydomonas*. *Plant Cell* **18**, 1454-1466.
- Gold, V.A.M., Salzer, R., Averhoff, B., and Kühlbrandt, W.** (2015). Structure of a type IV pilus machinery in the open and closed state. *eLife* **4**, e07380.
- Gounaris, K., Syndby, C., Andersson, B., and Barber, J.** (1983). Lateral heterogeneity of polar lipids in the thylakoid membranes of spinach chloroplast. *FEBS Letters* **156**, 170-174.

Bibliography

- Grasse, N., Mamedov, F., Becker, K., Styring, S., Rögner, M., and Nowaczyk, M.M.** (2011). Role of novel dimeric photosystem II (PSII)-Psb27 protein complex in PSII repair. *J Biol Chem* **286**, 29548-29555.
- Griese, M., Lange, C., and Soppa, J.** (2011). Ploidy in cyanobacteria. *FEMS Microbiol Lett* **323**, 124-131.
- Guan, C.d., Li, P., Riggs, P.D., and Inouye, H.** (1988). Vectors that facilitate the expression and purification of foreign peptides in *Escherichia coli* by fusion to maltose-binding protein. *Gene* **67**, 21-30.
- Guskov, A., Kern, J., Gabdulkhakov, A., Broser, M., Zouni, A., and Saenger, W.** (2009). Cyanobacterial photosystem II at 2.9-Å resolution and the role of quinones, lipids, channels and chloride. *Nat Struct Mol Biol* **16**, 334-342.
- Hagio, M., Gombos, Z., Varkanoyi, Z., Masamoto, N., Sato, N., Tsuzuki, H., and Wada, H.** (2000). Direct evidence for requirement of phosphatidylglycerol in photosystem II of photosynthesis. *Plant Physiology* **124**, 795-804.
- Hakala, M., Tuominen, I., Keranen, M., Tyystjarvi, T., and Tyystjarvi, E.** (2005). Evidence for the role of the oxygen-evolving manganese complex in photoinhibition of photosystem II. *Biochim Biophys Acta* **1706**, 68-80.
- Hakala, M., Rantamaki, S., Puputti, E.M., Tyystjarvi, T., and Tyystjarvi, E.** (2006). Photoinhibition of manganese enzymes: insights into the mechanism of photosystem II photoinhibition. *J Exp Bot* **57**, 1809-1816.
- Hanahan, D.** (1983). Studies on transformation of *Escherichia coli* with plasmids. *Journal of Molecular Biology* **166**, 557-580.
- Haußühl, K., Andersson, B., and Adamska, I.** (2001). A chloroplast DegP2 protease performs the primary cleavage of the photodamaged D1 protein in plant photosystem II. *The EMBO Journal* **20**, 713-722.
- Heinz, S., Liauw, P., Nickelsen, J., and Nowaczyk, M.** (2016a). Analysis of photosystem II biogenesis in cyanobacteria. *Biochim Biophys Acta* **1857**, 274-287.
- Heinz, S., Rast, A., Shao, L., Gutu, A., Gügel, I.L., Heyno, E., Labs, M., Rengstl, B., Viola, S., Nowaczyk, M.M., Leister, D., and Nickelsen, J.** (2016b). Thylakoid membrane architecture in *Synechocystis* depends on CurT, a homolog of the granal CURVATURE THYLAKOID1 Proteins. *Plant Cell* **28**, 2238-2260.
- Hernandez-Prieto, M.A., and Futschik, M.E.** (2012). CyanoExpress: A web database for exploration and visualisation of the integrated transcriptome of cyanobacterium *Synechocystis* sp. PCC6803. *Bioinformatics* **2**, 634-638.
- Hohmann-Marriott, M.F., and Blankenship, R.E.** (2011). Evolution of photosynthesis. *Annual Review of Plant Biology* **62**, 515-548.

Bibliography

- Holzwarth, A.R., Müller, M.G., Reus, M., Nowaczyk, M., Sander, J., and Rögner, M.** (2006). Kinetics and mechanism of electron transfer in intact photosystem II and in the isolated reaction center: pheophytin is the primary electron acceptor. *Proc Natl Acad Sci U S A* **103**, 6895-6900.
- Hospenthal, M.K., Costa, T.R.D., and Waksman, G.** (2017). A comprehensive guide to pilus biogenesis in gram-negative bacteria. *Nature reviews microbiology* **15**, 365-379.
- Huesgen, P.F., Scholz, P., and Adamska, I.** (2007). The serine protease HhoA from *Synechocystis* sp. strain PCC 6803: substrate specificity and formation of a hexameric complex are regulated by the PDZ domain. *J Bacteriol* **189**, 6611-6618.
- Huesgen, P.F., Miranda, H., Lam, X., Perthold, M., Schuhmann, H., Adamska, I., and Funk, C.** (2011). Recombinant Deg/HtrA proteases from *Synechocystis* sp. PCC 6803 differ in substrate specificity, biochemical characteristics and mechanism. *Biochem J* **435**, 733-742.
- Ifuku, K., and Noguchi, T.** (2016). Structural coupling of extrinsic proteins with the oxygen-evolving center in photosystem II. *Front Plant Sci* **7**, 84.
- Jarvis, P., Dormann, P., Peto, C.A., Lutes, J., Benning, C., and Chory, J.** (2000). Galactolipid deficiency and abnormal chloroplast development in the *Arabidopsis* MGD synthase 1 mutant. *Proc Natl Acad Sci U S A* **97**, 8175-8179.
- Jordan, P., Fromme, P., Witt, H.T., Klukas, O., Saenger, W., and Krauß, N.** (2001). Three-dimensional structure of cyanobacterial photosystem I at 2.5 Å resolution. *Nature* **411**, 909-917.
- Kale, R., Hebert, A.E., Frankel, L.K., Sallans, L., Bricker, T.M., and Pospíšil, P.** (2017). Amino acid oxidation of the D1 and D2 proteins by oxygen radicals during photoinhibition of photosystem II. *Proc Natl Acad Sci U S A* **114**, 2988-2993.
- Kaneko, T., Nakamura, Y., Sasamoto, S., Watanabe, A., Kohara, M., Matsumoto, M., Shimpo, S., Yamada, M., and Tabata, S.** (2003). Structural analysis of four large plasmids harboring in a unicellular cyanobacterium, *Synechocystis* sp. PCC 6803. *DNA Research* **10**, 221-225.
- Karplus, A.P., and Bruns, C.M.B.** (1994). Structure-Function relations for ferredoxin reductase. *Journal of Bioenergetics and Biomembranes* **26**, 89-99.
- Kashino, Y., Lauber, W.M., A., C.J., Wang, H.-L., Whitmarsh, J., Satoh, K., and Pakrasi, H.B.** (2002). Proteomic analysis of a highly active photosystem II preparation from the Cyanobacterium *Synechocystis* sp. PCC 6803. *Biochemistry* **41**, 8004-8012.
- Kato, K., Nagao, R., Jiang, T.Y., Ueno, Y., Yokono, M., Chan, S.K., Watanabe, M., Ikeuchi, M., Shen, J.R., Akimoto, S., Miyazaki, N., and Akita, F.** (2019). Structure of a cyanobacterial photosystem I tetramer revealed by cryo-electron microscopy. *Nat Commun* **10**, 4929.
- Kawakami, K., Umena, Y., Iwai, M., Kawabata, Y., Ikeuchi, M., Kamiya, N., and Shen, G.** (2011). Roles of PsbI and PsbM in photosystem II dimer formation and stability studied

Bibliography

- by deletion mutagenesis and X-ray crystallography. *Biochimica et Biophysica Acta (BBA) - Bioenergetics* **1807**.
- Kera, K., Yoshizawa, Y., Shigehara, T., Nagayama, T., Tsujii, M., Tochigi, S., and Uozumi, N.** (2020). Hik36–Hik43 and Rre6 act as a two-component regulatory system to control cell aggregation in *Synechocystis* sp. PCC6803. *Sci Rep* **10**.
- Keren, N., Berg, A., van Kan, P.J., Levanon, H., and Ohad, I.** (1997). Mechanism of photosystem II photoinactivation and D1 protein degradation at low light: The role of back electron flow. *Proc Natl Acad Sci U S A* **94**, 1579-1584.
- Kerfeld, C.A., and Melnicki, M.R.** (2016). Assembly, function and evolution of cyanobacterial carboxysomes. *Curr Opin Plant Biol* **31**, 66-75.
- Kirchhoff, H., Mukherjee, U., and Galla, H.-J.** (2002). Molecular architecture of the thylakoid membrane: Lipid diffusion space for plastoquinone. *Biochemistry* **41**, 4872-4772.
- Klinkert, B., Ossenbühl, F., Sikorski, M., Berry, S., Eichacker, L., and Nickelsen, J.** (2004). PratA, a periplasmic tetratricopeptide repeat protein involved in biogenesis of photosystem II in *Synechocystis* sp. PCC 6803. *J Biol Chem* **279**, 44639-44644.
- Knoppová, J., Yu, J., Konik, P., Nixon, P.J., and Komenda, J.** (2016). CyanoP is involved in the early steps of Photosystem II assembly in the cyanobacterium *Synechocystis* sp. PCC 6803. *Plant Cell Physiol* **57**, 1921-1931.
- Knoppová, J., Sobotka, R., Tichý, M., Yu, J., Konik, P., Halada, P., Nixon, P.J., and Komenda, J.** (2014). Discovery of a chlorophyll binding protein complex involved in the early steps of photosystem II assembly in *Synechocystis*. *Plant Cell* **26**, 1200-1212.
- Kok, B., Forbush, B., and McGloin, M.** (1970). Cooperation of charges in photosynthetic O₂ evolution-I. A linear step mechanism. *Photochemistry and Photobiology* **11**, 457-475.
- Komenda, J., Reisinger, V., Müller, B.C., Dobáková, M., Granvogl, B., and Eichacker, L.A.** (2004). Accumulation of the D2 protein is a key regulatory step for assembly of the photosystem II reaction center complex in *Synechocystis* PCC 6803. *J Biol Chem* **279**, 48620-48629.
- Komenda, J., Kuviková, S., Granvogl, B., Eichacker, L., Diner, B.A., and Nixon, P.J.** (2007a). Cleavage after residue Ala352 in the C-terminal extension is an early step in the maturation of the D1 subunit of photosystem II in *Synechocystis* PCC 6803. *Bioenergetics* **1767**, 829-837.
- Komenda, J., Nickelsen, J., Tichý, M., Prášil, O., Eichacker, L.A., and Nixon, P.J.** (2008). The cyanobacterial homologue of HCF136/YCF48 is a component of an early photosystem II assembly complex and is important for both the efficient assembly and repair of photosystem II in *Synechocystis* sp. PCC 6803. *J Biol Chem* **283**, 22390-22399.
- Komenda, J., Barker, M., Kuviková, S., de Vries, R., Mullineaux, C.W., Tichý, M., and Nixon, P.J.** (2006). The FtsH protease slr0228 is important for quality control of

Bibliography

- photosystem II in the thylakoid membrane of *Synechocystis* sp. PCC 6803. *J Biol Chem* **281**, 1145-1151.
- Komenda, J., Tichý, M., Prášil, O., Knoppová, J., Kuviková, S., de Vries, R., and Nixon, P.J.** (2007b). The exposed N-terminal tail of the D1 subunit is required for rapid D1 degradation during photosystem II repair in *Synechocystis* sp PCC 6803. *Plant Cell* **19**, 2839-2854.
- Komenda, J., Knoppová, J., Kopečná, J., Sobotka, R., Halada, P., Yu, J., Nickelsen, J., Boehm, M., and Nixon, P.J.** (2012). The Psb27 assembly factor binds to the CP43 complex of photosystem II in the cyanobacterium *Synechocystis* sp. PCC 6803. *Plant Physiol* **158**, 476-486.
- Kopf, M., Klähn, S., Scholz, I., Matthiessen, J.K., Hess, W.R., and Voss, B.** (2014). Comparative analysis of the primary transcriptome of *Synechocystis* sp. PCC 6803. *DNA Res* **21**, 527-539.
- Kroll, D., Meierhoff, K., Bechtold, N., Kinoshita, M., Westphal, S., Vothknecht, U.C., Soll, J., and Westhoff, P.** (2001). VIPP1, a nuclear gene of *Arabidopsis thaliana* essential for thylakoid membrane formation. *Proc Natl Acad Sci U S A* **98**, 4238-4242.
- Kufryk, G.I., Sachet, M., Schmetterer, G., and Vermaas, W.F.J.** (2002). Transformation of the cyanobacterium *Synechocystis* sp. PCC 6803 as a tool for genetic mapping: optimization of efficiency. *FEMS Microbiology Letters* **206**, 215-219.
- Kurusu, G., Zhang, H., Smith, J.L., and Cramer, W.A.** (2003). Structure of the Cytochrome *b₆f* complex of oxygenic photosynthesis: Tuning the cavity. *Science* **302**, 1009-1014.
- Lamb, J.J., Røkke, G., and Hohmann-Marriott, M.F.** (2018). Chlorophyll fluorescence emission spectroscopy of oxygenic organisms at 77 K. *Photosynthetica* **56**, 105-124.
- Lea-Smith, D.J., Bombelli, P., Vasudevan, R., and Howe, C.J.** (2016). Photosynthetic, respiratory and extracellular electron transport pathways in cyanobacteria. *Biochim Biophys Acta* **1857**, 247-255.
- Lee, A.G.** (2000). Membrane lipids: It's only a phase. *Current Biology* **10**, 377-380.
- Lelong, C., Boekema, E.J., Kruij, J., Bottin, H., Rögner, M., and Sétif, P.** (1996). Characterization of a redox active cross-linked complex between cyanobacterial photosystem I and soluble ferredoxin. *The EMBO Journal* **15**, 2160-2168.
- Liberton, M., Howard Berg, R., Heuser, J., Roth, R., and Pakrasi, H.B.** (2006). Ultrastructure of the membrane systems in the unicellular cyanobacterium *Synechocystis* sp. strain PCC 6803. *Protoplasma* **227**, 129-138.
- Liu, H., Weisz, D.A., and Pakrasi, H.B.** (2015). Multiple copies of the PsbQ protein in a cyanobacterial photosystem II assembly intermediate complex. *Photosynthesis Research* **126**, 375-383.

Bibliography

- Liu, Z., Yan, H., Wang, K., Kuang, T., Zhang, J., Gui, L., An, X., and Chang, W.** (2004). Crystal structure of spinach major light-harvesting complex at 2.72 Å resolution *Nature* **428**, 287-292.
- Loll, B., Kern, J., Saenger, W., Zouni, A., and Biesiadka, J.** (2005). Towards complete cofactor arrangement in the 3.0 Å resolution structure of photosystem II. *Nature* **438**, 1040-1044.
- Mahbub, M., Hemm, L., Yang, Y., Kaur, R., Carmen, H., Engl, C., Huokko, T., Riediger, M., Watanabe, S., Liu, L., Wilde, A., Hess, W.R., and Mullineaux, C.W.** (2020). mRNA localization, reaction centre biogenesis and thylakoid membrane targeting in cyanobacteria. *Nature Plants* **6**, 1179–1191.
- Malakhov, M.P., Malakhova, O.A., and Murata, N.** (1999). Balanced regulation of expression of the gene for Cytochrome c_M and that of genes for Plastocyanin and Cytochrome c_6 in *Synechocystis* *FEBS Letters* **444**, 281-284.
- Malakhov, M.P., Wada, H., Los, D.A., Semenko, V.E., and Murata, N.** (1994). A new type of cytochrome *c* from *Synechocystis* PCC6803. *Journal of Plant Physiology* **144**, 259-264.
- Matsusako, T., Toya, Y., Yoshikawa, K., and Shimizu, H.** (2017). Identification of alcohol stress tolerance genes of *Synechocystis* sp. PCC 6803 using adaptive laboratory. *Biotechnology of Biofuels* **10**, 1-9.
- Mazumder, R., Iyer, L.M., Vasudevan, S., and Aravind, L.** (2002). Detection of novel members, structure-function analysis and evolutionary classification of the 2H phosphoesterase superfamily. *Nucleic Acids Res* **30**, 5229-5243.
- Merino-Puerto, V., Mariscal, V., Mullineaux, C.W., Herrero, A., and Flores, E.** (2010). Fra proteins influencing filament integrity, diazotrophy and localization of septal protein SepJ in the heterocyst-forming cyanobacterium *Anabaena* sp. *Mol Microbiol* **75**, 1159-1170.
- Merino-Puerto, V., Mariscal, V., Schwarz, H., Maldener, I., Mullineaux, C.W., and Flores, E.** (2011a). FraH is required for reorganization of intracellular membranes during heterocyst differentiation in *Anabaena* sp. Strain PCC 7120. *Journal of Bacteriology* **193**, 6815-6823.
- Merino-Puerto, V., Mariscal, V., Schwarz, H., Maldener, I., Mullineaux, C.W., Herrero, A., and Flores, E.** (2011b). FraH is required for reorganization of intracellular membranes during heterocyst differentiation in *Anabaena* sp. strain PCC 7120. *J Bacteriol* **193**, 6815-6823.
- Mitchell, P.** (1966). Chemiosmotic coupling in oxidative and photosynthetic phosphorylation. *Biological Reviews* **445-502**, 445-502.
- Morris, J.N., Eaton-Rye, J.J., and Summerfield, T.C.** (2016). Phenotypic variation in wild-type substrains of the model cyanobacterium *Synechocystis* sp. PCC 6803. *New Zealand Journal of Botany* **55**, 25-35.

Bibliography

- Mühlhoff, U., Zhao, J., and Bryant, D.A.** (1996). Interaction between photosystem I and flavodoxin from the cyanobacterium *Synechococcus* sp. PCC 7002 as revealed by chemical cross-linking. *Eur J Biochem* **235**, 324-331.
- Mühlhoff, U., Haehnel, W., Witt, H., and Herrmann, R.G.** (1993). Genes encoding eleven subunits of photosystem I from the thermophilic cyanobacterium *Synechococcus* sp. *Gene* **127**, 71-78.
- Mullet, J.E., Burke, J.J., and Arntzen, C.J.** (1980). Chlorophyll proteins of photosystem I. *Plant Physiology* **65**, 814-822.
- Mullineaux, C.W.** (1992). Excitation energy transfer from phycobilisomes to photosystem I in a cyanobacterium. *Biochimica et Biophysica Acta (BBA) - Bioenergetics* **1100**, 285-292.
- Mullineaux, C.W., and Allen, J.F.** (1990). State 1-State 2 transition in the cyanobacterium *Synechococcus* 6301 by the redox state of electron carriers between photosystem I and II. *Photosynth Res* **23**, 297-311.
- Munekage, Y., Hashimoto, M., Miyake, C., Tomizawa, K.-I., Endo, T., Tasaka, T., and Shikanai, T.** (2004). Cyclic electron flow around photosystem I is essential for photosynthesis. *Nature* **429**, 579-582.
- Murata, N., and Miyao, M.** (1985). Extrinsic membrane proteins in the photosynthetic oxygen-evolving complex. *Trends Biochemical Science* **10**.
- Murray, J., and Barber, J.** (2006). Identification of a calcium-binding site in the PsbO protein of photosystem II. *Biochemistry* **45**, 4128-4130.
- Nanba, O., and Satoh, K.** (1987). Isolation of a photosystem II reaction center consisting of D-1 and D-2 polypeptides and cytochrome *b*-559. *Proc Natl Acad Sci U S A* **84**, 109-112.
- Nixon, P.J., Barker, M., Boehm, M., de Vries, R., and Komenda, J.** (2005). FtsH-mediated repair of the photosystem II complex in response to light stress. *J Exp Bot* **56**, 357-363.
- Nixon, P.J., Michoux, F., Yu, J., Boehm, M., and Komenda, J.** (2010). Recent advances in understanding the assembly and repair of photosystem II. *Ann Bot* **106**, 1-16.
- Noji, H., Yasuda, R., and Kinosita, K.J.** (1997). Direct observation of the rotation of F₁-ATPase. *Nature* **386**, 299-302.
- Nowaczyk, M.M., Hebel, R., Schlodder, E., Meyer, H.E., Warscheid, B., and Rögner, M.** (2006). Psb27, a cyanobacterial lipoprotein, is involved in the repair cycle of photosystem II. *Plant Cell* **18**, 3121-3131.
- Nudleman, E., and Kaiser, D.** (2004). Pulling Together with Type IV Pili. *J. Mol. Microbiol. Biotechnol.* **7**, 52-62.

Bibliography

- Ohad, I., Kyle, D., and Arntzen, C.J.** (1984). Membrane protei damage and repair: Removal and replacement of inactivated 32-kilodalton polypeptides in chloroplast membranes. *Journal of Cell Biology* **99**, 481-485.
- Ossenbühl, F., Inaba-Sulpice, M., Meurer, J., Soll, J., and Eichacker, L.A.** (2006). The *Synechocystis* sp PCC 6803 *oxa1* homolog is essential for membrane integration of reaction center precursor protein pD1. *Plant Cell* **18**, 2236-2246.
- Özkul, K., and Karakaya, H.** (2015). Characterisation of an *opcA* mutant of the unicellular cyanobacterium *Synechocystis* sp. PCC 6803. *Current Microbiology* **71**, 572-578.
- Pandini, V., Aliverti, A., and Zanetti, G.** (1999). Interaction of the soluble recombinant PsaD subunit of spinach photosystem I with ferredoxin I. *Biochemistry* **38**, 10707-10713.
- Peschke, M., Moog, D., Klingl, A., Maier, U.G., and Hempel, F.** (2013). Evidence for glycoprotein transport into complex plastids. *PNAS* **110**, 10860-10865.
- Phinney, B.S., and Thelen, J.J.** (2005). Proteomic characterization of a triton-insoluble fraction from chloroplasts defines a novel group of proteins associated with macromolecular structured. *Journal of Proteome Research* **4**, 497-506.
- Pospíšil, P.** (2009). Production of reactive oxygen species by photosystem II. *Biochim Biophys Acta* **1787**, 1151-1160.
- Pribil, M., Sandoval-Ibáñez, O., Xu, W., Sharma, A., Labs, M., Liu, Q., Galgenmüller, C., Schneider, T., Wessels, M., Matsubara, S., Jansson, S., Wanner, G., and Leister, D.** (2018). Fine-tuning of photosynthesis requires CURVATURE THYLAKOID1-mediated thylakoids plasticity. *Plant Physiol* **176**, 2351-2364.
- Ranjbar, C., R., Wientjes, E., Struik, P.C., Kirilovsky, D., and van Amerongen, H.** (2018). State transitions in the cyanobacterium *Synechococcus elongatus* 7942 involve reversible quenching of the photosystem II core. *Biochim Biophys Acta Bioenerg.*
- Rast, A., Heinz, S., and Nickelsen, J.** (2015). Biogenesis of thylakoid membranes. *Biochim Biophys Acta* **1847**, 821-830.
- Rast, A., Rengstl, B., Heinz, S., Klingl, A., and Nickelsen, J.** (2016). The Role of Slr0151, a Tetratricopeptide Repeat Protein from *Synechocystis* sp. PCC 6803, during photosystem II Assembly and Repair. *Front Plant Sci* **7**, 605.
- Rast, A., Schaffer, M., Albert, S., Wan, W., Pfeffer, S., Beck, F., Pitzko, J.M., Nickelsen, J., and Engel, B.D.** (2019). Biogenic regions of cyanobacterial thylakoids form contact sites with the plasma membrane. *Nature Plants* **5**, 436-446.
- Raymond, J., and Segrè, D.** (2006). The effect of oxygen on biochemical networks and the evolution of complex life. *Science* **311**, 1764-1767.
- Rengstl, B., Oster, U., Stengel, A., and Nickelsen, J.** (2011). An intermediate membrane subfraction in cyanobacteria is involved in an assembly network for photosystem II biogenesis. *J Biol Chem* **286**, 21944-21951.

Bibliography

- Rengstl, B., Knoppová, J., Komenda, J., and Nickelsen, J.** (2013). Characterization of a *Synechocystis* double mutant lacking the photosystem II assembly factors YCF48 and SII0933. *Planta* **237**, 471-480.
- Richarme, G.** (1983). Associative properties of the *Escherichia coli* galactose-binding protein and maltose-binding protein. *Molecular Enzymology* **748**, 99-108.
- Rieske, J.S., Hansen, R.E., and Zaugg, W.S.** (1964). Studies on the electron transfer: LVIII Properties of a new oxidation-reduction component of the respiratory chain as studied by electron paramagnetic resonance spectroscopy. *The Journal of Biological Chemistry* **229**, 3017-3022.
- Rippka, R., and Herdman, M.** (1992). Catalogue of strains. Pasteur culture collection of cyanobacterial strains in axenic cultures. Catalogue of strains, Institute Pasteur, Paris, France **1**, 103pp.
- Rippka, R., Derulles, J., Waterbury, J.B., Herdman, M., and Stanier, R.Y.** (1979). Generic assignments, strain histories and properties of pure cultures of cyanobacteria. *Journal of General Microbiology* **110**, 1-61.
- Rögner, M., Nixon, P.J., and Diner, B.A.** (1990). Purification and characterization of photosystem I and photosystem II core complexes from Wild-type and phycocyanin-deficient strains of the cyanobacterium *Synechocystis* PCC 6803. *The Journal of Biological Chemistry* **265**, 6189-6196.
- Roose, J.L., and Pakrasi, H.B.** (2008). The Psb27 protein facilitates manganese cluster assembly in photosystem II. *J Biol Chem* **283**, 4044-4050.
- Roose, J.L., Kashino, Y., and Pakrasi, H.B.** (2007). The PsbQ protein defines cyanobacterial photosystem II complexes with highest activity and stability. *Proc Natl Acad Sci U S A* **104**, 2548-2553.
- Rousseau, F., Sétif, P., and Lagoutte, B.** (1993). Evidence for the involvement of PSI-E subunit in the reduction of ferredoxin by photosystem I. *The EMBO Journal* **12**, 1755-1765.
- Rütgers, M., and Schroda, M.** (2013). A role of VIPP1 as a dynamic structure within thylakoid centers as sites of photosystem biogenesis? *Plant Signal Behav* **8**, e27037.
- Sacharz, J., Bryan, S.J., Yu, J., Burroughs, N.J., Spence, E.M., Nixon, P.J., and Mullineaux, C.W.** (2015). Sub-cellular location of FtsH proteases in the cyanobacterium *Synechocystis* sp. PCC 6803 suggests localised PSII repair zones in the thylakoid membranes. *Mol Microbiol* **96**, 448-462.
- Sachelaru, I., Petriman, N.A., Kudva, R., Kuhn, P., Welte, T., Knapp, B., Drepper, F., Warscheid, B., and Koch, H.G.** (2013). YidC occupies the lateral gate of the SecYEG translocon and is sequentially displaced by a nascent membrane protein. *J Biol Chem* **288**, 16295-16307.

Bibliography

- Sakurai, I., Mizusawa, N., Wada, H., and Sato, N.** (2007). Digalactosyldiacylglycerol is required for stabilization of the oxygen-evolving complex in photosystem II. *Plant Physiol* **145**, 1361-1370.
- Sato, N., Hagio, M., Wada, H., and Tsuzuki, M.** (2000). Requirement of phosphatidylglycerol for photosynthetic function in thylakoid membranes. *Proc Natl Acad Sci U S A* **97**, 10655-10660.
- Satoh, K.** (1980). F-695 emission from the purified photosystem II chlorophyll a- protein complex. *FEBS Letters* **110**.
- Schottkowski, M., Ratke, J., Oster, U., Nowaczyk, M., and Nickelsen, J.** (2009a). Pitt, a novel tetratricopeptide repeat protein involved in light-dependent chlorophyll biosynthesis and thylakoid membrane biogenesis in *Synechocystis* sp. PCC 6803. *Mol Plant* **2**, 1289-1297.
- Schottkowski, M., Gkalympoudis, S., Tzekova, N., Stelljes, C., Schünemann, D., Ankele, E., and Nickelsen, J.** (2009b). Interaction of the periplasmic PrtA factor and the PsbA (D1) protein during biogenesis of photosystem II in *Synechocystis* sp. PCC 6803. *J Biol Chem* **284**, 1813-1819.
- Schubert, W.-D., Klukas, O., Saenger, W., Witt, H.T., Fromme, P., and Krauß, N.** (1998). A common ancestor for oxygenic and anoxygenic photosynthetic systems: A comparison based on the structural model of photosystem I. *Journal of Molecular Biology* **280**, 297-314.
- Schuller, J.M., Birrell, J.M., Tanaka, H., Konuma, T., Wulfhorst, H., Cox, N., Schuller, S.K., Thiemann, J., Lubitz, W., Sétif, P., Ikegami, T., Engel, B.D., Kurisu, G., and Nowaczyk, M.M.** (2019). Structural adaptations of photosynthetic complex I enable ferredoxin-dependent electron transfer. *Science* **363**, 257-260.
- Seki, Y., Nitta, K., and Kaneko, Y.** (2014). Observation of polyphosphate bodies and DNA during the cell division cycle of *Synechococcus elongatus* PCC 7942. *Plant Biol (Stuttg)* **16**, 258-263.
- Shen, G., and Vermaas, W.F.J.** (1994). Chlorophyll in a *Synechocystis* sp. PCC 6803 mutant without Photosystem I and Photosystem II core complexes. Evidence for peripheral antenna chlorophylls in cyanobacteria **269**, 13904-13910.
- Shen, J.R., and Inoue, Y.** (1993). Binding and functional properties of two new extrinsic components, cytochrome c-550 and a 12-kDa Protein, in cyanobacterial photosystem II. *Biochemistry* **32**, 1825-1832.
- Shimoni, E., Rav-Hon, O., Ohad, I., Brumfeld, V., and Reich, Z.** (2005). Three-dimensional organization of higher-plant chloroplast thylakoid membranes revealed by electron tomography. *Plant Cell* **17**, 2580-2586.
- Shuvalov, V.A., Allakhverdiev, S.I., Sakamoto, A., Malakhov, M., and Murata, N.** (2001). Optical study of Cytochrome c_M formation in *Synechocystis*. *IUBMB Life* **51**, 93-97.

Bibliography

- Siebenaller, C., Junglas, B., and Schneider, D.** (2019). Functional implications of multiple IM30 oligomeric states. *Front Plant Sci* **10**, 1500.
- Solymosi, D., Muth-Pawlak, D., Nikkanen, L., Duncan, F., Vasudevan, R., Howe, C.J., Lea-Smith, D.J., and Allahverdiyeva, Y.** (2019). Cytochrome c_M downscale photosynthesis under photomixotrophy in *Synechocystis* sp. PCC 6803.
- Sommer, F., Drepper, F., and Hippler, M.** (2002). The luminal helix I of PsaB is essential for recognition of plastocyanin or cytochrome c_6 and fast electron transfer to photosystem I in *Chlamydomonas reinhardtii*. *J Biol Chem* **277**, 6573-6581.
- Sommer, F., Drepper, F., Haehnel, W., and Hippler, M.** (2004). The hydrophobic recognition site formed by residues PsaA-Trp651 and PsaB-Trp627 of photosystem I in *Chlamydomonas reinhardtii* confers distinct selectivity for binding of plastocyanin and cytochrome c_6 . *J Biol Chem* **279**, 20009-20017.
- Sonoike, K., Hatanaka, H., and Katoh, S.** (1993). Small subunits of photosystem I reaction center complexes from *Synechococcus elongatus*. II. The *psaE* gene product has a role to promote interaction between the terminal electron acceptor and ferredoxin. *Biochimica et Biophysica Acta* **1141**, 52-57.
- Spence, E., Bailey, S., Nenninger, A., Møller, S.G., and Robinson, C.** (2004). A homolog of Albino3/Oxal is essential for thylakoid biogenesis in the cyanobacterium *Synechocystis* sp. PCC6803. *J Biol Chem* **279**, 55792-55800.
- Spetea, C., Hundal, T., Lohmann, F., and Andersson, B.** (1999). GTP bound to chloroplast thylakoid membranes is required for light-induced, multi-enzyme degradation of the photosystem II D1 protein. *Proc Natl Acad Sci U S A* **96**, 6547-6552.
- Standfuss, J., Terwisscha van Scheltinga, A.C., Lamborghini, M., and Kühlbrandt, W.** (2005). Mechanisms of photoprotection and nonphotochemical quenching in pea light-harvesting complex at 2.5 Å resolution. *EMBO J* **24**, 919-928.
- Stanier, R.Y., Kunisawa, R., and Mandel, M.** (1971). Purification and properties of unicellular blue-green algae (Order *Chroococcales*). *Bacteriological Reviews* **35**, 171-205.
- Stengel, A., Gügel, I.L., Hilger, D., Rengstl, B., Jung, H., and Nickelsen, J.** (2012). Initial steps of photosystem II de novo assembly and preloading with manganese take place in biogenesis centers in *Synechocystis*. *Plant Cell* **24**, 660-675.
- Stroebel, D., Choquet, Y., Popot, J.-L., and Picot, D.** (2003). An atypical haem in the cytochrome b_6f complex. *Nature* **426**, 413-418.
- Studier, W.F., and Moffat, B.A.** (1986). Use of bacteriophage T7 RNA Polymerase to direct selective high-level expression of cloned genes. *Journal of Molecular Biology* **189**, 17.
- Suga, M., Akita, F., Hirata, K., Ueno, G., Murakami, H., Nakajima, Y., Shimizu, T., Yamashita, K., Yamamoto, M., Ago, H., and Shen, J.R.** (2015). Native structure of photosystem II at 1.95 Å resolution viewed by femtosecond X-ray pulses. *Nature* **517**, 99-103.

Bibliography

- Sukhov, V., Surova, L., Sherstneva, O., Katicheva, L., and Vodeneev, V.** (2015). Variation potential influence on photosynthetic cyclic electron flow in pea. *Frontiers in Plant Science* **5**, 1-13.
- Sun, J., Xu, W., Hervás, M., Navarro, J.A., De La Rosa, M.A., and Chitnis, P.R.** (1999). Oxidizing side of the cyanobacterial photosystem I. Evidence for interaction between the electron donor proteins and a luminal surface helix of the PsaB subunit*. *Journal of Biological Chemistry* **274**, 19048-19054.
- Tang, Q., Tan, X., and Xu, X.** (2010). Effects of a type-II RNA-binding protein on fatty acid composition in *Synechocystis* sp. PCC 6803. *Chinese Science Bulletin* **55**, 2416–2421.
- Theis, J., Gupta, T.K., Klingler, J., Wan, W., Albert, S., Keller, S., Engel, B.D., and Schroda, M.** (2019). VIPP1 rods engulf membranes containing phosphatidylinositol phosphates. *Sci Rep* **9**, 8725.
- Thompson, L.K., and Brudvig, G.W.** (1988). Cytochrome b-559 may function to protect photosystem II from photoinhibition. *Biochemistry* **27**, 6653-6658.
- Thornton, L.E., Ohkawa, H., Roose, J.L., Kashino, Y., Keren, N., and Pakrasi, H.B.** (2004). Homologs of plant PsbP and PsbQ proteins are necessary for regulation of photosystem II activity in the cyanobacterium *Synechocystis* 6803. *Plant Cell* **16**, 2164-2175.
- Trautner, C., and Vermaas, W.F.** (2013). The *sll1951* gene encodes the surface layer protein of *Synechocystis* sp. strain PCC 6803. *J Bacteriol* **195**, 5370-5380.
- Trebst, A.** (1979). Inhibition of photosynthetic electron flow by phenol and diphenylether herbicides in control and trypsin-treated chloroplast. *Zeitschrift für Naturforschung C* **34**, 986-991.
- Tyystjärvi, E., Mäenpää, P., and Aro, E.-M.** (1994). Mathematical modelling of photoinhibition and photosystem II repair cycle.
I. Photoinhibition and D1 protein degradation *in vitro* and the absence of chloroplast protein synthesis *in vivo*. *Photosynthesis Research* **41**, 439-449.
- Umena, Y., Kawakami, K., Shen, J.R., and Kamiya, N.** (2011). Crystal structure of oxygen-evolving photosystem II at a resolution of 1.9 Å. *Nature* **473**, 55-60.
- Uniacke, J., and Zerges, W.** (2007). Photosystem II assembly and repair are differentially localized in *Chlamydomonas*. *Plant Cell* **19**, 3640-3654.
- van de Meene, A.M., Hohmann-Marriott, M.F., Vermaas, W.F., and Roberson, R.W.** (2006). The three-dimensional structure of the cyanobacterium *Synechocystis* sp. PCC 6803. *Arch Microbiol* **184**, 259-270.
- van de Meene, A.M.L., Sharp, W., McDaniel, J.H., Friedrich, H., Vermaas, W.F.J., and Roberson, R.W.** (2012). Gross morphological changes in thylakoid membrane structure are associated with photosystem I deletion in *Synechocystis* sp. PCC 6803. *Biochimica et Biophysica Acta* **1818**, 1427-1434.

Bibliography

- van Niel, C.B.** (1932). On the morphology and physiology of the purple and green sulphur bacteria. *Archiv für Mikrobiologie* **1**, 1-112.
- Vasil'ev, S., Orth, P., Zouni, A., Owens, T.G., and Bruce, D.** (2001). Excited-state dynamics in photosystem II: insights from the x-ray crystal structure. *Proc Natl Acad Sci U S A* **98**, 8602-8607.
- Vavilin, D., Yao, D., and Vermaas, W.** (2007). Small Cab-like proteins retard degradation of photosystem II-associated chlorophyll in *Synechocystis* sp. PCC 6803: kinetic analysis of pigment labeling with ¹⁵N and ¹³C. *J Biol Chem* **282**, 37660-37668.
- Veerman, J., Bentley, F.K., Eaton-Rye, J.J., Mullineaux, C.W., Vasil'ev, S., and Bruce, D.** (2005). The PsbU subunit of photosystem II stabilizes energy transfer and primary photochemistry in the phycobilisome- photosystem II assembly of *Synechocystis* sp. PCC 6803. *Biochemistry* **44**, 16939-16948.
- Veit, S., Takeda, K., Tsunoyama, Y., Baymann, F., Nevo, R., Reich, Z., Rögner, M., Miki, K., and Rexroth, S.** (2016). Structural and functional characterisation of the cyanobacterial PetC3 Rieske protein family. *Biochim Biophys Acta* **1857**, 1879-1891.
- Vermaas, W., Madsen, C., Yu, J., Visser, J., Metz, J., Nixon, P.J., and Bruce, D.** (1995). Turnover of the D1 protein and of photosystem II in a *Synechocystis* 6803 mutant lacking Tyr_z. *Photosynthesis Research* **45**, 99-104.
- Watanabe, M., Semchonok, D.A., Webber-Birungi, M.T., Ehira, S., Kondo, K., Narikawa, R., Ohmori, M., Boekema, E.J., and Ikeuchi, M.** (2014). Attachment of phycobilisomes in an antenna-photosystem I supercomplex of cyanobacteria. *PNAS* **111**, 2512-2517.
- Westphal, S., Heins, L., Soll, J., and Vothknecht, U.C.** (2001). Vipp1 deletion mutant of *Synechocystis*: a connection between bacterial phage shock and thylakoid biogenesis? *Proc Natl Acad Sci U S A* **98**, 4243-4248.
- Wienken, C.J., Baaske, P., Rothbauer, U., Braun, D., and Duhr, S.** (2010). Protein-binding assays in biological liquids using microscale thermophoresis. *Nature communications* **1**, 7.
- Xu, Q., Hoppe, D., Chitnis, V.P., Odom, W.R., Guikema, J.A., and Chitnis, P.R.** (1995). Mutational analysis of photosystem I polypeptides in the cyanobacterium *Synechocystis* sp. PCC 6803. Targeted inactivation of *psaI* reveals the function of PsaI in the structural organization of PsaL. *The Journal of Biological Chemistry* **270**, 16243-16250.
- Yang, H., Liao, L., Bo, T., Zhao, L., Sun, X., Lu, X., Norling, B., and Huang, F.** (2014). Slr0151 in *Synechocystis* sp. PCC 6803 is required for efficient repair of photosystem II under high-light condition. *J Integr Plant Biol* **56**, 1136-1150.
- Yeremenko, N., Jeanjean, R., Prommeenate, P., Krasikov, V., Nixon, P.J., Vermaas, W.F., Havaux, M., and Matthijs, H.C.** (2005). Open reading frame *ssr2016* is required for antimycin A-sensitive photosystem I-driven cyclic electron flow in the cyanobacterium *Synechocystis* sp. PCC 6803. *Plant Cell Physiol* **46**, 1433-1436.

Bibliography

- Yoshihara, S., Geng, X., and Ikeuchi, M.** (2002). *pilG* gene cluster and split *pilL* genes involved in pilus biogenesis, motility and genetic transformation in the cyanobacterium *Synechocystis* sp. PCC 6803. *Plant and Cell Physiology* **43**, 513-521.
- Yoshihara, S., Geng, X., Okamoto, S., Yura, K., Murata, T., Go, M., Ohmori, M., and Ikeuchi, M.** (2001). Mutational analysis of genes involved in pilus structure, motility and transformation competency in the unicellular motile cyanobacterium *Synechocystis* sp. PCC 6803. *Plant Cell Physiol.* **42**, 63-73.
- Yu, J., Knoppová, J., Michoux, F., Bialek, W., Cota, E., Shukla, M.K., Straskova, A., Pascual Aznar, G., Sobotka, R., Komenda, J., Murray, J.W., and Nixon, P.J.** (2018). Ycf48 involved in the biogenesis of the oxygen-evolving photosystem II complex is a seven-bladed beta-propeller protein. *Proc Natl Acad Sci U S A* **115**, E7824-E7833.
- Yu, L., Mühlhoff, U., Bryant, D.A., and Goldbeck, J.H.** (1993). PsaE is required for in vivo cyclic electron flow around photosystem I in the cyanobacterium *Synechococcus* sp. PCC 7002. *Plant Physiology* **103**, 171-180.
- Zanetti, G., and Merati, G.** (1987). Interaction between photosystem I and ferredoxin: Identification by chemical cross-linking of the polypeptide which binds ferredoxin. *European Journal of Biochemistry* **169**, 143-147.
- Zheleva, D., Sharma, J., Panico, M., Morris, H.R., and Barber, J.** (1993). Isolation and characterization of monomeric and dimeric CP47-Reaction center photosystem II complex. *Journal of Biological Chemistry* **273**, 16122-16127.
- Zinchenko, V.V., V, P.I., Melnik, V.A., and Shestakov, S.V.** (1991). Vectors for the complementation analysis of cyanobacterial mutants. *Russian Journal of Genetics* **35**, 228-232.
- Zouni, A., Witt, H.-T., Kern, J., Fromme, P., Krauß, N., Saenger, W., and Orth, P.** (2001). Crystal structure of photosystem II from *Synechococcus elongatus* at 3.8 Å resolution. *Nature* **409**, 739-743.

Abbreviations

ABBREVIATIONS

Acetonitrile	ACN
Adenosine triphosphate	ATP
Adenosine triphosphate synthase	ATPase
Ammoniumpersulfate	APS
Ångström	Å
<i>Aqua destillata</i>	<i>A.dest</i>
Blue Native	BN
C-terminal processing protease	CtpA
Carbon dioxide	CO ₂
Chlorophyll synthase	ChlG
Co-Immunoprecipitation	Co-IP
Collision induced dissociation	CID
Cytochrome <i>b</i> ₅₅₉	Cyt <i>b</i> ₅₅₉
Cytochrome <i>b</i> _{6f} complex	Cyt <i>b</i> _{6f}
Cytochrome <i>c</i> _M	Cyt <i>c</i> _M
Digalactosyldiacylglycerol	DGDG
Dimethyl sulfoxide	DMSO
Dissociation constant	K _d
Domain of unknown function	DUF
Electrochemiluminescence	ECL
<i>Escherichia Coli</i>	<i>E.Coli</i>
Ethylenediaminetetraacetate disodium salt dihydrate	Na-EDTA
Ferredoxin	Fd
Ferredoxin NADP Reductase	FNR
Ft	Flow through
High temperature requirement homologue A	HhoA
high-light-inducible protein	Hlip
intermediate form of D1	iD1
Isopropyl-β-D-thiogalactopyranosid	ITPG
Kilodalton	kDa
Light harvesting complexes	LHC
liquid lysogeny broth	LB
Maltose binding protein	MBP
Mature form of D1	mD1
Mega base pairs	Mbp

Abbreviations

Microscale thermophoresis	MST
Monogalactosyldiacylglycerol	MGDG
<i>n</i> -Dodecyl- β -D-Maltoside	β -DM
<i>N</i> -Morpholino)propansulfonacid	MOPS
<i>N,N,N',N'</i> -tetramethylethane-1,2-diamine	TEMED
Nicotinamide adenine dinucleotide hydrophosphate	NADPH
Optical density	OD
Oxygen	O ₂
Oxygen evolving complex	OEC
Sodium dodecyl sulfate polyacrylamide gel electrophoresis	SDS-PAGE
Pasteur Culture Collection	PCC
Phenylmethylsulfonyl fluoride	PMSF
Phosphate buffered saline	PBS
phosphatidylglycerol	PG
Photosystem I	PSI
Photosystem II	PSII
Pilin protein Q	PilQ
Plastohydroquinone	PQH ₂
Plastoquinone A	Q _A
Plastoquinone B	Q _B
Polymerase chain reaction	PCR
PratA defined membrane	PDM
Precursor form of D1	pD1
Processing associated tetraco peptide (TPR) protein reaction centre complex	PratA RC
Reaction centre of PSI	P ₇₀₀
Reaction centre of PSII	P ₆₈₀
Ribulose-1,5-bisphosphate carboxylase	RubisCO
Room temperature	RT
sodium dodecyl sulfate	SDS
sulfoquinovosyldiacylglycerol	SQDG
Supernatant	SN
Surface layer	S-Layer
<i>Synechocystis</i> sp. PCC 6803	<i>Synechocystis</i>
the vesicle inducing protein in plastids 1	Vipp1
Thylakoid membrane	TM
Transmission Electron Microscopy	TEM

Abbreviations

Tris-acetate-EDTA
Ultraviolet and visible
Water
Wild-type

TAE
UV-Vis
H₂O
WT

ANNEX

Table 18: Mass spectrometry analysis of the Co-IP with α CurT on PDM fractions. As negative control the strain *ancM curT* was used. Ten of the potential ORF was listed after highest abundance in mass spectrometry analysis. Bioinformatical analysis are shown in column 3-5. The hits are listed after the score.

ORF	Function	Mass weight [kDa] ^a	Predicted TM helices ^b	Co-expression with CurT/AncM ^c	Score ^d
<i>ancM</i>	AncM	31.87	1	CurT	24.85
<i>slr0193</i>	RNA-binding protein, Rbp3	16.62	0	CurT	19.86
<i>sll0617</i>	VIPP1	28.90	2	no	16.79
<i>sll0822</i>	hypothetical protein	13.96	0	CurT	15.84
<i>sll1244</i>	50S ribosomal protein L9	16.64	1	no	8.7
<i>sll1028</i>	carbon dioxide concentrating mechanism protein CcmK	11.13	0	no	8.52
<i>slr1034</i>	hypothetical protein YCF41	14.41	0	no	7.94
<i>sll0359</i>	hypothetical protein	17.22	0	no	7.82
<i>slr0952</i>	fructose-1.6-bisphosphatas e	38.26	3	no	7.36
<i>sll1837</i>	periplasmic protein, function unknown	15.47	1	AncM	5.87
<i>sll1261</i>	elongation factor TS	24.24	1	no	5.21
<i>ssl3437</i>	30S ribosomal protein S17	9.23	0	no	4.99
<i>ssr2799</i>	50S ribosomal protein L27	9.45	0	no	4,93

Annex

ORF	Function	Mass weight [kDa] ^a	Predicted TM helices ^b	Co-expression with CurT/AncM ^c	Score ^d
<i>sll1123</i>	hypothetical protein	28.90	2	no	4.91
<i>slr1329</i>	ATP synthase beta subunit	51.73	5	CurT	4.59
<i>sll0199</i>	plastocyanin	13.15	2	no	4.35
<i>sll1873</i>	unknown protein	12.91	0	no	3.56
<i>sll1807</i>	50S ribosomal protein L24	12.82	0	no	3.32
<i>sll1810</i>	50S ribosomal protein L6	19.65	0	no	3.20
<i>slr1256</i>	urease gamma subunit	11.06	0	no	2.92
<i>sll0008</i>	unknown protein	19.02	1	no	2.85
<i>sll5034</i>	hypothetical protein	23.20	1	no	2.67
<i>sll1883</i>	arginine biosynthesis bifunctional protein ArgJ	43.32	3	no	2.61
<i>slr0483</i>	CurT	16.88	2	no	2.34
<i>sll1809</i>	30S ribosomal protein S8	14.67	1	no	2.31
<i>ssr0482</i>	30S ribosomal protein S16	9.56	0	no	2.31

^a) Theoretical mass weight was calculated using https://web.expasy.org/compute_pi/

^b) Transmembrane domains theoretical analysed using the tools https://embnet.vital-it.ch/software/TMPRED_form.html and <http://www.cbs.dtu.dk/services/TMHMM/>

^c) Co-expression data was analysed using <http://cyanoexpress.sysbiolab.eu>

^d) The score value is calculated for each peptide by matching the predicted ions to the ions observed in the mass spectrum (Eng *et al.*, 1994).

Annex

Table 19: Mass spectrometry analysis of the Co-IP with α CurT on the TM fraction 8-9. As negative control the strain *ancM curT* was used. Potential ORF was listed after abundance in mass spectrometry analysis. Bioinformatical analysis are shown in column 3-5.

ORF	Function	Mass weight [kDa] ^a	Predicted TM helices ^b	Co-expression with CurT/AncM ^c	Score ^d
<i>sll1808</i>	50S ribosomal protein L5	20.23	0	no	25.71
<i>slr1128</i>	hypothetical protein	35.73	1	no	21.61
<i>sll0469</i>	ribose-phosphate pyrophosphokinase	36.40	2	no	16.47
<i>slr0404</i>	hypothetical protein	34.87	3	no	15.72
<i>slr1537</i>	unknown protein	32.42	1	no	13.76
<i>slr1238</i>	glutathione synthetase	35.07	4	no	10.33
<i>sll1837</i>	periplasmic protein, function unknown	15.47	1	AncM	9.88
<i>slr0012</i>	ribulose bisphosphate carboxylase small subunit	13.24	1	no	9.58
<i>slr0543</i>	tryptophan synthase beta subunit	45.07	3	no	8.75
<i>sll0891</i>	malate dehydrogenase	34.35	4	no	8.73
<i>sll1745</i>	50s ribosomal protein L10	18.68	1	no	8.28
<i>sll1688</i>	threonine synthase	47.01	4	no	7.17
<i>slr0965</i>	DNA polymerase III beta subunit	42.09	3	no	6.97
<i>sll1583</i>	unknown protein	61.47	3	no	6,28
<i>slr0228</i>	cell division protein FtsH	68.50	4	no	6.09
<i>slr1678</i>	50S ribosomal protein L21	13.67	0	no	6.05
<i>slr0400</i>	hypothetical protein	33.40	5	no	6.02
<i>slr1894</i>	probable DNA-binding stress protein	17.76	0	no	5.99
<i>slr1963</i>	water-soluble carotenoid protein	34.66	3	no	5.93

Annex

ORF	Function	Mass weight [kDa] ^a	Predicted TM helices ^b	Co-expression with CurT/AncM ^c	Score ^d
<i>sll1621</i>	AhpC/TSA family protein	21.17	2	no	5.64
<i>sll1815</i>	adenylate kinase	20.25	1	no	5.60
<i>sll1260</i>	30S ribosomal protein S2	30.15	0	no	5.59
<i>slr0930</i>	hypothetical protein	49.36	3	no	5.38
<i>slr0757</i>	circadian clock protein KaiB homolog	11.94	0	no	5.36
<i>slr0426</i>	GTP cyclohydrolase I	26.64	0	no	5.34
<i>slr1274</i>	probable fimbrial assembly protein PilM, required for motility	40.88	1	no	5.06
<i>sll0427</i>	photosystem II manganese-stabilising polypeptide, PsbO	29.99	1	no	4.73
<i>sll0524</i>	hypothetical protein	47.48	9	no	4.09
<i>sll1817</i>	30S ribosomal protein S11	13.76	0	no	3.92
<i>ssl2982</i>	probable DNA-directed RNA polymerase omega subunit	8.74	0	no	3.91
<i>sll0018</i>	fructose-bisphosphate aldolase, class II	38.97	1	CurT	3.91
<i>slr1890</i>	bacterioferritin	20.23	0	no	3.74
<i>sll1101</i>	30S ribosomal protein S10	12.04	0	no	3.74
<i>slr0527</i>	transcription regulator ExsB homolog	24.97	3	no	3.63
<i>sll0428</i>	unknown protein	40.26	1	no	3.49
<i>sll1212</i>	GDP-mannose 4,6-dehydratase	41.33	0	no	3.48
<i>sll1803</i>	50S ribosomal protein L22	13.50	0	no	3.45
<i>ssr2317</i>	unknown protein	10.29	0	no	3.45

Annex

ORF	Function	Mass weight [kDa] ^a	Predicted TM helices ^b	Co-expression with CurT/AncM ^c	Score ^d
<i>slr1719</i>	DrgA protein homolog	23.70	2	CurT	3.45
<i>sll0227</i>	peptidyl-prolyl cis-trans isomerase B, periplasmic protein	26.58	1	no	3.44
<i>slr0676</i>	adenylylsulfate kinase	19.67	2	no	3.42
<i>sll1809</i>	30S ribosomal protein S8	14.67	1	no	3.41
<i>slr0875</i>	large-conductance mechanosensitive channel	15.81	2	no	3.35
<i>slr0912</i>	unknown protein	29.35	2	no	3.33
<i>sll1806</i>	50S ribosomal protein L14	13.29	0	no	3.28
<i>slr1718</i>	hypothetical protein	26.04	2	no	3.26
<i>sll1640</i>	hypothetical protein	35.59	2	no	3.26
<i>sll1456</i>	unknown protein	33.52	1	no	3.26
<i>slr1176</i>	glucose-1-phosphate adenylyltransferase	49.37	1	no	3.26
<i>slr0729</i>	hypothetical protein	10.95	1	no	3.20
<i>sll1035</i>	uracil phosphoribosyltransferase	23.64	3	no	3.19
<i>slr0111</i>	unknown protein	19.38	0	no	3.14
<i>sll0851</i>	photosystem II CP43 protein	50.3	7	no	3.05
<i>sll1570</i>	unknown protein	26.62	2	no	2.99
<i>sll1743</i>	50S ribosomal protein L11	14.98	0	no	2.98
<i>slr1541</i>	hypothetical protein	24.19	0	no	2.97
<i>sll1430</i>	adenine phosphoribosyltransferase	19.00	2	no	2.96
<i>slr5051</i>	unknown protein	14.28	1	no	2.96
<i>sll1327</i>	ATP synthase gamma chain	34.61	3	no	2.91

Annex

ORF	Function	Mass weight [kDa] ^a	Predicted TM helices ^b	Co-expression with CurT/AncM ^c	Score ^d
<i>ssr1600</i>	similar to anti-sigma f factor antagonist	7.55	1	no	2.90
<i>sll1742</i>	transcription antitermination protein NusG	23.46	0	no	2.90
<i>slr1658</i>	unknown protein	22.66	1	no	2.84
<i>slr1511</i>	3-oxoacyl-[acyl-carrier-protein] synthase III	35.17	2	no	2.83
<i>slr1616</i>	unknown protein	37.35	4	no	2.81
<i>slr0520</i>	phosphoribosyl formylglycinamide synthase	24.43	3	no	2.78
<i>sll0711</i>	isopentenyl monophosphate kinase	34.08	3	no	2.77
<i>slr1276</i>	hypothetical protein	30.01	2	no	2.77
<i>slr0194</i>	ribose 5-phosphate isomerase	24.75	3	no	2.76
<i>sll1127</i>	1.4-dihydroxy-2-naphthoate synthase	30.31	1	no	2.67
<i>sll1823</i>	adenylosuccinate synthetase	48.79	1	no	2.63
<i>sll1325</i>	ATP synthase delta chain of CF(1)	20.09	1	no	2.61
<i>slr0483</i>	CurT	16.88	2	no	2.34
<i>sll1804</i>	30S ribosomal protein S3	27.15	1	no	2.56
<i>slr1854</i>	unknown protein	22.29	1	no	2.55
<i>sll0228</i>	arginase	33.46	1	no	2.55
<i>slr1751</i>	periplasmic carboxyl-terminal protease	46.83	1	no	2.54
<i>sll1883</i>	arginine biosynthesis bifunctional protein ArgJ	43.32	3	no	2.52
<i>sll0272</i>	hypothetical protein	17.66	1	no	2.52

Annex

ORF	Function	Mass weight [kDa] ^a	Predicted TM helices ^b	Co-expression with CurT/AncM ^c	Score ^d
<i>sll1316</i>	cyt <i>b₆f</i> complex iron-sulphur subunit (Rieske iron sulphur protein)	19.00	2	no	2.50
<i>slr2144</i>	periplasmic protein, function unknown	45.58	2	no	2.45
<i>ssl2084</i>	acyl carrier protein	8.59	0	no	2.41
<i>sll7043</i>	unknown protein	21.55	0	no	2.40
<i>sll1018</i>	dihydroorotase	48.17	1	no	2.40
<i>slr0966</i>	tryptophan synthase alpha chain	28.02	2	no	2.38
<i>slr1600</i>	hypothetical protein	17.13	0	no	2.37
<i>sll1029</i>	carbon dioxide concentrating mechanism protein CcmK	12.10	1	no	2.35

^a) Theoretical mass weight was calculated using https://web.expasy.org/compute_pi/

^b) Transmembrane domains theoretical analysed using the tools https://embnet.vital-it.ch/software/TMPRED_form.html and <http://www.cbs.dtu.dk/services/TMHMM/>

^c) Co-expression data was analysed using <http://cyanoexpress.sysbiolab.eu>

^d) The score value is calculated for each peptide by matching the predicted ions to the ions observed in the mass spectrum (Eng *et al.*, 1994).

Annex

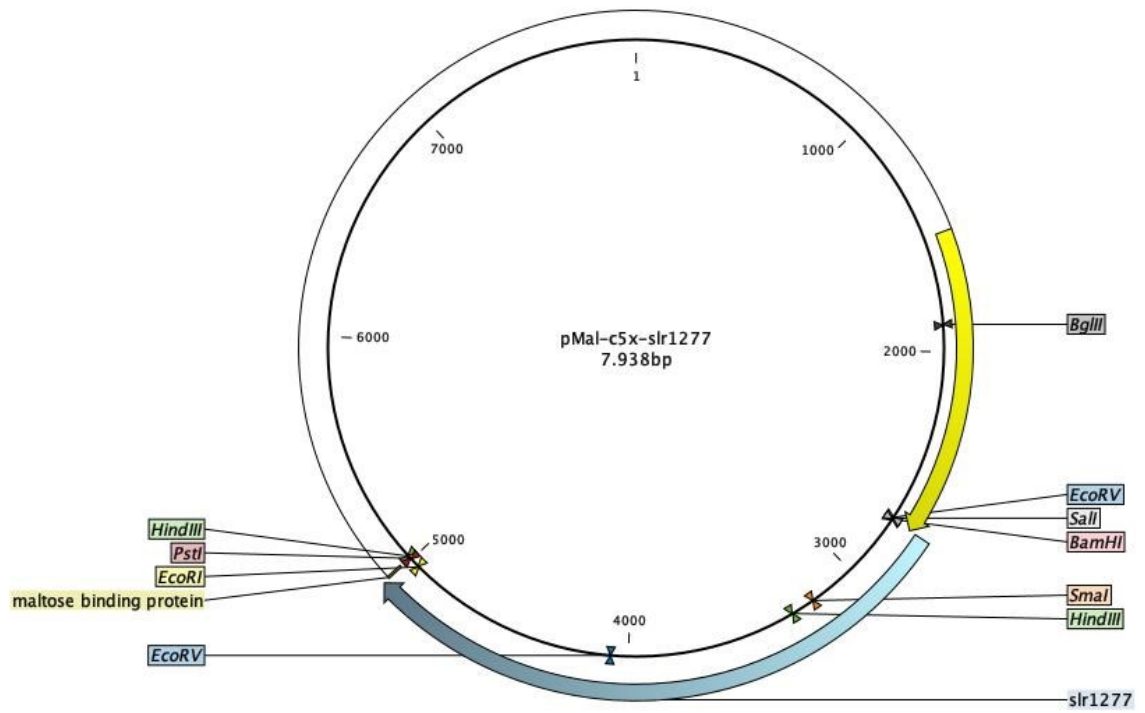


Figure 39 Vector pMal-c5x-slr1277.

Annex

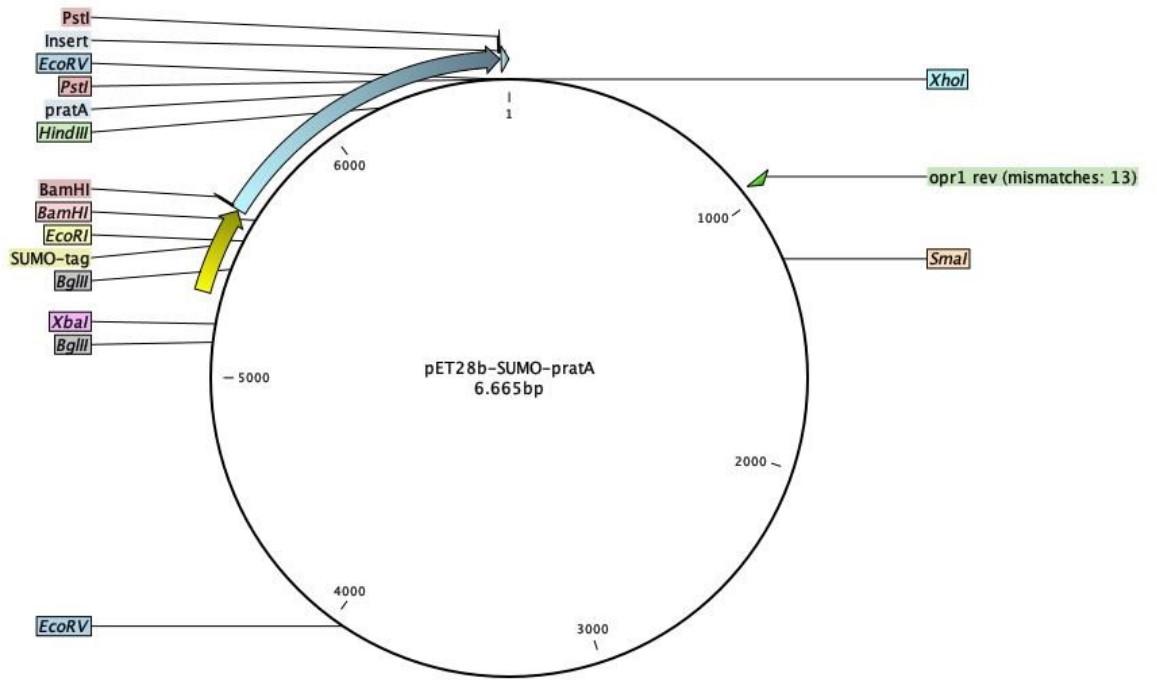


Figure 40 pET28b-SUMO-pratA

Annex

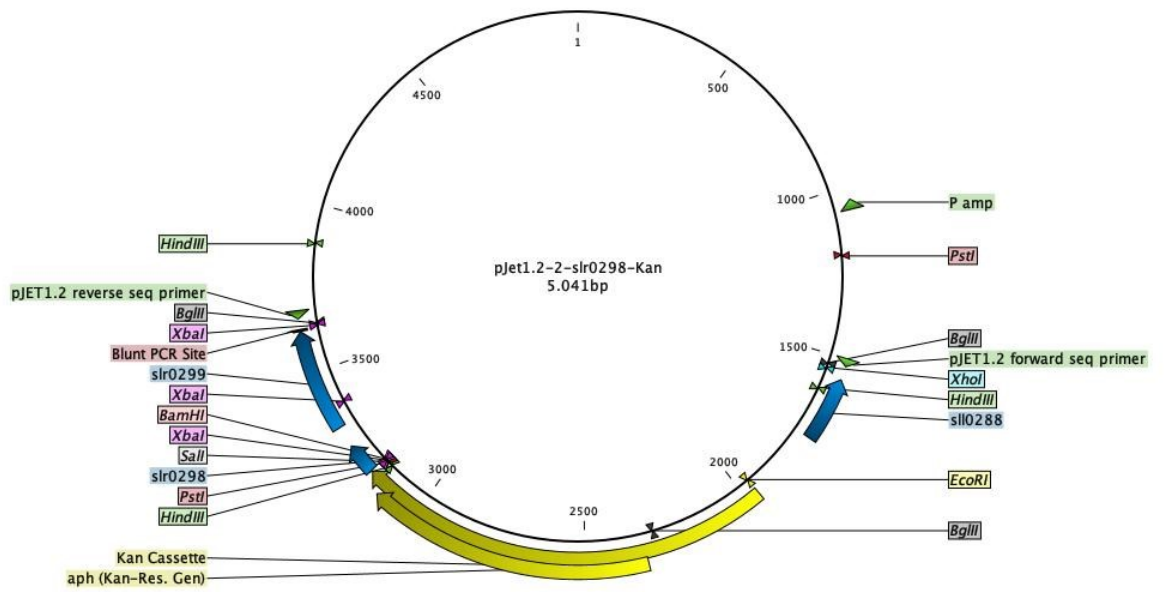


Figure 41 pJet1.2-2-slr0298

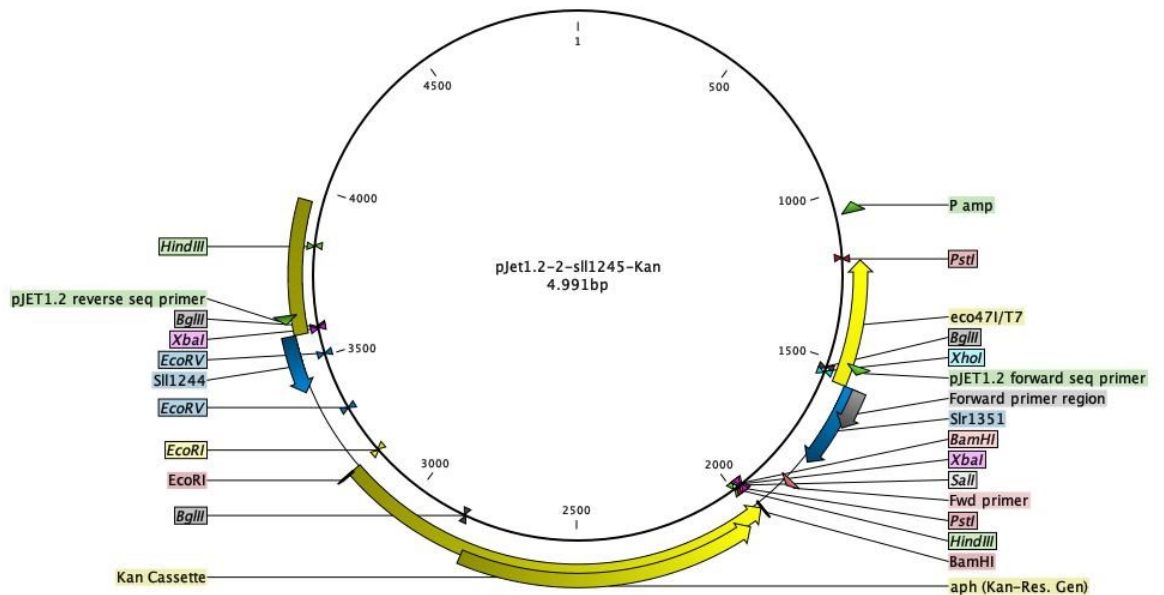


Figure 42 pJet1.2-2-sll1245-Kan

Annex

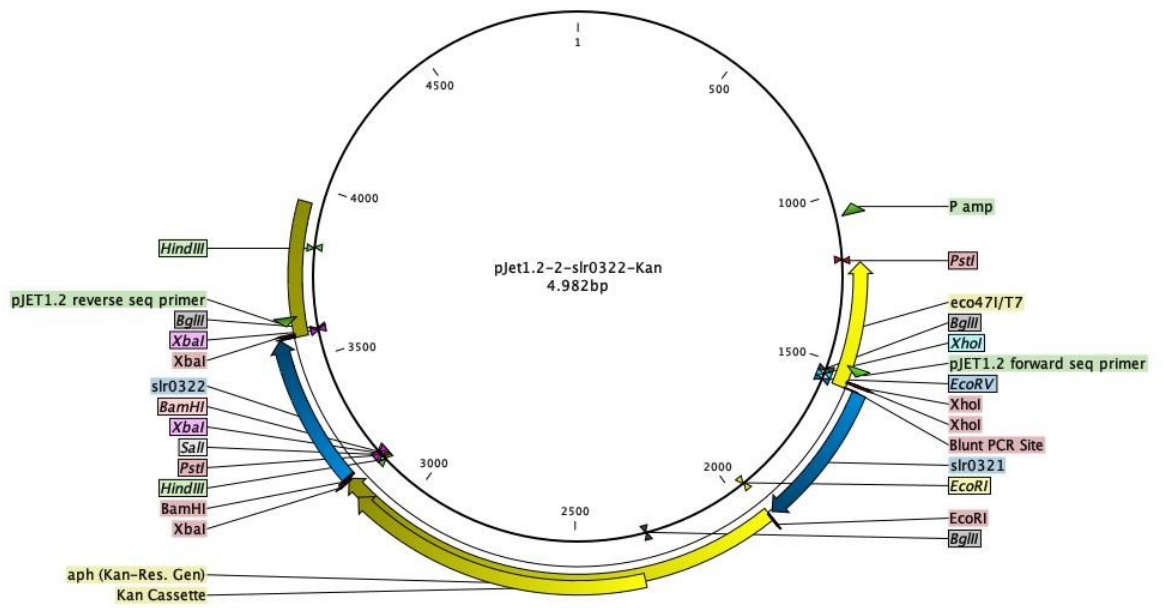


Figure 43 pJet1.2-2-slr0322-Kan

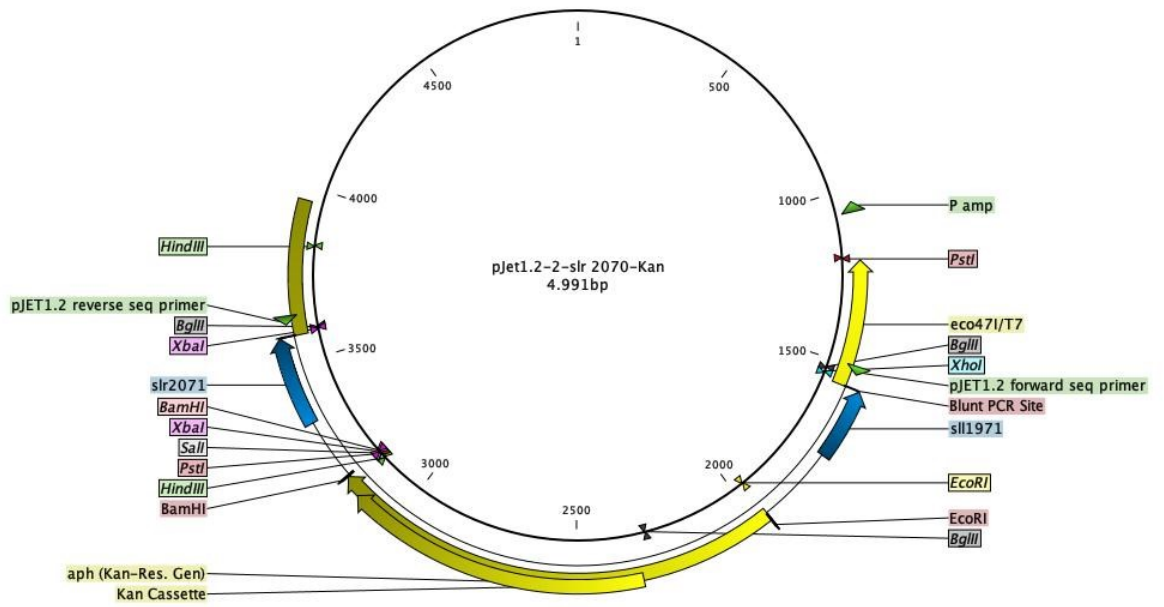


Figure 44 pJet1.2-2-slr2070-Kan

Annex

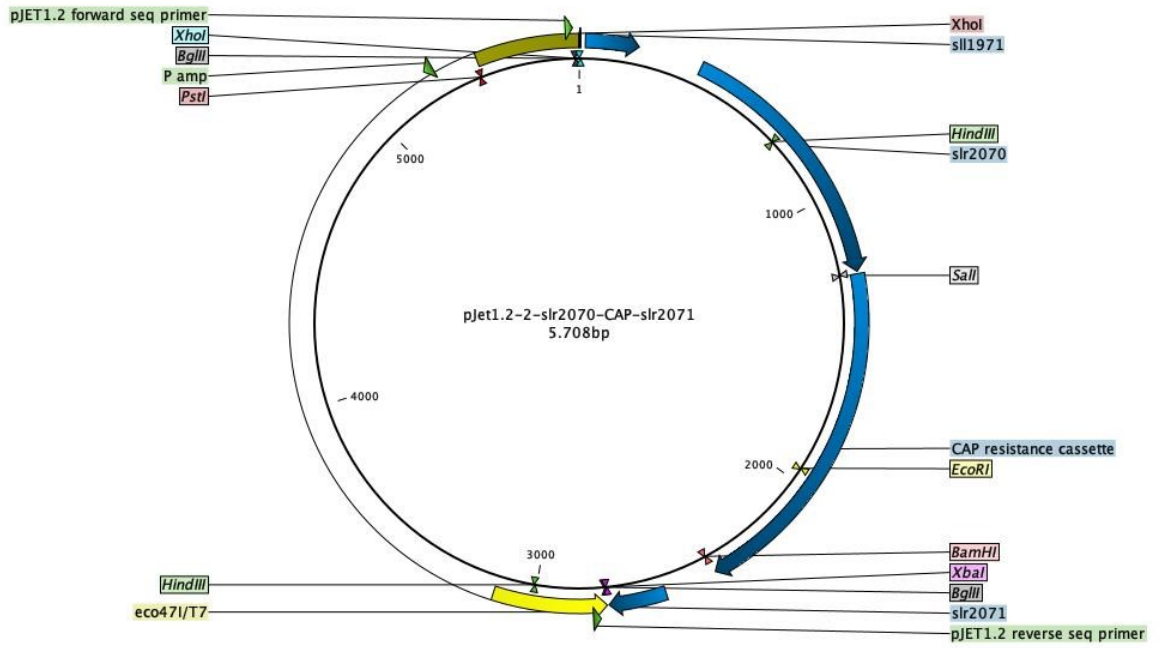


Figure 45 pJet1.2-2-slr2070-CAP-slr2071

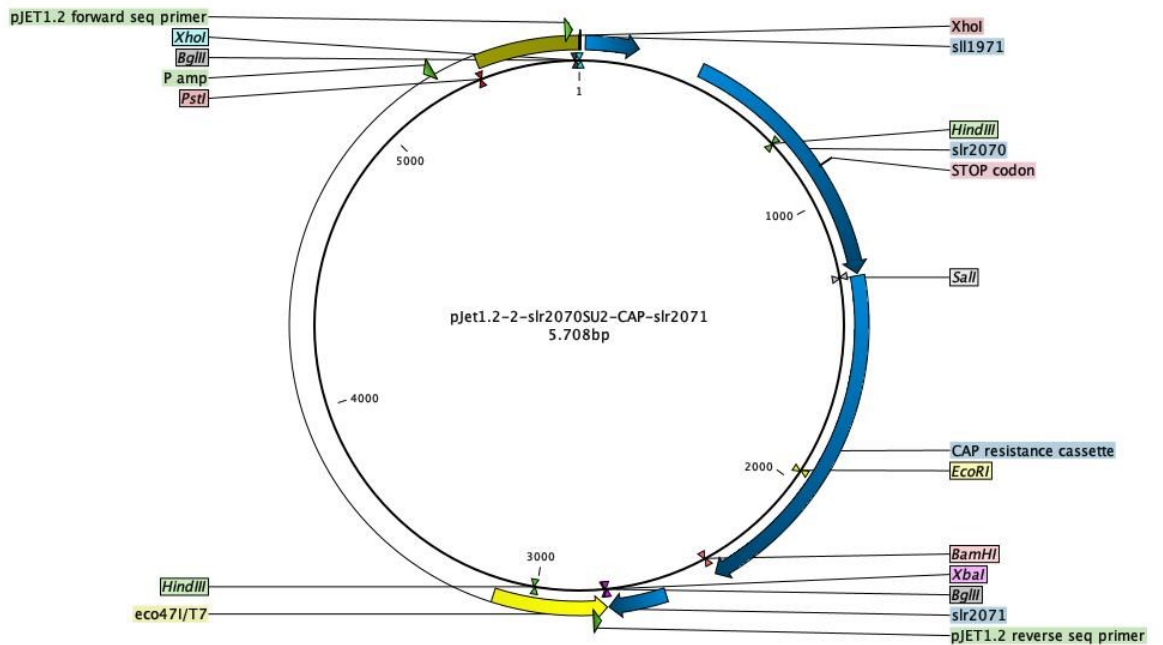


Figure 46 pJet1.2-2-slr2070SU2-CAP-slr2071

Annex

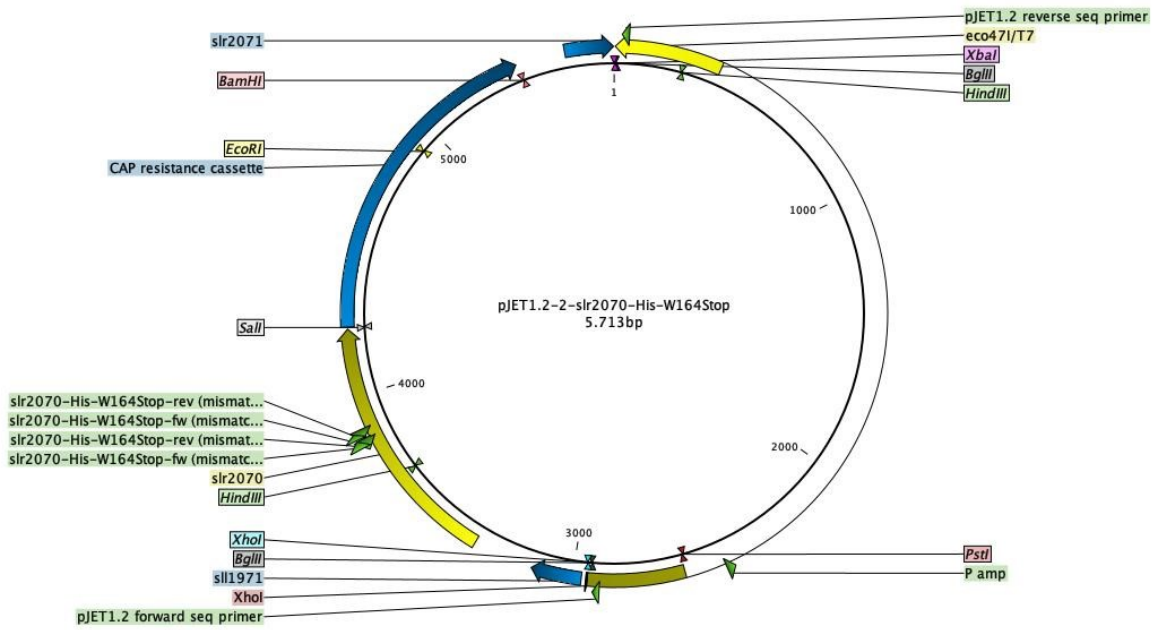


Figure 47 pJet1.2-2-slr2070-His-W164Stop

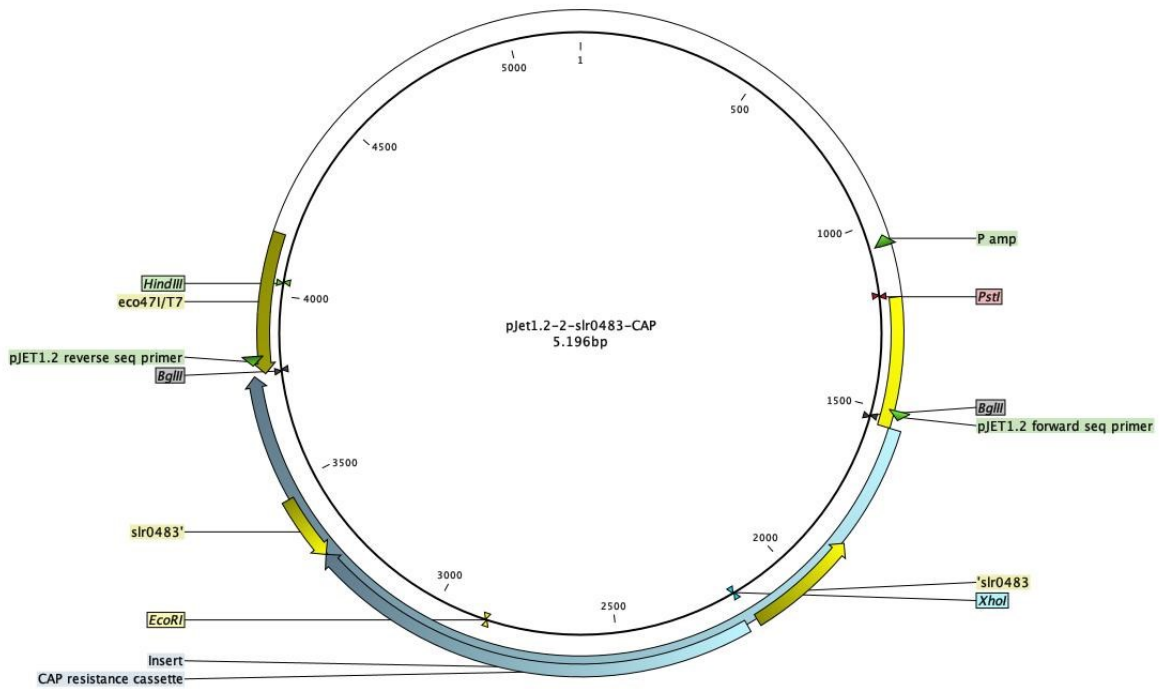


Figure 48 pJet-slr0483-CAP

Annex

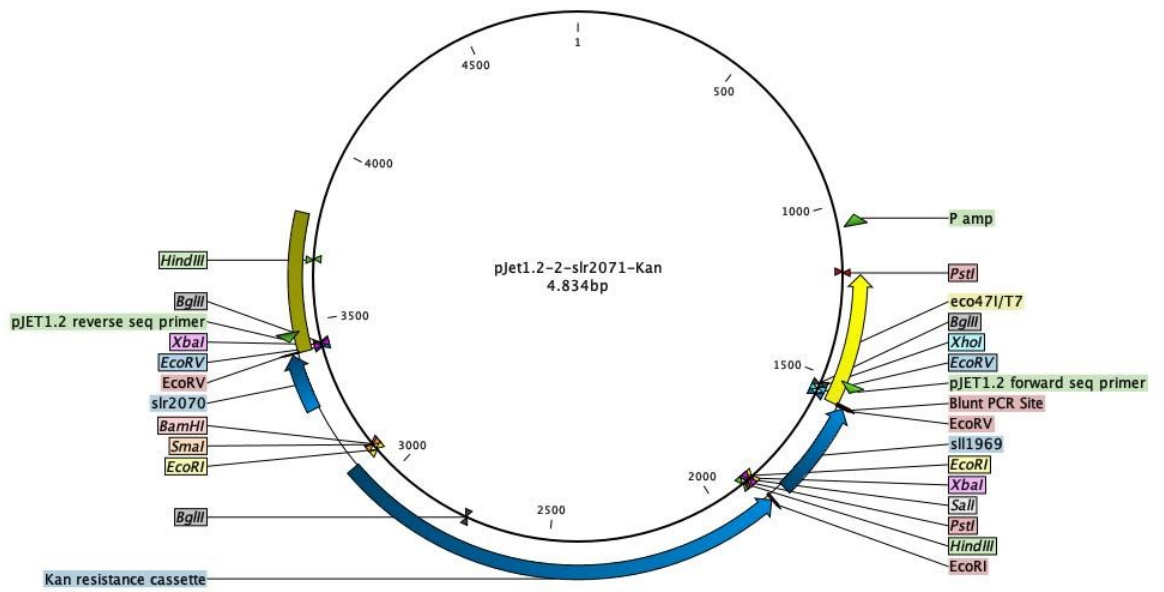


Figure 49 pJet1.2-2-slr2071-Kan

Annex

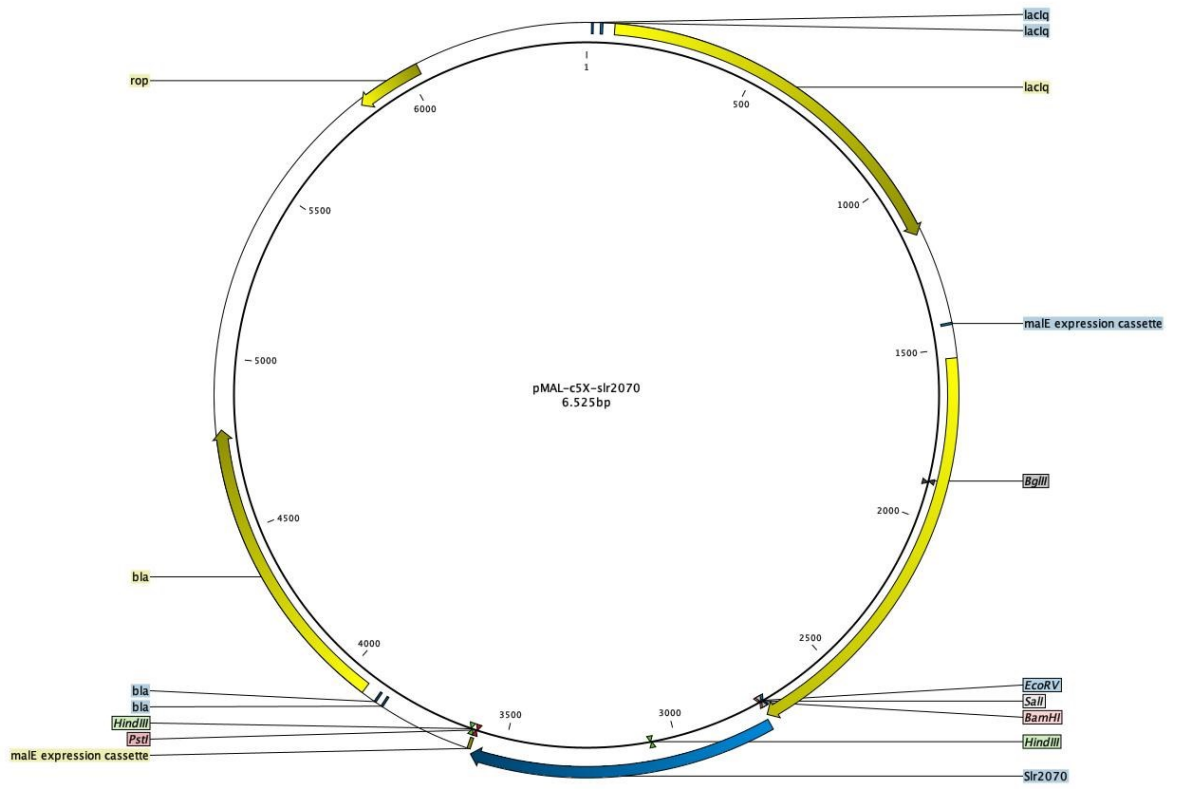


Figure 50 pMal-c5x-slr2070

CURRICULUM VITAE

Name Julia Hamm
Date of Birth 21.03.1991
Place of Birth Viernheim (Hessen)
Nationality German

Work Experience

Since 11/2020 Sales Specialist – Life Science
VWR, part of avantor

Research Experience

Since 08/2016 Phd at Ludwigs-Maximilians University Munich
Research Group Molecular Plant Science, Prof. Dr. Jörg
Nickelsen

Academic Education

2014-2016 Ruhr-Universität Bochum
Master of Science in Biology
Optimierung des Elektronentransports von Photosystem II in
Biohybridsystemen – Prof. Dr. Rögner

2013-2014 TU Kaiserslautern
Biology and Chemical Engineering

2010-2013 TU Kaiserslautern
Bachelor of Science in Biological Science
Der Import von Grx2 in das IMS von Mitochondrien – Prof. Dr. Jan
Riemer

School Education

2007-2010 Helene-Lange Schule, Mannheim
Allgemeine Hochschulreife

2001-2007 Carl-Engler Realschule, Hemsbach
Mittlere Reife

1997-2001 Hebelschule, Hemsbach

Volunteer Work

2020-2021 Elected Member of Bezirksausschuss Schwabing-
Freimann

LIST OF PUBLICATION

Matthias Ostermeier, Steffen Heinz, **Julia Hamm**, Jure Zabret, Anna Rast, Andreas Klingl, Marc M. Nowaczyk and Jörg Nickelsen (in preparation). Thylakoid attachment to the plasma membrane requires the AncM protein in *Synechocystis* sp. PCC 6803

DANKSAGUNG

Zunächst möchte ich mich bei Prof. Dr. Nickelsen für die exzellente Betreuung sowie die Bereitstellung des spannenden Themas bedanken. Darüber hinaus möchte ich mein Dank für die stets offene Tür und die zahlreichen wissenschaftlichen Diskussionen aussprechen.

Darüber hinaus möchte ich der gesamten Arbeitsgruppe Molekulare Pflanzenwissenschaften für die inspirierende Arbeitsatmosphäre bedanken. Insbesondere danken möchte ich Steffen Heinz und Matthias Ostermeister für die stets kritischen und wissenschaftlichen Gesprächen sowie die zahlreichen zündenden Ideen. Ein ausgesprochen großer Dank geht an die wunderbaren technischen Assistentinnen Simone Boos und Karin Findeisen für die stets aufmunternden Worte und hilfreichen Ratschlägen rund um die Laborarbeit.

Den Mitgliedern der Forschergruppe FOR2092 möchte ich für inspirierende Tagungen und interessante Gespräche danken. Insbesondere möchte ich mich bei den Mitarbeitern Jan Lambertz und Jure Zabret der Arbeitsgruppe *Molecular Mechanisms of Photosynthesis* in Bochum unter Leitung von Prof. Dr. Marc Nowaczyk für die tolle Zusammenarbeit bedanken.

Ein weiterer Dank geht an Prof. Dr. Ralf Heermann für die Zusammenarbeit mit der Bioanalytik Serviceeinheit der LMU München sowie an Dr. Andreas Brachmann und Prof. Dr. Klingl für die freundliche Unterstützung bei der Genomsequenzierung und der Elektronen Mikroskopie.

Danken möchte ich auch Dr. Steffen Heinz und Leonie Kertess für das Korrektur lesen dieser Arbeit.

Zum Schluss möchte ich meiner Familie und meinem Partner für die großartige Unterstützung während der gesamten Zeit danken.

EIDESSTAATLICHE VERSICHERUNG UND ERKLÄRUNG

Eidesstaatliche Versicherung

Ich versichere hiermit an Eides statt, dass die vorgelegte Dissertation von mir selbstständig und ohne unerlaubte Hilfe angefertigt ist.

München, den 26. Mai 2021

Julia Hamm

Erklärung

Hiermit erkläre ich, dass die Dissertation nicht ganz oder in wesentlichen Teilen einer anderen Prüfungskommission vorgelegt worden ist. Des Weiteren habe ich mich **nicht** anderweitig einer Doktorprüfung ohne Erfolg unterzogen.

München, den 26. Mai 2021

Julia Hamm